NASA Technical Memorandum 4541

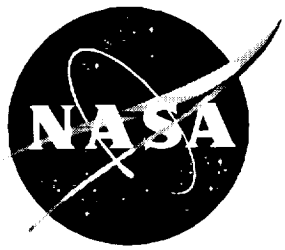

Aerodynamic Characteristics of a Propeller-Powered High-Lift Semispan Wing

Garl L. Gentry, Jr.
Langley Research Center • Hampton, Virginia

M. A. Takallu
Lockheed Engineering & Sciences Company • Hampton, Virginia

Zachary T. Applin
Langley Research Center • Hampton, Virginia

National Aeronautics and Space Administration
Langley Research Center • Hampton, Virginia 23681-0001

April 1994

Abstract

A small-scale semispan high-lift wing-flap system equipped under the wing with a turboprop engine assembly was tested in the Langley 14- by 22-Foot Subsonic Tunnel. Experimental data were obtained for various propeller rotational speeds, nacelle locations, and nacelle inclinations. To isolate the effects of the high-lift system, data were obtained with and without the flaps and leading-edge device. The effects of the propeller slipstream on the overall longitudinal aerodynamic characteristics of the wing-propeller assembly were examined. Test results indicated that the lift coefficient of the wing could be increased by the propeller slipstream when the rotational speed was increased and high-lift devices were deployed. Decreasing the nacelle inclination (increased pitch down) enhanced the lift performance of the system much more than varying the vertical or horizontal location of the nacelle. Furthermore, decreasing the nacelle inclination led to higher lift curve slope values, which indicated that the powered wing could sustain higher angles of attack near maximum lift performance. Any lift augmentation was accompanied by a drag penalty due to the increased wing lift.

Introduction

As part of the NASA Advanced Turboprop (ATP) Program, investigations were conducted at Langley Research Center on the engine-airframe integration aerodynamics for potential transport aircraft configurations (refs. 1–2). Some of these detailed studies have demonstrated the potential for major economic benefits through the use of advanced turboprop propulsion systems (refs. 3–5). These studies have focused primarily on providing high-efficiency cruise performance through the use of aft-fuselage-mounted turboprop arrangements or integrated wing-mounted nacelles designed to minimize interference effects. Advanced turboprops are also very attractive for short take-off and landing (STOL) transport applications, but little work has been reported regarding their propulsive-lift benefits.

Designs of high-bypass-ratio turbofans were studied in considerable detail during the 1970's (ref. 6). These studies examined systems with relatively large diameter slipstreams and the effect of the turbofans on aircraft performance. While the effort is continuing in this area (ref. 7), the task of designing the advanced turboprop systems becomes more challenging because of the large helical slipstream of the highly loaded blades. The response of the lifting surfaces to the slipstream varies with the system configuration and position of the slipstream; however, the highly loaded turboprop system integrated on a high-lift wing may increase the understanding of problems associated with some of the most critical phases of aircraft operations, such as take-off or missed approach procedure.

The objective of this investigation was to conduct a series of tests to investigate the potential for obtaining propulsive-lift benefits in a high-lift system using a wing-mounted, turboprop propulsion system. The investigation focused on varying the position of the propulsion system to determine the system aerodynamics. The results of the investigation were exploratory in nature, useful for any future analysis of a design of a general transport model with similar flow characteristics.

In the following sections, the model setup and test conditions for the investigation are described, and the results of the study are presented and described in detail. Presentation of the results includes a discussion of the measured system aerodynamic force and moment coefficients, followed by detailed discussions about estimation of force and moment coefficients due to the propeller slipstream only. This report focuses on three different wing configurations: (1) cruise wing, (2) wing with double-slotted flaps at 60° deflection, and (3) the second configuration with a leading-edge Krueger flap added.

Symbols

C_D	drag coefficient, Drag force/qS
C_L	lift coefficient, Lift force/qS
C_m	pitching-moment coefficient, Pitching moment/qSc
c	wing chord of cruise configuration, ft
$\bar{c}$	mean aerodynamic chord

i_{nac}	nacelle inclination with respect to wing chord, deg
q	free-stream dynamic pressure, lb/ft^2
S	wing area, ft^2
T_C	static thrust, lb
x, y, z	Cartesian coordinate system, in.
x/c	nondimensionalized longitudinal propeller location from wing leading edge
z/c	nondimensionalized vertical propeller location from wing leading edge
α	wing angle of attack, deg
Δ	differential
δ	component deflection, positive downward, deg

Subscripts:

f	flap
K	Krueger
l	wing lower surface
u	wing upper surface
v	vane
w	wing

Abbreviations:

ATP	Advanced Turboprop Program
QCSEE	quiet clean short-haul experimental engine
WM	windmill condition

Model Setup and Apparatus

A photograph of the model assembly, installed in the test section of the Langley 14- by 22-Foot Subsonic Tunnel, is presented in figure 1. The semispan wing had a rectangular planform with a 20-in. chord and a 48-in. span as shown in figure 2(a). The wing was equipped with a leading-edge flap (Krueger type) and a double-slotted flap system (fig. 2(b)), and incorporated a constant-chord QCSEE (quiet clean short-haul experimental engine) airfoil section (ref. 8). The cruise wing configuration is shown in figure 2(c). Wing and high-lift system sectional coordinates are given in tables I–V. The propulsion system consisted of an eight-bladed, single-rotation propeller driven by an air turbine motor mounted in a nacelle. The cylindrical nacelle was mounted with prefabricated support links to the wing and could be placed at several different longitudinal (x/c) and vertical (z/c) locations (fig. 3). Similar support links were used to vary the nacelle inclination with respect to the wing chord line. Variations in the nacelle inclination (thrust line angle) as a result of using two different support links changed the nacelle vertical and horizontal positions by small increments, but were negligible when compared with the variation of the nacelle location.

The 1-ft-diameter, eight-bladed propeller was a scale model of the SR-7L propeller designed and developed jointly by Hamilton Standard Propellers and NASA Lewis Research Center (ref. 9). The air motor that was used to power the propeller was a compact, high power-to-weight ratio, four-stage turbine designed to deliver approximately 150 hp at 19 000 rpm and was housed in the 5-in-diameter nacelle. The drive air was exhausted through a nozzle at the nacelle exit directly in the nacelle axial direction. The high-pressure air line (see trombone-shaped ducts in fig. 2(a)) for the power system was routed through the tunnel system to a rigid mount at the bottom of the model support system into a rigid point on the wing and bridged the external balance. Motor rotational speed was measured with a 30-per-revolution signal decoded by a tachometer. Overall forces and moments of the wing-propeller assembly were measured with a six-component strain-gage balance located inside the wing with a balance moment center at 0.4c. (See fig. 2(a).) There were no provisions for direct measurements of thrust and torque for the propulsion system.

The investigation was performed in the Langley 14- by 22-Foot Subsonic Tunnel (ref. 10), which has a test section of 14.50 ft high, 21.75 ft wide, and 50.00 ft long. This atmospheric wind tunnel is capable of test section speeds from 0 to 200 knots. The model system was situated in the center of the tunnel on a masthead. This entire system was on a turning table 45 in. above the tunnel floor, which was well above the floor wall boundary layer (ref. 10).

Test Conditions

Experiments were conducted at a free-stream dynamic pressure of 15 lb/ft^2 (66.5 knots), which yielded a Reynolds number of 0.66×10^6 based on the wing reference chord of 20 in. Wing angle of attack was varied within the stall boundaries from $-30°$ to $40°$. The dynamic pressure and the propeller speeds of 11 000 and 14 000 rpm were selected to simulate highly loaded blade configurations (refs. 11–14), corresponding to critical phases of flight operations such as climb out and missed approach. The blade

pitch angle at 75 percent radial station was set to 40° throughout the tests (ref. 11). Operating conditions were established by first setting the tunnel dynamic pressure and then setting the propeller rpm, which were held constant throughout the given angle-of-attack range. All the data presented were time averaged and were acquired at a rate of 5 samples/sec for 5 sec.

Discussion of Results

The effects of the nacelle and propeller slipstream on the overall force and moment characteristics of the wing-propeller assembly were obtained and are presented in detail in the following sections. Presentation of the results will include the discussion of the measured system aerodynamic force and moment coefficients followed by detailed discussion of the force and the moment coefficients due to the propeller slipstream only. Three different wing configurations were studied: (1) cruise wing, (2) wing with double-slotted flaps at 60° deflection, and (3) the second configuration with a leading-edge Krueger flap added. The results are presented to show the effects of different components of the system on the longitudinal aerodynamic characteristics of the entire system. The basic test matrix is presented in table VI.

Presentation of Basic Data

Figures 4–15 show the effects of nacelle inclination angle i_{nac} on the longitudinal aerodynamic characteristics of the wing-nacelle assembly. These figures present test results for the propeller rotational speeds for windmill conditions, 11 000 rpm and 14 000 rpm. Each set of figures presents results for constant nacelle position in the following order: $x/c = 0.60$ and $z/c = 0.25$, $x/c = 0.60$ and $z/c = 0.30$, $x/c = 0.75$ and $z/c = 0.30$, and $x/c = 0.75$ and $z/c = 0.25$.

Cruise wing configuration. Test results for the cruise wing configuration are depicted in figures 4–7. When the propeller rotational speed was increased, the immediate effect was seen in larger negative values of the measured drag, increase in maximum lift coefficient, and increase in pitching-moment coefficients. Negative values of drag occurred because the thrust increased and the strain gage balance measured the axial forces (combined wing-propeller) in the direction of the propeller drag. The above data indicate that during windmill conditions the lift curve experiences a negative zero-lift angle of attack. This camber-like behavior is possibly due to a complex flow field moving past such a large nacelle-propeller assembly. Furthermore, changes in nacelle position and inclination angle have very little effect on the results for the cruise wing configuration.

Flapped wing configuration. For the flapped wing configuration the vane was deflected 30°, and the double-slotted flaps were deflected 60° (fig. 2(b)). The test results in figures 8–15 show that the deflection of 60° with double-slotted flaps significantly affected the longitudinal aerodynamic characteristics of the wing-nacelle assembly in comparison with the results of the above cruise configurations (figs. 4–7). Unlike the cruise configuration, the performance curves for 11 000 rpm and 14 000 rpm show that both lift and pitching moment increased for all inclination angles with increasing propeller rotational speed. These increases indicate that performance changes due to nacelle inclination are more pronounced for the flapped wing configuration than for the cruise wing.

Flapped wing with leading-edge device. The high-lift configuration included the Krueger leading-edge device, which was deflected to $\delta_K = 60°$. The test results for this configuration are shown in figures 12–15. Although figures 12–15 present results for only a constant rotational speed of 11 000 rpm, lift augmentation normally gained from installation of Krueger flaps was not evident. In comparison with the results for the flapped case, the results in figures 12–15 showed some relative reduction in the lift performance. Reductions occurred in both the lift curve slope for angle of attack larger than 10° and in maximum lift coefficient. Both the gap and deflection of the Krueger flap were not adequate for the present flow characteristics. In spite of the deficiencies of the Krueger flaps, the effects of the nacelle inclination on the aerodynamic characteristics were both noticeable and similar to the trends seen for the flapped wing configuration.

Estimate of Propeller Thrust

Wing-mounted propulsion systems have significant effects on the wing aerodynamic characteristics, and these effects are more pronounced when the high-lift components are deployed. Various aerodynamic components contribute to the rise of these effects. Some of these effects are external to the wing performance and affect the measurement of the aerodynamic characteristics of the combined assembly. Examples of these effects are the propeller thrust, the location of the thrust line, the size and location of the exhaust nozzle, and the thrust from the exhaust nozzle alone. Another group of effects are pure aerodynamic effects, such as the propeller slipstream and the flow past the nacelle and nacelle attachments. The previous results were the measurements of the forces and moments generated by the combined wing

and the propulsion system. To estimate the contribution of the propeller wake on the wing aerodynamic characteristics, the thrust of the propeller must be quantified and its contribution must be removed from the overall measurements. As it was mentioned earlier, the six-component balance was positioned in the wing assembly; therefore, a direct measurement of propeller performance or performance of the isolated propeller was not available. Thus, the normal and axial forces were obtained for the combination of propeller and cruise wing at zero inclination and no wind conditions. Data were obtained for a wide range of propeller rotational speeds, and results are shown in figure 16. Care was taken to account for all static forces and moments arising from the relative positions of the center of thrust and the thrust line to the strain-gage balance for various inclination angles and nacelle positions. These forces (interpolated for a given rpm) were then numerically removed from the measured data discussed earlier.

Analysis of Thrust-Removed Data

With the method described in the previous section, the contribution of the propeller thrust was removed from data presented in figures 4–15, and the results are presented in figures 17–27. The effect of the propeller slipstream was more pronounced for the high-lift configuration; thus, the presentation of thrust-removed data is limited to data for the high-lift configurations.

Flapped wing configuration. The results for the wing with no leading-edge devices and with double-slotted flap configuration for $\delta_f = 60°$, with a nacelle location of $x/c = 0.60$, and $z/c = 0.30$, and with a nacelle inclination of $i_{nac} = 0°$ are discussed here to illustrate typical results. Figure 17 compares results of measured data and the direct-thrust-removed data and includes a curve showing the effects on the exhaust discharge of removing the blades while the core pressure remains constant.

The powered nacelle without the propeller blades produced a maximum lift coefficient of 2.9 at $\alpha = 15°$ and a minimum drag coefficient of 0.05 (fig. 17). This comparison was in contrast to the cases with blades on, where less drag (more thrust) and more lift were measured (i.e., the curve indicating the direct measurements shows a maximum lift coefficient of 4.4 at $\alpha = 20°$ and a minimum drag coefficient of -0.2 at $\alpha = -20°$). This drastic change was because of the contributions of both the propeller thrust and the propeller slipstream. The lift curve with all the thrust contributions removed shows little change from the measured lift curve; however, the lift curve with blades removed brings about a larger change from the measured lift curve. This similarity of lift characteristics indicates a supercirculation (refs. 6–8) effect with the propeller slipstream as the major source of lift augmentation. Added drag values were caused by a lack of thrust contribution and induced drag was caused by the lift augmentation.

Figure 18 shows comparisons between thrust-removed data and measured data at propeller rotational speeds of 11 000 rpm and 14 000 rpm. Again, the lift performance of the thrust-removed data is only slightly less than that of the measured data, which indicates the lift augmentation effects on the propeller slipstream. Figures 19 and 20 show, in more detail, the thrust-removed performance characteristics with variations in rpm, nacelle position, and inclination. In all the cases illustrated, higher lift benefits were gained from the additional flow over the wing than from the apparent lift due to the thrust component when the propeller rotational speed (disk loading) was increased. However, when the thrust values were removed from the data, there was a net increase in the drag coefficient. This drag penalty was due to added lift with an associated increase in induced drag and some skin friction drag caused by the stronger propeller slipstream. Furthermore, a comparison of the moment coefficients shows no significant change due to increased rotational speed (disk loading). One may conclude that in the case of an aircraft no additional trim moment may be needed for higher disk loading. Figures 19 and 20 also show that as the nacelle inclination decreased, the lift performance improved proportionally. This lift augmentation was associated with an increased drag and decreasing pitching-moment coefficients. Furthermore, the change in nacelle inclination caused a shift in the lift curve slope accordingly. In particular, decreasing nacelle inclination (increased pitch-down) resulted in increasing lift over the entire angle-of-attack range.

Flapped wing with leading-edge device. The thrust-removed data are shown for a high-lift configuration in figures 23–26 (i.e., when both double-slotted flaps and Krueger leading-edge devices are deployed at $\delta_f = 60°$ and $\delta_K = 60°$, respectively). The results are shown for a constant propeller rotational speed of 11 000 rpm and for all four nacelle locations. The thrust-removed longitudinal aerodynamic characteristics of this high-lift configuration also showed that as the nacelle pitch is lowered (decreasing nacelle inclination) the lift curve performance improves proportionally. Again, lift augmentation was associated with increasing drag and decreasing (more negative) pitching-moment coefficient. Furthermore, for the

high-lift configuration, the decreasing nacelle inclination (increased pitch-down) resulted in an increasing lift curve slope, but not the shift in lift curve that was observed in figures 19–22, which is a trend typical of wings with leading-edge devices.

Effect of Nacelle Position on Thrust-Removed Data

In the following section, the results that were presented previously are plotted in a different form to facilitate a detailed look at incremental changes that the system experiences because of the specific position or inclination of the propeller-nacelle assembly with respect to the wing.

Effect of longitudinal and vertical positions of propeller-nacelle. In figure 27 the aerodynamic coefficients for the powered propeller are presented for the four nacelle locations tested. Results are shown for the wing with $\delta_f = 60°$, $i_{nac} = 0°$, and two propeller rotational speeds. A close examination of figure 27 indicates that a longitudinal or vertical change in the location of the nacelle with respect to the wing resulted in a shift in the lift curve. In particular, a change in the vertical location affected the performance data more than the variations in the horizontal direction. In both cases, the incremental changes were more pronounced at higher propeller rotational speed. These trends seem to confirm previous observations that the amount of projection of the propeller disk exposed to high-lift devices may influence the magnitude of the supercirculation.

Effect of inclination. The nacelle inclination changes the direction of the propeller slipstream and affects the aerodynamic characteristics of the powered high-lift wing system. To examine these characteristics in detail, the longitudinal aerodynamic coefficients of the flapped configuration, $\delta_f = 60°$, were selected. The differences between the performance coefficients at various nacelle inclinations and zero nacelle inclination were computed and the results are plotted in figures 28–31. Two different propeller rotational speeds were selected. Again, results are shown for all four nacelle locations. Lift, drag, and pitching-moment coefficients increased with increased pitch-down values of nacelle inclination. In addition, both lift and drag increased with different angles of attack; therefore, a pitch-down change in the nacelle inclination during high angle-of-attack operations can effectively produce substantial lift augmentation for the system. The incremental values of the moment coefficients moderately changed with decreasing inclination angle but did not vary strongly as angle of attack was increased. In real aircraft operations, the increased drag and losses due to trim must be overcome by added thrust during some crucial maneuvers such as level off to minimum descent altitude or a missed approach procedure. These maneuvers require high-lift performance and full propeller thrust (to stop the descent or to initiate a climb out) with alignment of the thrust line and free-stream direction. This configuration suggests an innovative design where a pitch-down movement of the nacelle during these maneuvers could align the thrust line with the free-stream direction to counteract added drag more effectively and to expand the range of maximum lift. A possible additional benefit of nacelle and free-stream alignment would be the reduction in asymmetric propeller disc loading and the elimination of some stability and control concerns. An asymmetric disc loading is known to cause undesirable changes in the frequency spectrum of the propeller radiated noise.

Concluding Remarks

An experimental investigation was conducted on the engine-airframe integration aerodynamics for a high-lift wing configuration. The model consisted of an untapered semispan wing with a double-slotted flap system with and without a Krueger leading-edge device. The advanced propeller and the powered nacelle were tested, and aerodynamic characteristics of the combined system were presented.

Results indicate that the lift coefficient of the powered wing could be increased by the propeller slipstream when the rotational speed (disk loading) was increased and high-lift devices were incorporated. Moving the nacelle with respect to the wing leading edge in vertical and longitudinal directions increased lift augmentation through a distinct shift in the lift curve with no change in the lift curve slope. Vertical displacement showed more effective lift augmentation than longitudinal displacement. Decreasing the nacelle inclination (increased pitch-down) increased the lift performance of the flapped system over the entire angle-of-attack range. The combination of large pitch-down inclination angle and high angle of attack showed the largest increase in lift increment. Any lift augmentation was accompanied with an additional increase in drag due to the increased wing lift.

NASA Langley Research Center
Hampton, VA 23681-0001
December 15, 1993

References

1. Applin, Zachary T.; and Gentry, Garl L., Jr.: *Low-Speed Stability and Control Characteristics of a Transport Model With Aft-Fuselage-Mounted Advanced Turboprops.* NASA TP-2535, 1986.

2. Dunham, Dana Morris; Gentry, Garl L.; Manuel, Gregory S.; Applin, Zachary T.; and Quinto, P. Frank: *Low-Speed Aerodynamic Characteristics of a Twin-Engine General Aviation Configuration With Aft-Fuselage-Mounted Pusher Propellers.* NASA TP-2763, 1987.

3. Goldsmith, I. M.: *A Study To Define the Research and Technology Requirements for Advanced Turbo/Propfan Transport Aircraft.* NASA CR-166138, 1981.

4. Levin, Alan D.; Smith, Ronald C.; and Wood, Richard D.: *Aerodynamic and Propeller Performance Characteristics of a Propfan-Powered, Semispan Model.* NASA TM-86705, 1985.

5. Whitlow, J. B., Jr.; and Sievers, G. K.: *Fuel Savings Potential of the NASA Advanced Turboprop Program.* NASA TM-83736, [1984].

6. Johnson, William G., Jr.: *Aerodynamic Characteristics of a Powered, Externally Blown Flap STOL Transport Model With Two Engine Simulator Sizes.* NASA TN D-8057, 1975.

7. Favier, D.; Maresca, C.; Barbi, C.; and Fratello, G.: Experimental and Numerical Study of the Propeller/Fixed Wing Interaction. AIAA-88-2571, 1988.

8. Phelps, Arthur E., III: *Static and Wind-On Tests of an Upper-Surface-Blown Jet-Flap Nozzle Arrangement for Use on the Quiet Clean Short-Haul Experimental Engine (QCSEE).* NASA TN D-8476, 1977.

9. Parzych, D.; Shenkman, A.; and Cohen, S.: *Large-Scale Advanced Propfan (LAP) Performance, Acoustic and Weight Estimation, January, 1984.* NASA CR-174782, 1985.

10. Gentry, Garl L., Jr.; Quinto, P. Frank; Gatlin, Gregory M.; and Applin, Zachary T.: *The Langley 14- by 22-Foot Subsonic Tunnel: Description, Flow Characteristics, and Guide for Users.* NASA TP-3008, 1990.

11. Gentry, Garl L., Jr.; Booth, Earl R., Jr.; and Takallu, M. A.: *Effect of Pylon Wake With and Without Pylon Blowing on Propeller Thrust.* NASA TM-4162, 1990.

12. Takallu, M. A.; and Dunham, Dana Morris: A Hybrid Method for Prediction of Propeller Performance. AIAA-90-0440, Jan. 1990.

13. Takallu, M.; and Lessard, V.: Periodic Blade Loads of a High Speed Propeller at Small Angle of Attack. AIAA-91-2250, June 1991.

14. Takallu, M. A.; and Gentry, G. L., Jr.: Aerodynamic Characteristics of a Propeller Powered High Lift Semi-Span Wing. AIAA-92-0388, Jan. 1992.

Table I. Coordinates of Cruise Wing Section

x (a)	z_u (a)	z_ℓ (a)
0.00	0.000	0.000
1.25	2.920	-3.120
2.50	3.970	−4.140
5.00	5.180	−5.340
7.50	5.910	−6.060
10.00	6.480	−6.580
15.00	7.330	−7.300
20.00	7.920	−7.770
25.00	8.310	−8.040
30.00	8.610	−8.180
35.00	8.800	−8.160
40.00	8.920	−8.050
45.00	8.902	−7.734
50.00	8.850	−7.370
55.00	8.615	−6.450
60.00	8.340	−5.475
65.00	7.925	−3.715
70.00	7.360	−2.000
75.00	6.500	−1.005
80.00	5.610	−0.300
85.00	4.425	−0.040
90.00	3.140	−0.100
95.00	1.620	−0.450
100.00	0.000	−0.770

[a]Coordinates are given in percent of local wing chord. $c_w = 20$ in.

Table II. Coordinates of High-Lift Wing Section

x (a)	z_u (a)	z_ℓ (a)
0.00	0.000	0.000
1.25	2.920	−3.120
2.50	3.920	−4.140
5.00	5.180	−5.340
7.50	5.910	−6.060
10.00	6.480	−6.580
15.00	7.330	−7.300
20.00	7.920	−7.770
25.00	8.310	−8.040
30.00	8.610	−8.180
35.00	8.800	−8.160
40.00	8.920	−8.050
45.00	8.900	−7.750
50.00	8.850	−7.370
55.00	8.640	−6.695
60.00	8.340	−5.870
65.00	7.950	1.820
70.00	7.360	5.550
79.00	5.610	5.550

[a]Coordinates are given in percent of local wing chord. $c_w = 20$ in.

Table III. Coordinates of Flap Vane Airfoil Section

x (a)	z_u (a)	z_ℓ (a)
0.00	−12.500	−12.500
1.25	−6.525	−16.500
5.00	−0.297	−19.490
7.50	2.331	−20.210
10.00	4.801	−20.490
15.00	8.496	−20.130
20.00	11.530	−19.190
25.00	14.110	−17.990
30.00	16.270	−16.500
40.00	19.410	−13.810
50.00	21.060	−11.500
52.01	21.250	1.102
54.00	21.420	4.110
60.00	21.840	9.979
70.00	21.820	13.700
80.00	21.120	15.850
90.00	19.920	16.720
100.00	18.010	16.550

[a]Coordinates are given in percent of flap vane chord. $c_v = 0.236 c_w$.

Table IV. Coordinates of Flap Airfoil Section

x (a)	z_u (a)	z_ℓ (a)
0.00	−4.000	−4.000
1.25	0.000	−7.390
2.50	1.910	−8.410
5.00	4.790	−8.690
7.50	6.930	−8.450
10.00	8.670	−7.880
15.00	11.000	−6.700
20.00	12.630	−0.640
25.00	13.790	−4.680
30.00	14.530	−3.750
40.00	15.060	−2.160
50.00	14.240	−1.020
60.00	12.330	−0.440
80.00	6.690	−1.000
90.00	3.260	−1.800
100.00	−0.440	−2.710

[a]Coordinates are given in percent of local flap chord.
$c_f = 0.264c_w$.

Table V. Coordinates of Krueger Flap

x (a)	z_u (a)	z_ℓ (a)
0.00	0.000	0.000
1.25	5.000	−5.000
2.50	6.950	−6.950
5.00	10.000	−10.000
7.50	12.000	−12.000
10.00	13.550	−13.550
15.00	15.590	−15.590
15.00	15.590	5.680
20.00	16.950	5.680
30.00	17.910	5.680
40.00	17.500	5.680
50.00	16.180	5.680
60.00	14.200	5.680
70.00	11.590	5.680
80.00	8.550	5.680
90.00	5.250	5.680
100.00	1.700	5.680

[a]Coordinates are given in percent of local Krueger chord.
$c_K = 0.22c_w$.

Table VI. Wing-Nacelle Configurations

Figure	i_{nac}, deg						x/c	z/c	Configuration	Propeller speed, rpm	q_∞, lb/ft^2
	0	−2	−4	−6	−8	−10					
4(a)	x						0.60	0.25	Cruise	WM	15
4(b)	x						0.60	0.25	Cruise	11 000	15
4(c)	x	x	x	x			0.60	0.25	Cruise	14 000	15
5(a)	x	x	x				0.60	0.30	Cruise	WM	15
5(b)	x	x	x				0.60	0.30	Cruise	11 000	15
5(c)	x	x	x				0.60	0.30	Cruise	14 000	15
6(a)	x	x	x	x	x	x	0.75	0.30	Cruise	WM	15
6(b)	x	x	x	x	x	x	0.75	0.30	Cruise	11 000	15
6(c)	x	x	x	x	x	x	0.75	0.30	Cruise	14 000	15
7(a)	x	x	x				0.75	0.25	Cruise	WM	15
7(b)	x	x	x				0.75	0.25	Cruise	11 000	15
7(c)	x	x	x				0.75	0.25	Cruise	14 000	15
8(a)	x	x	x			x	0.60	0.25	Flaps	WM	15
8(b)	x	x	x		x	x	0.60	0.25	Flaps	11 000	15
8(c)	x	x	x		x	x	0.60	0.25	Flaps	14 000	15
9(a)	x	x	x	x	x	x	0.60	0.30	Flaps	WM	15
9(b)	x	x	x	x	x	x	0.60	0.30	Flaps	11 000	15
9(c)	x	x	x	x	x	x	0.60	0.30	Flaps	14 000	15
10(a)	x	x	x	x	x	x	0.75	0.25	Flaps	WM	15
10(b)	x	x	x	x	x	x	0.75	0.25	Flaps	11 000	15
10(c)	x	x	x	x	x	x	0.75	0.25	Flaps	14 000	15
11(a)	x	x	x	x	x	x	0.75	0.30	Flaps	WM	15
11(b)	x	x	x	x	x	x	0.75	0.30	Flaps	11 000	15
11(c)	x	x	x	x	x	x	0.75	0.30	Flaps	14 000	15
12	x	x	x	x	x	x	0.60	0.25	Flaps + K	11 000	15
13	x	x	x	x	x	x	0.60	0.30	Flaps + K	11 000	15
14	x	x	x	x	x	x	0.75	0.30	Flaps + K	11 000	15
15	x	x	x	x	x	x	0.75	0.25	Flaps + K	11 000	15
16(a)	x	x	x	x		x	0.60	0.25	Flaps	Range	15
16(b)	x	x	x	x	x	x	0.60	0.30	Flaps	Range	15
16(c)	x	x	x	x	x	x	0.75	0.30	Flaps	Range	15
16(d)	x	x	x		x	x	0.75	0.25	Flaps	Range	15

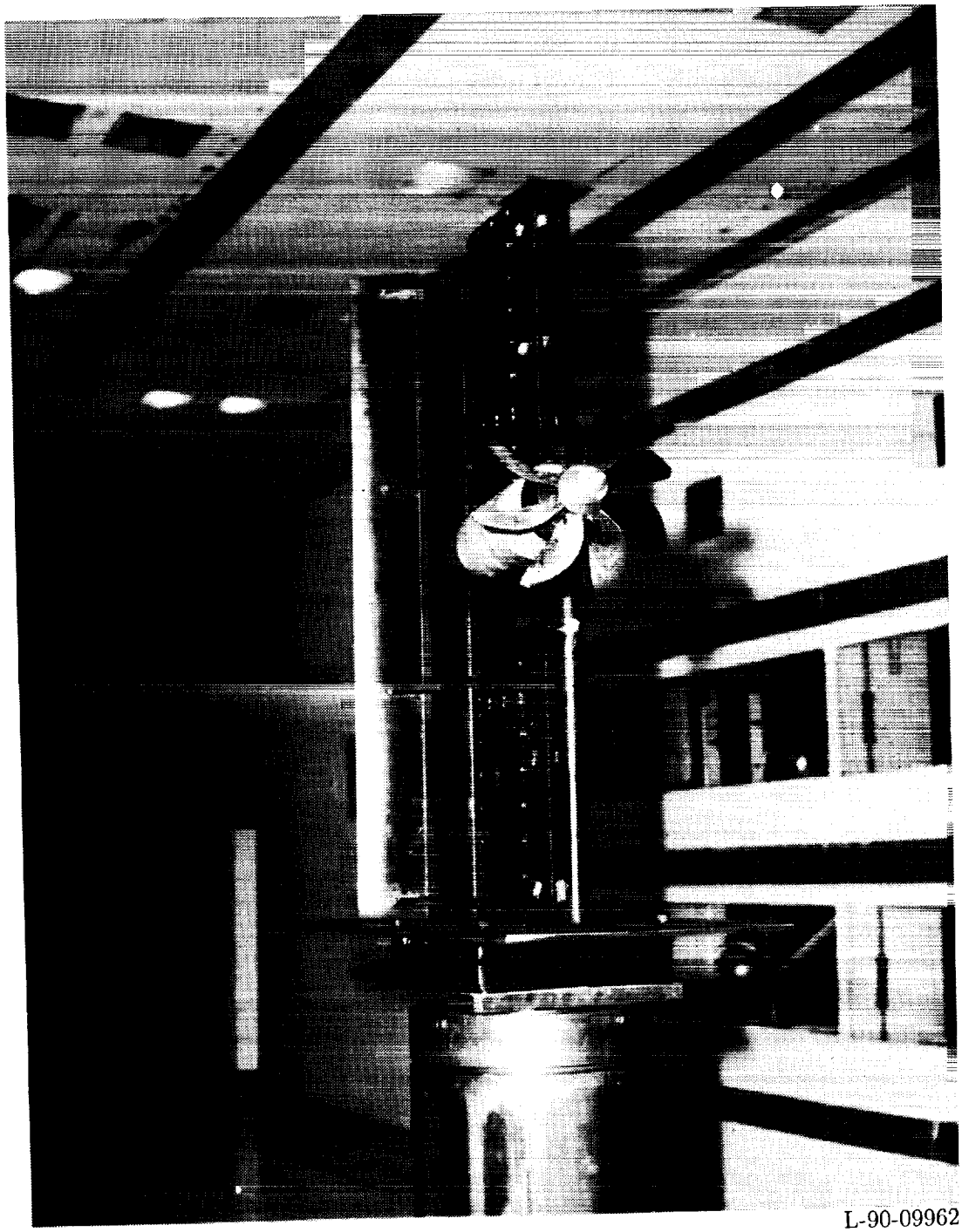

(a) Three-quarter view of trailing-edge flap configuration.

Figure 1. Photograph of semispan model installed in Langley 14- by 22-Foot Subsonic Tunnel.

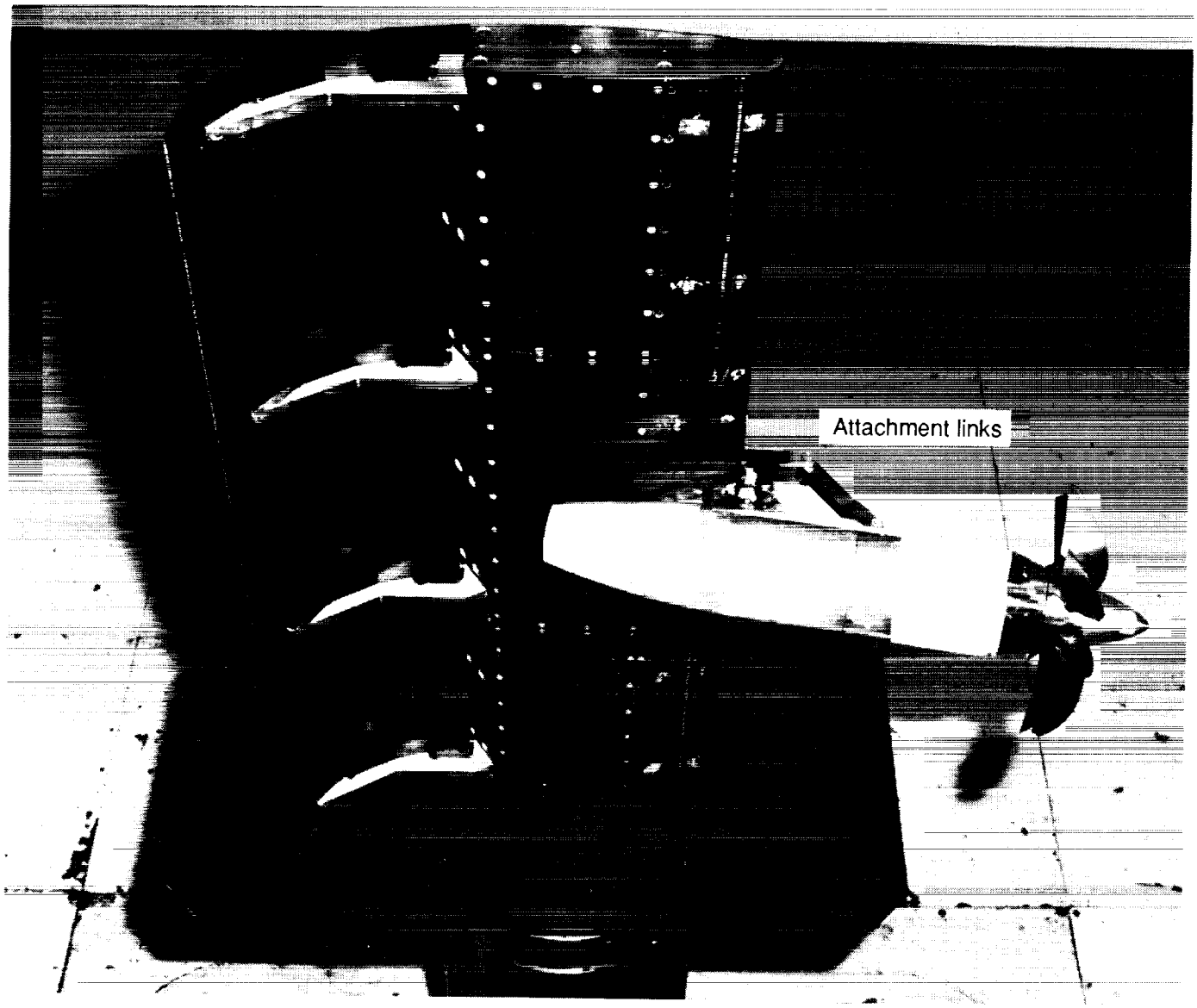

(b) Bottom view of trailing-edge flap configuration.

Figure 1. Concluded.

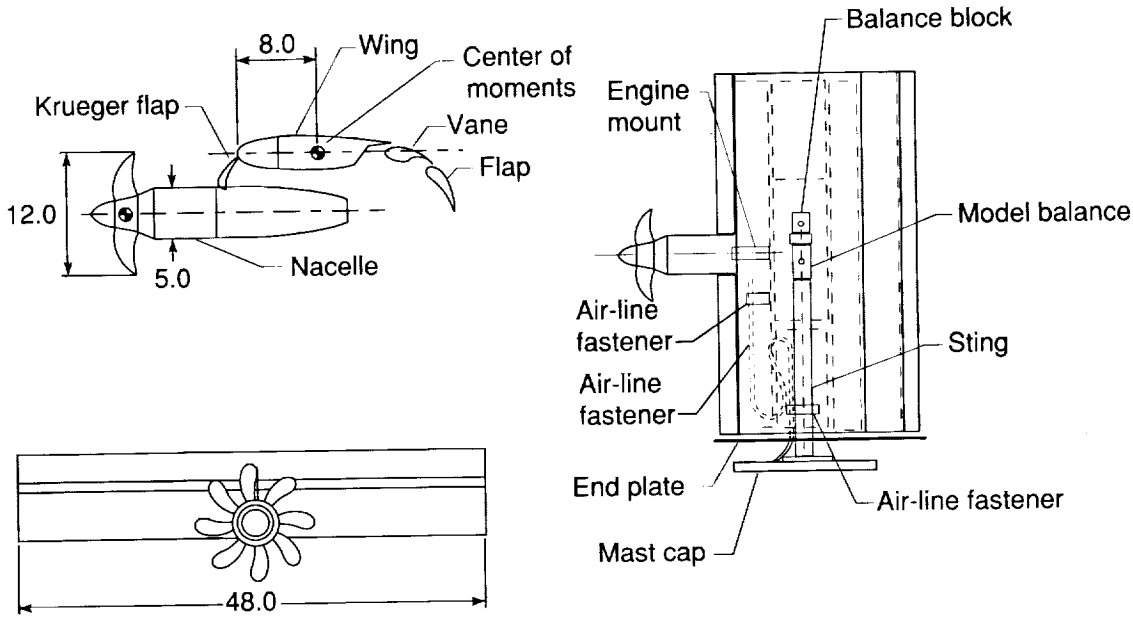

(a) Three-view sketch of semispan high-lift wing with propeller-nacelle assembly.

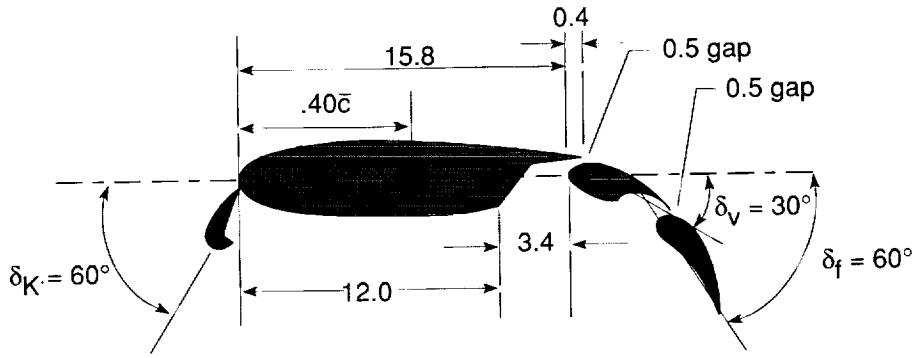

(b) High-lift configuration.

(c) Cruise configuration.

Figure 2. Schematics of test model. All dimensions are in inches.

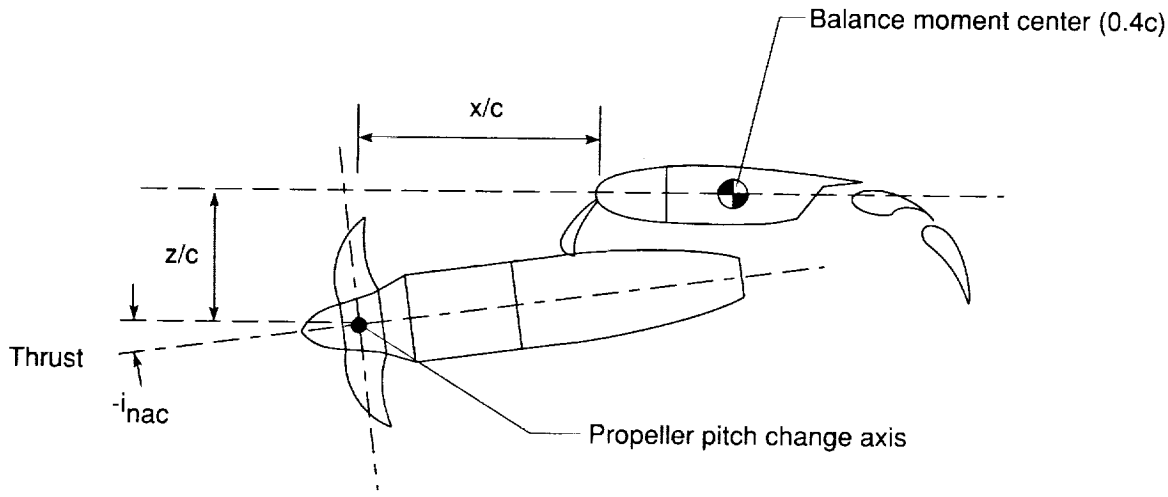

Figure 3. Schematic of propeller-nacelle position.

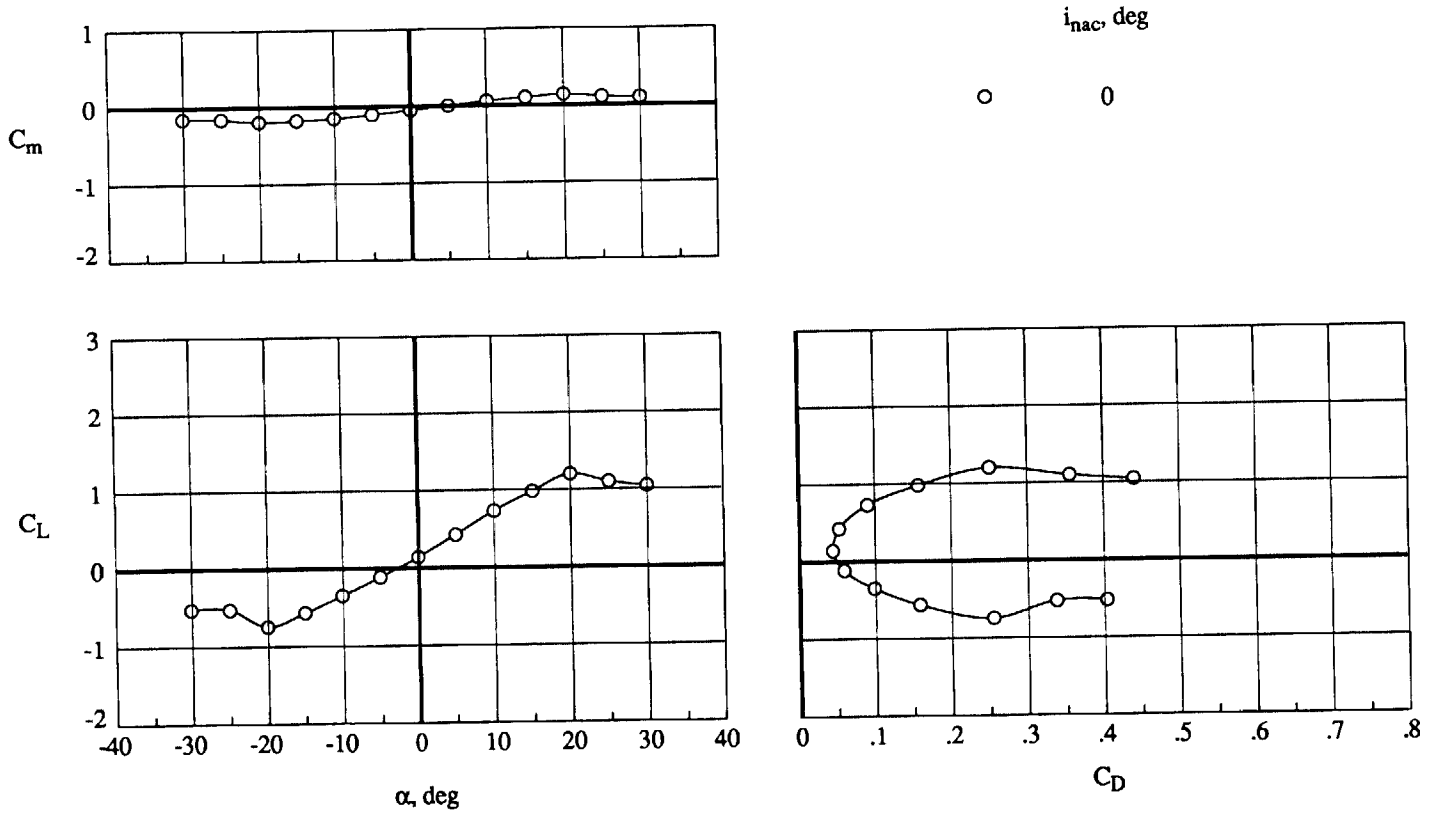

(a) Windmill conditions.

Figure 4. Effect of nacelle inclination on aerodynamic characteristics for $q = 15$ lb/ft^2, $x/c = 0.60$, $z/c = 0.25$, and $\delta_f = 0°$.

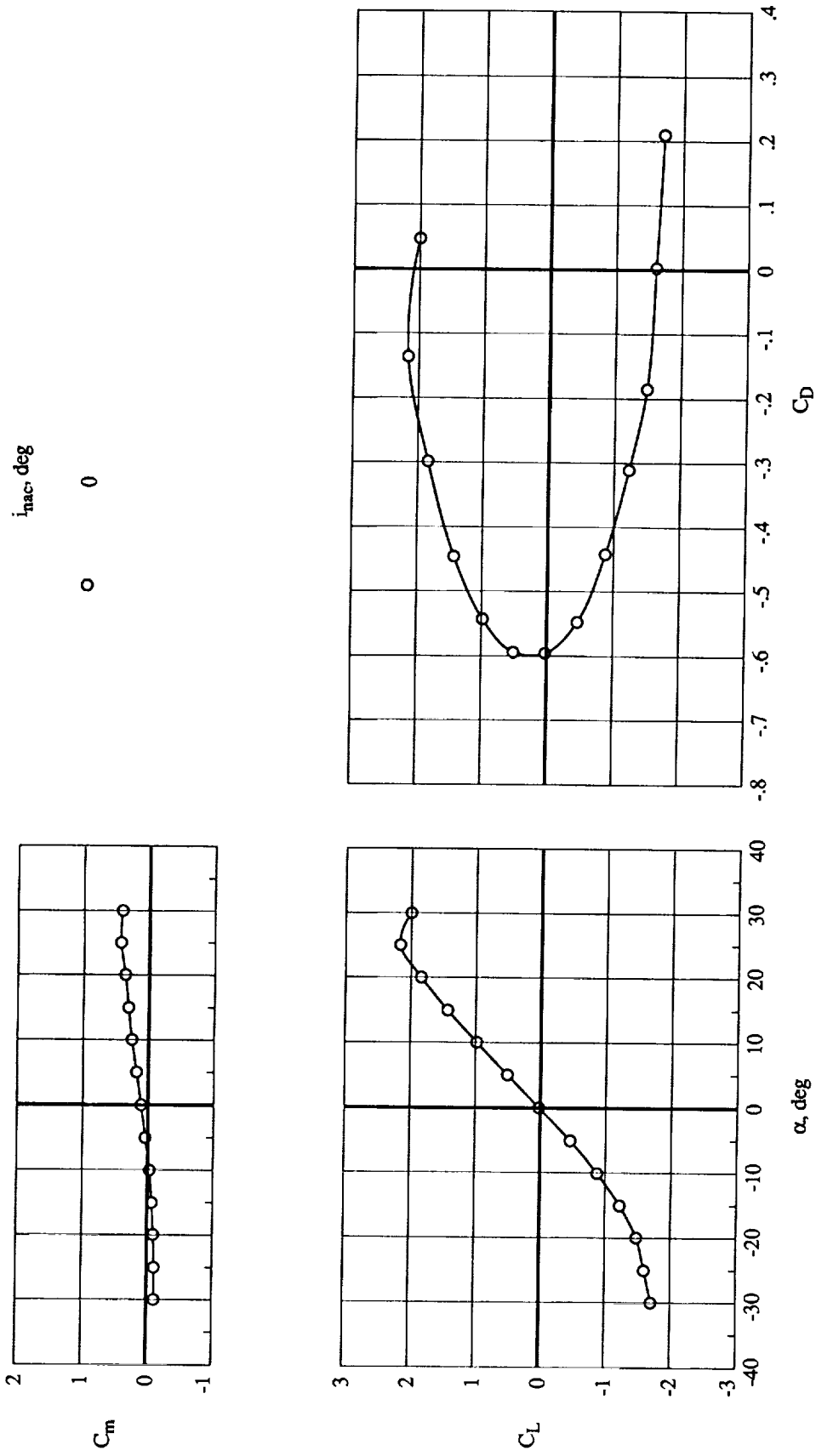

(b) Propeller speed = 11 000 rpm.

Figure 4. Continued.

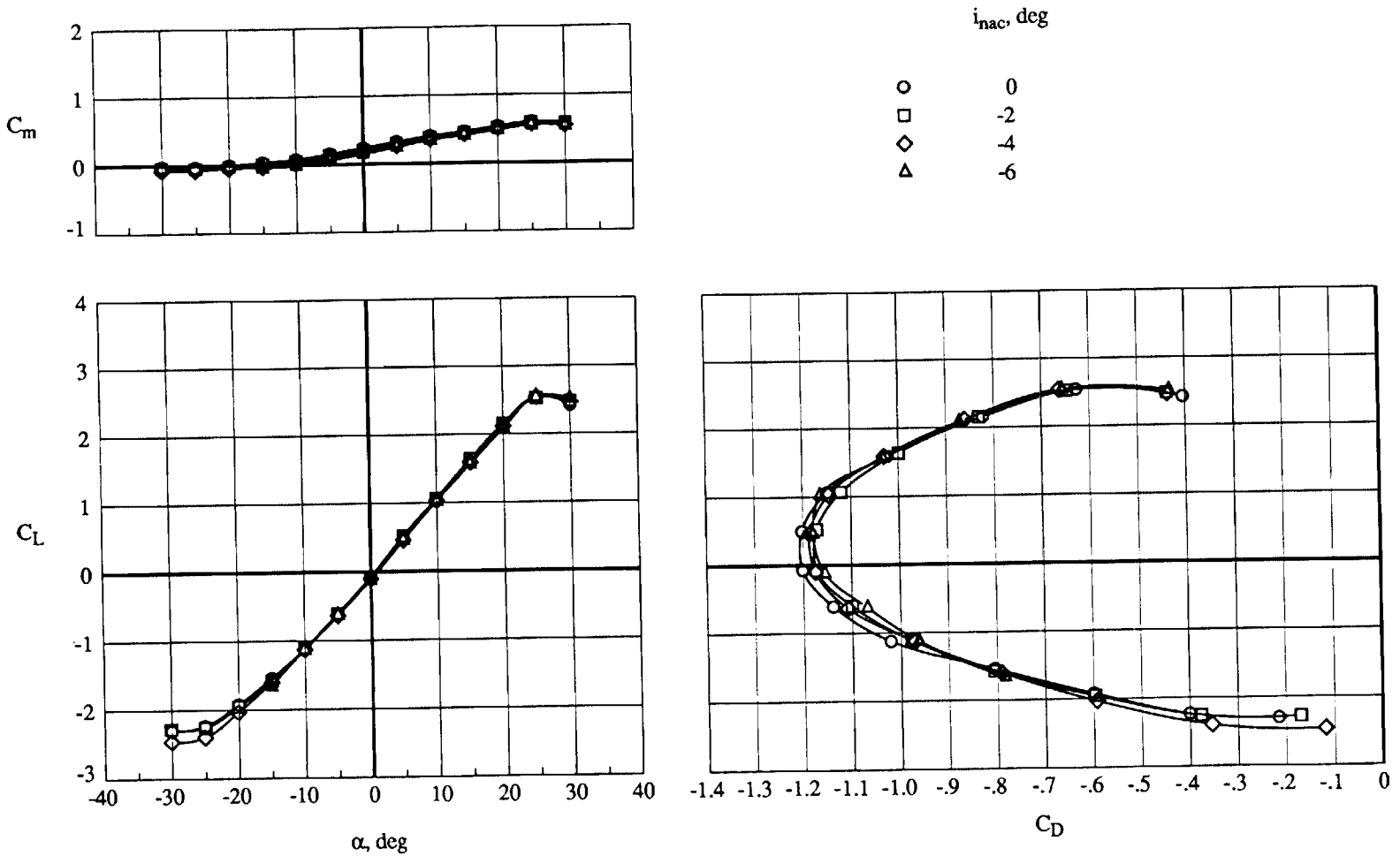

(c) Propeller speed = 14 000 rpm.

Figure 4. Concluded.

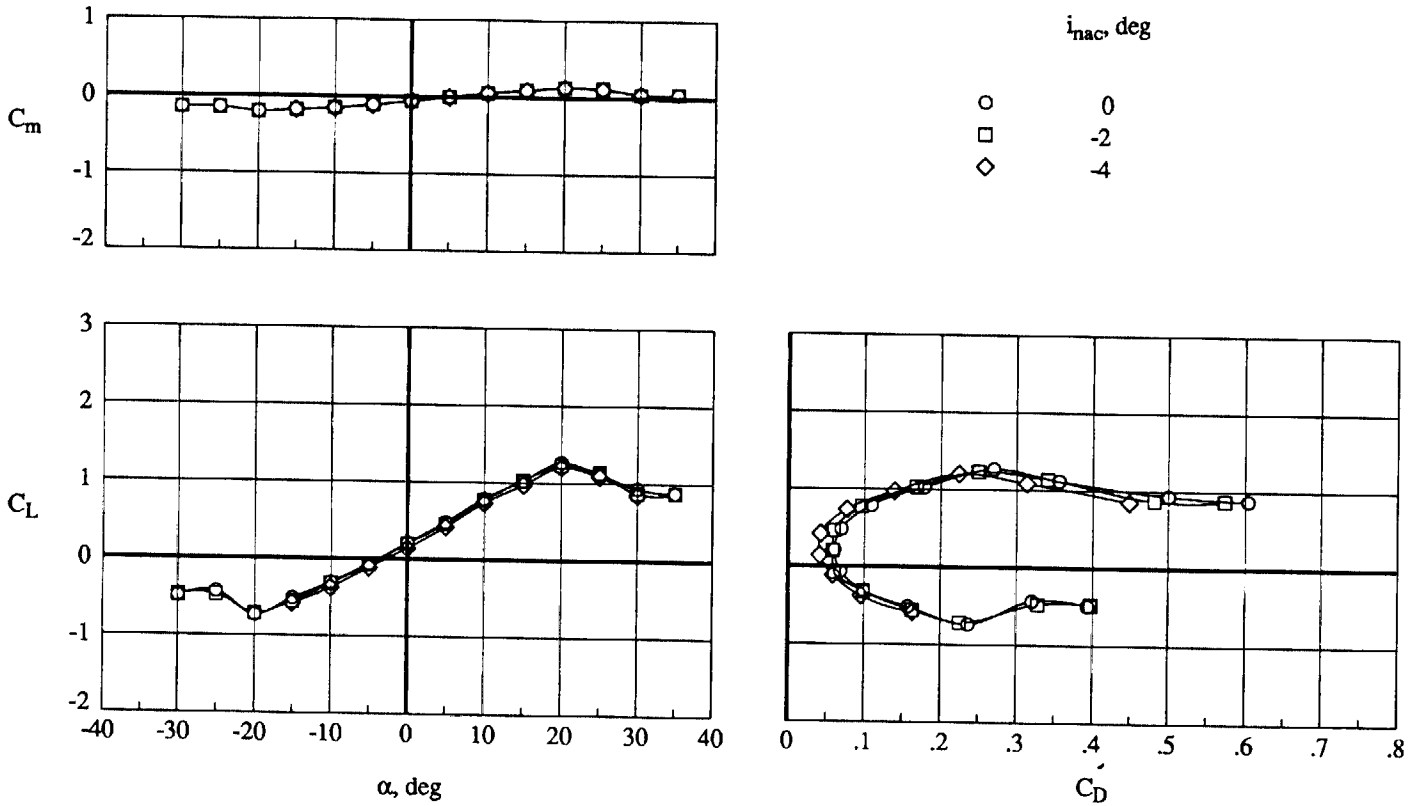

(a) Windmill conditions.

Figure 5. Effect of nacelle inclination on aerodynamic characteristics for $q = 15$ lb/ft^2, $x/c = 0.60$, $z/c = 0.30$, and $\delta_f = 0°$.

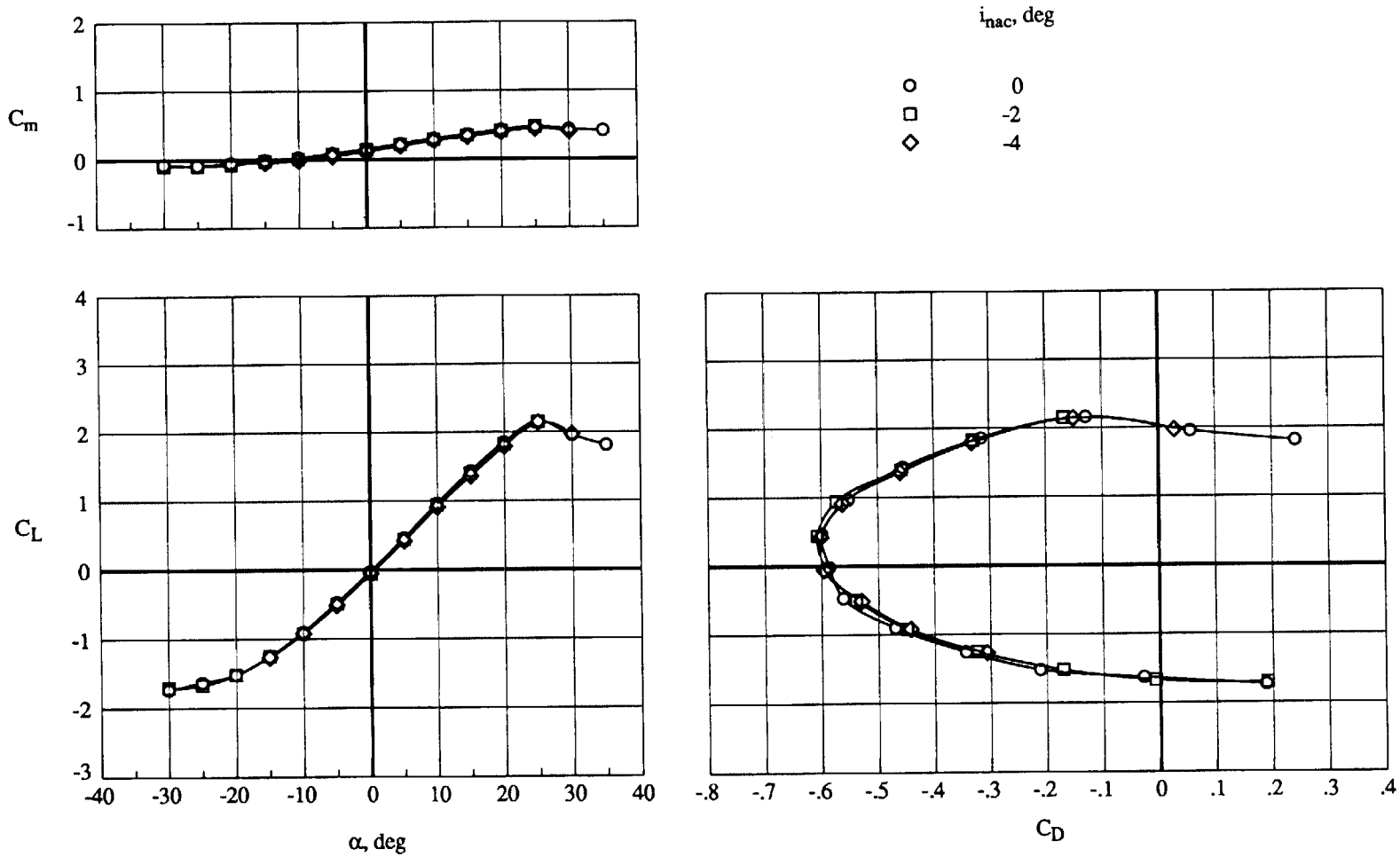

(b) Propeller speed = 11 000 rpm.

Figure 5. Continued.

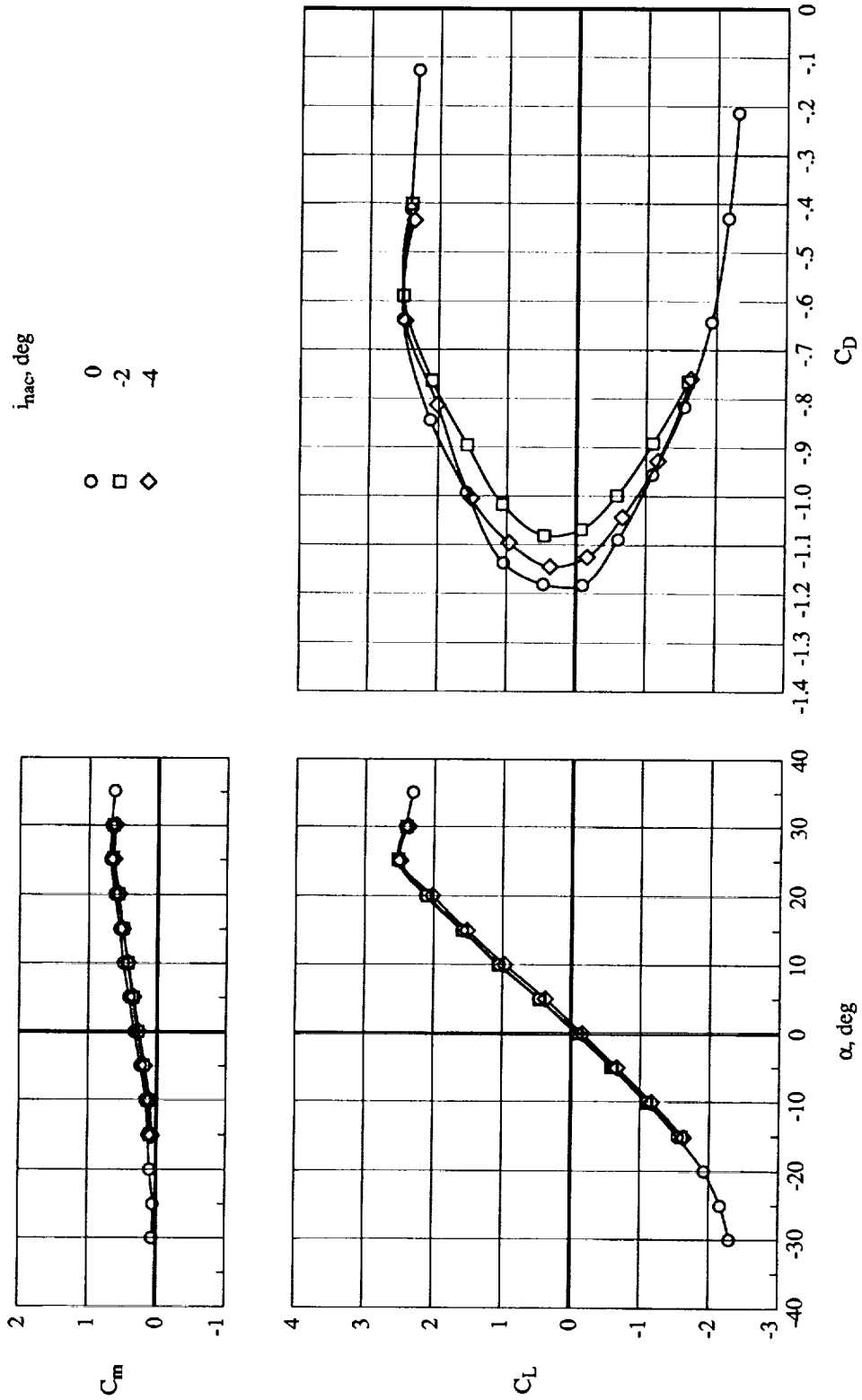

(c) Propeller speed = 14 000 rpm.

Figure 5. Concluded.

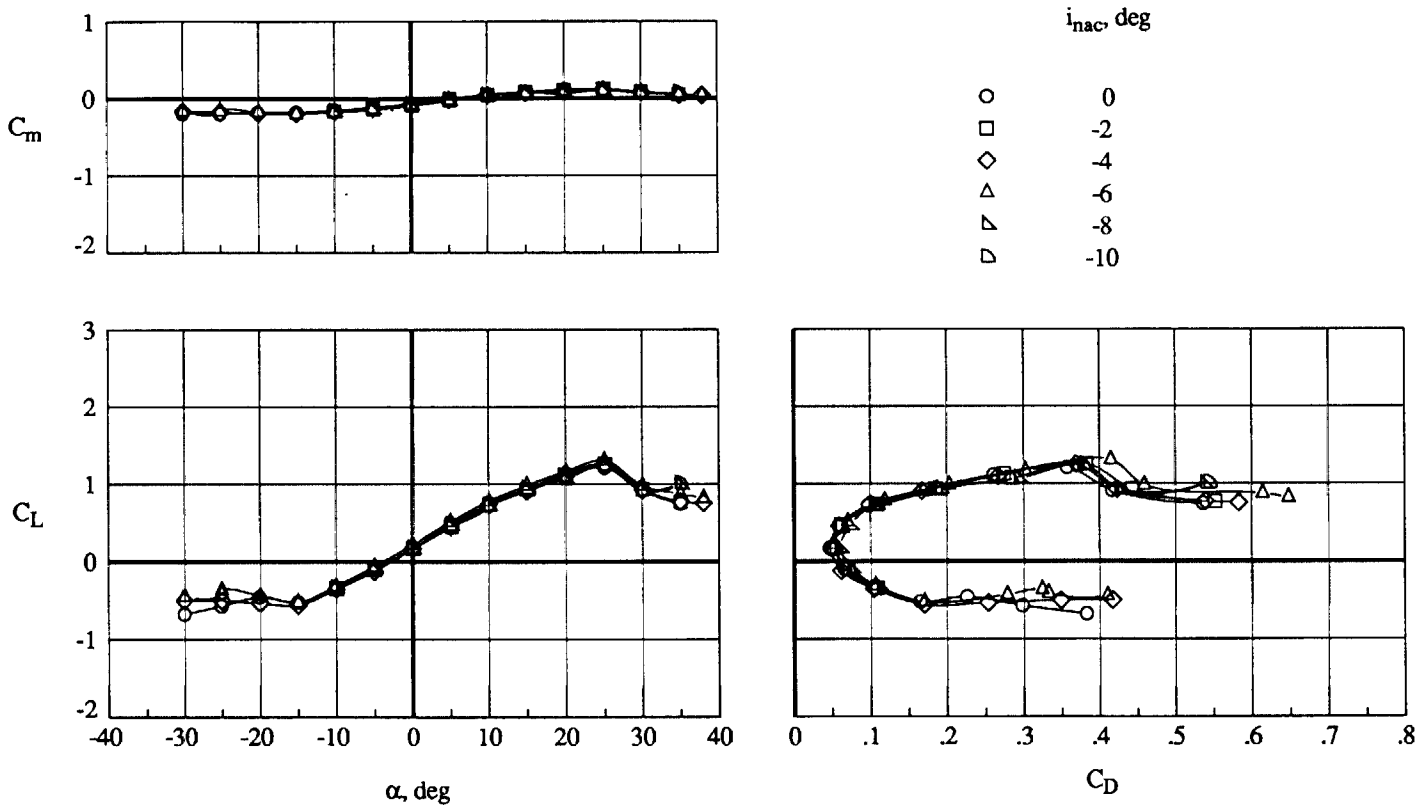

(a) Windmill conditions.

Figure 6. Effect of nacelle inclination on aerodynamic characteristics for $q = 15$ lb/ft^2, $x/c = 0.75$, $z/c = 0.30$, and $\delta_f = 0°$.

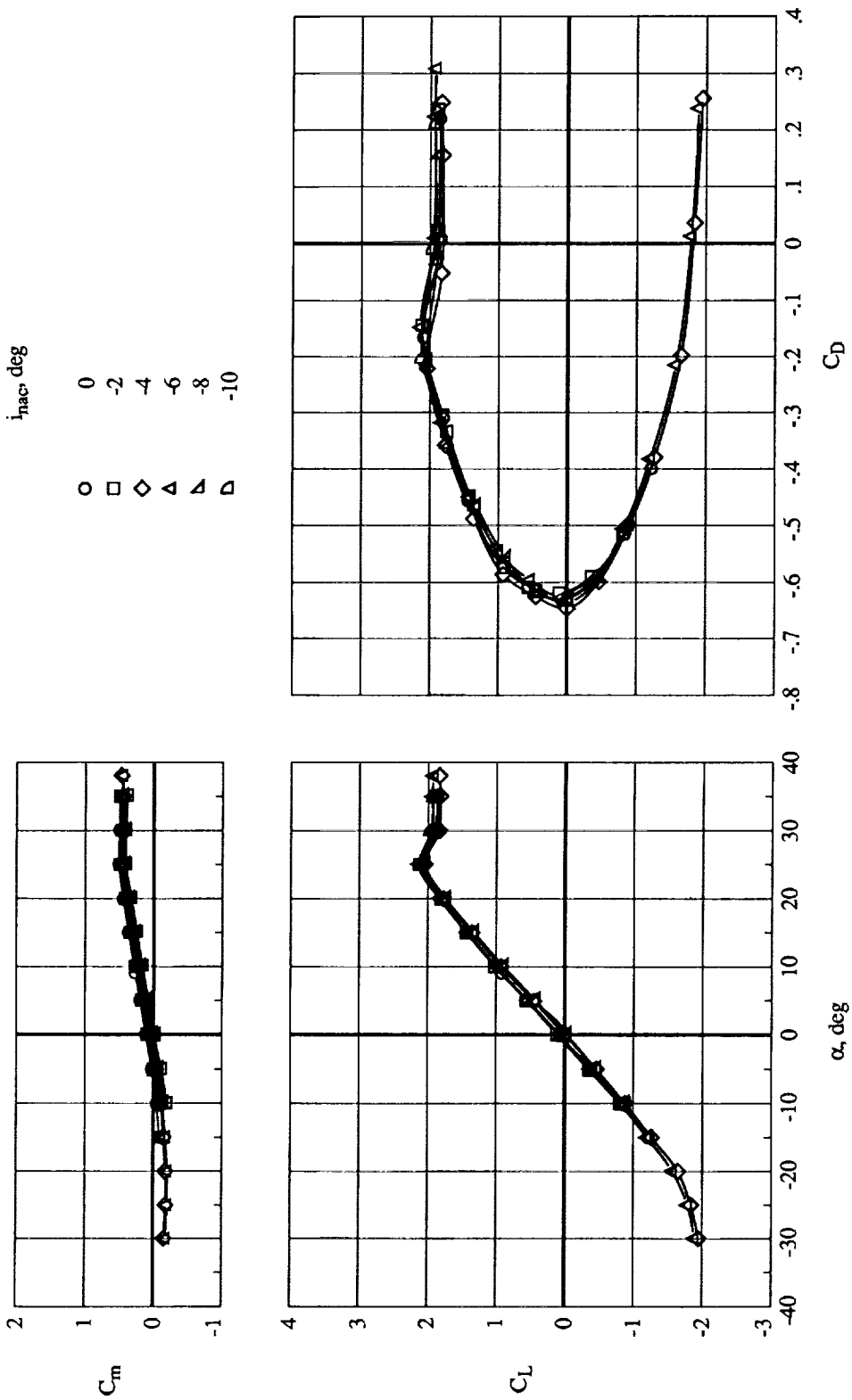

(b) Propeller speed = 11 000 rpm.

Figure 6. Continued.

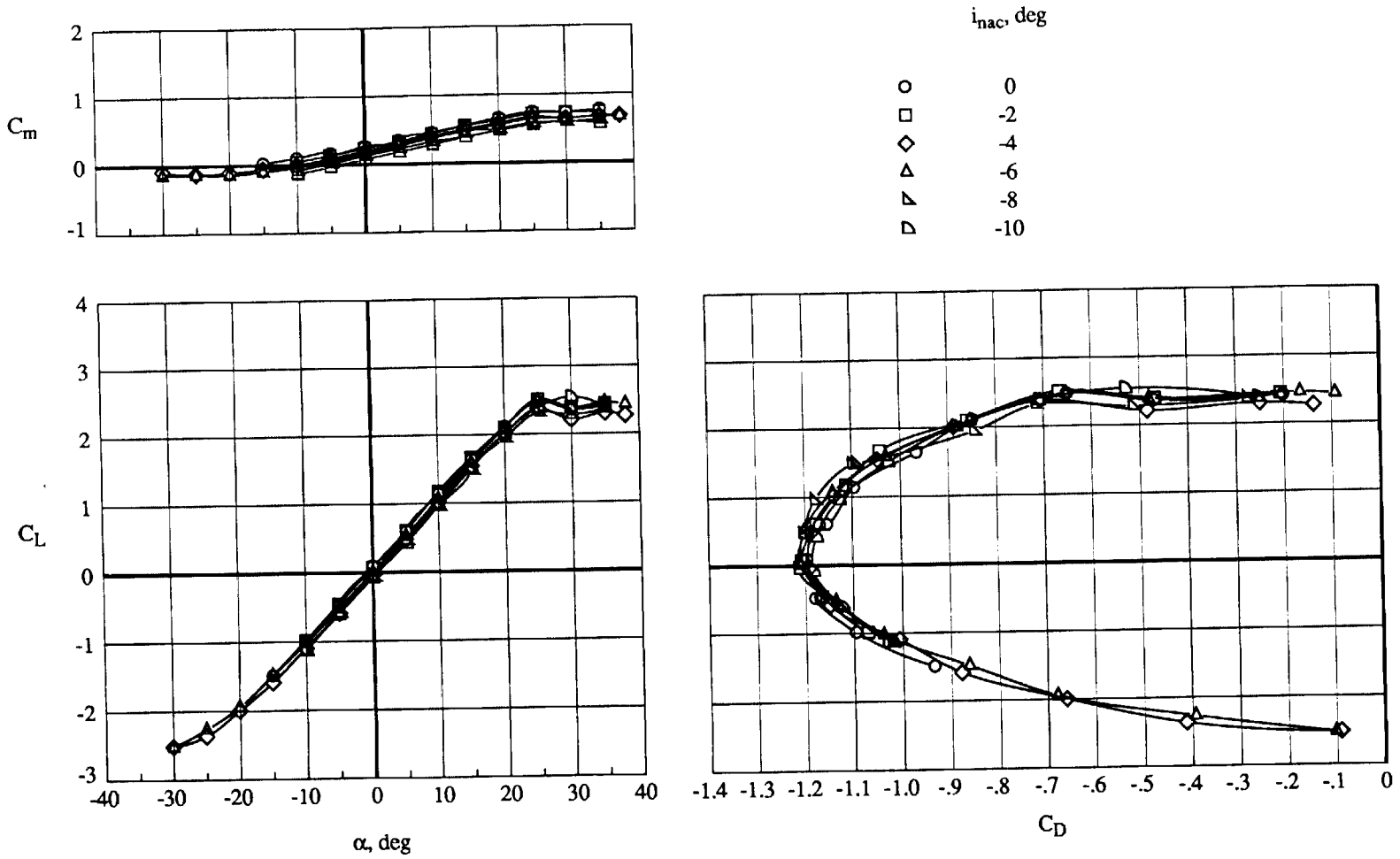

(c) Propeller speed = 14 000 rpm.

Figure 6. Concluded.

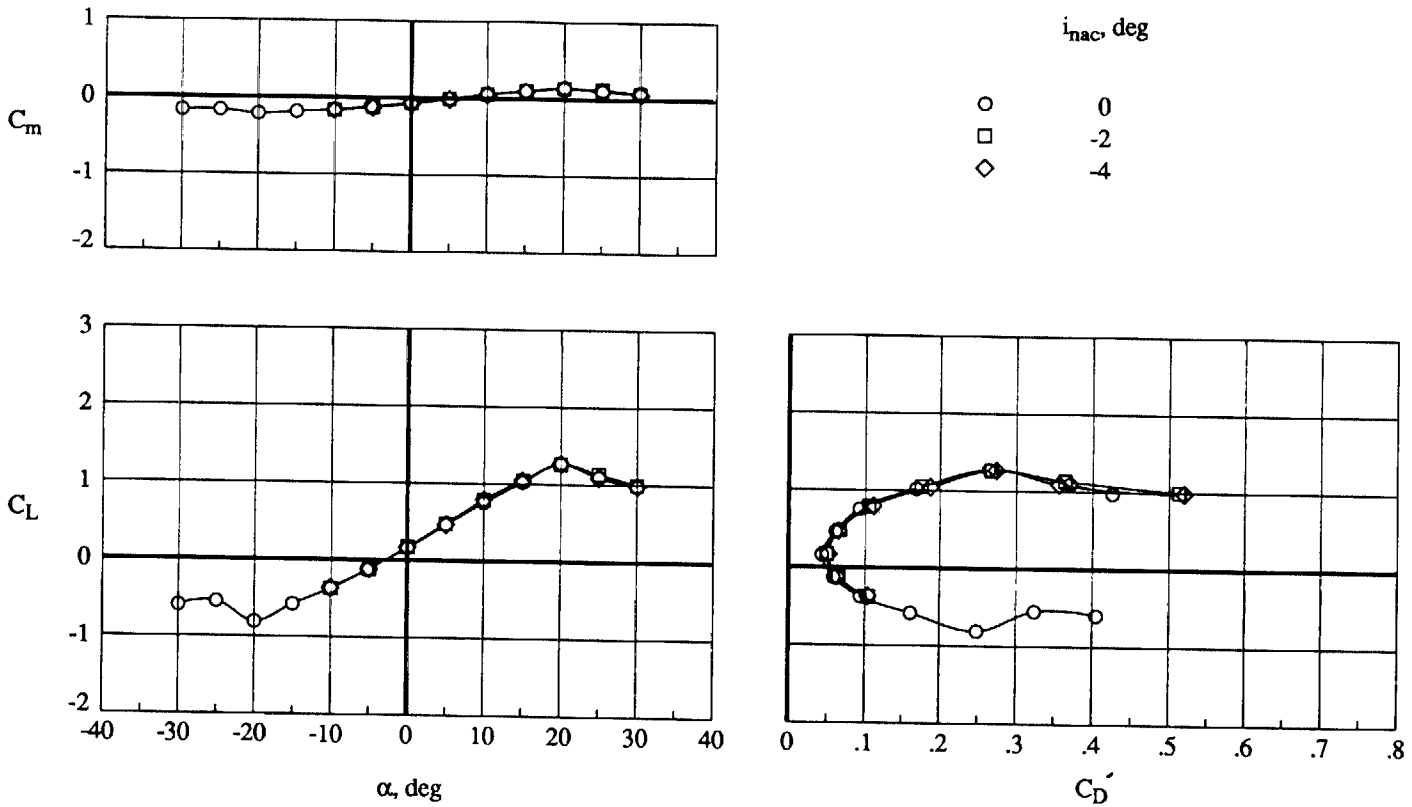

(a) Windmill conditions.

Figure 7. Effect of nacelle inclination on aerodynamic characteristics for $q = 15$ lb/ft^2, $x/c = 0.75$, $z/c = 0.25$, and $\delta_f = 0°$.

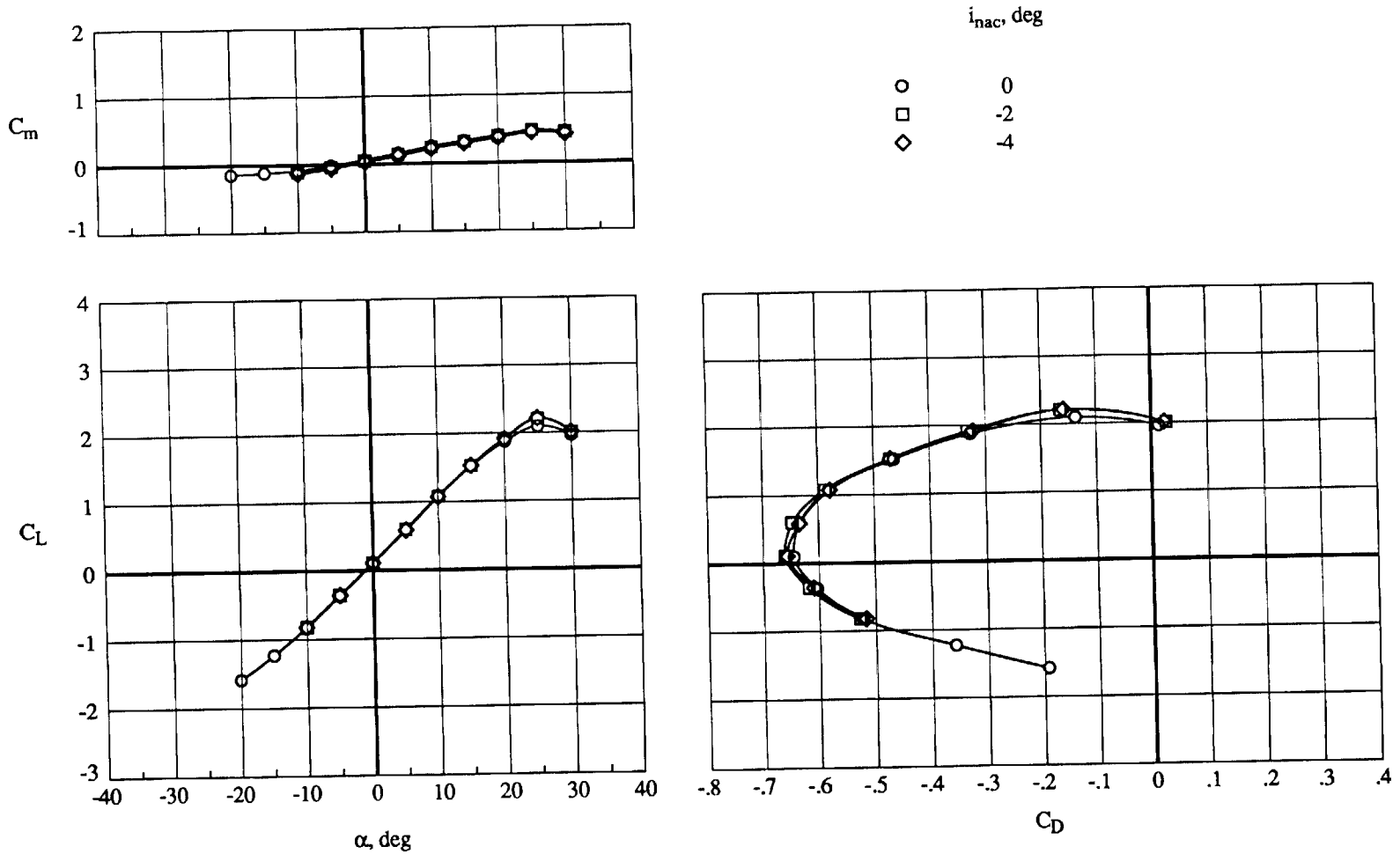

(b) Propeller speed = 11 000 rpm.

Figure 7. Continued.

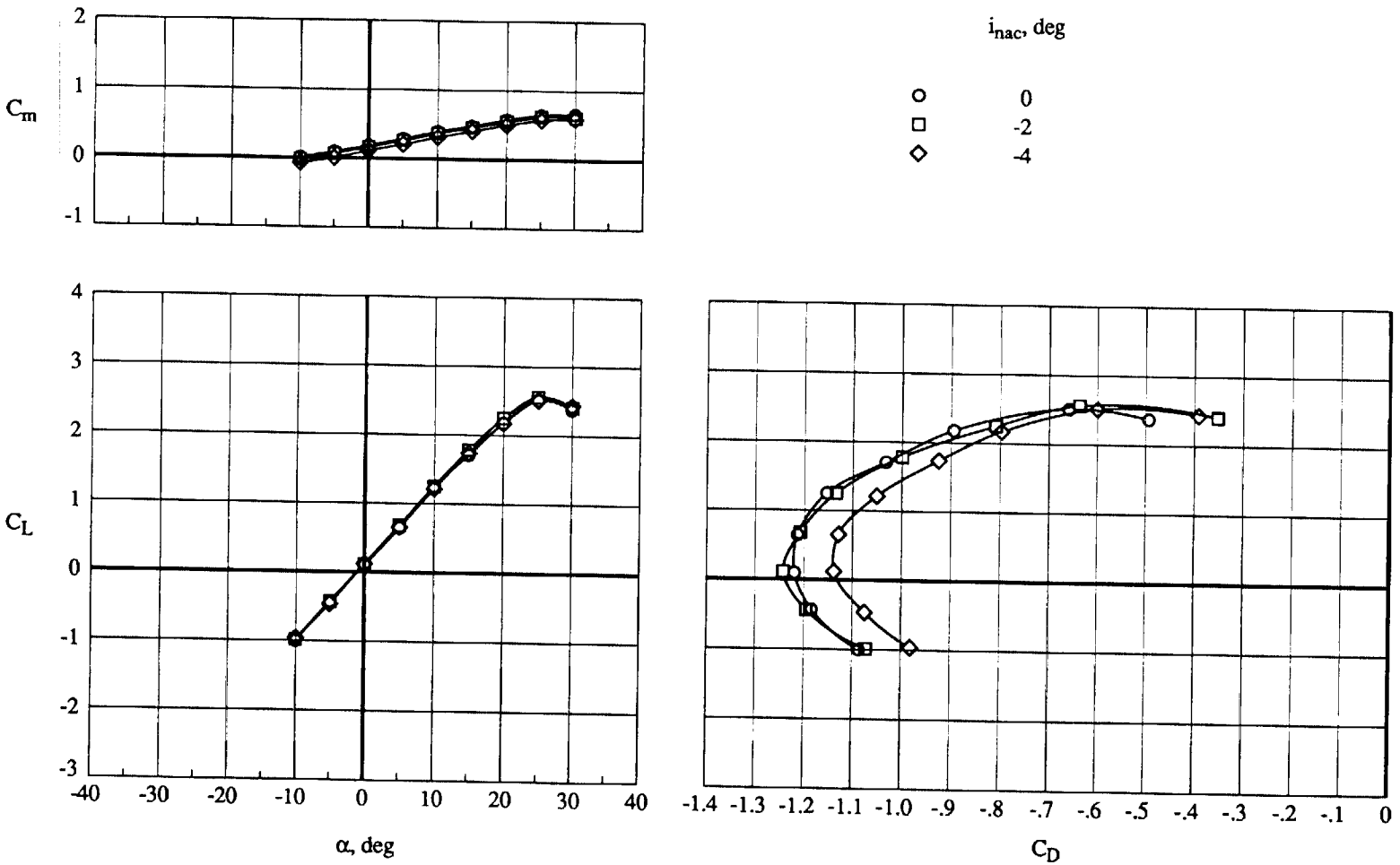

(c) Propeller speed = 14 000 rpm.

Figure 7. Concluded.

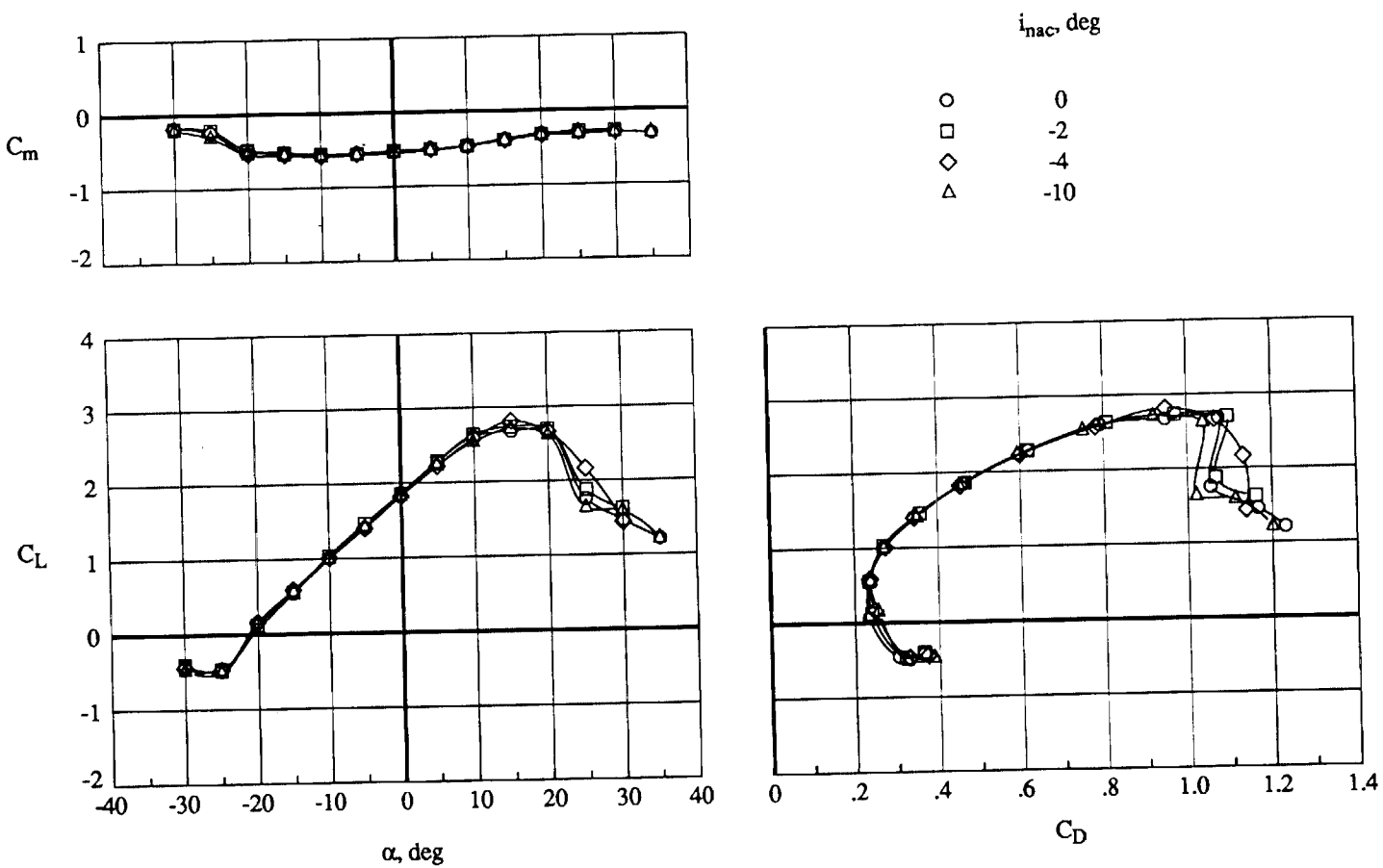

(a) Windmill conditions.

Figure 8. Effect of nacelle inclination on aerodynamic characteristics for $q = 15$ lb/ft^2, $x/c = 0.60$, $z/c = 0.25$, and $\delta_f = 60°$.

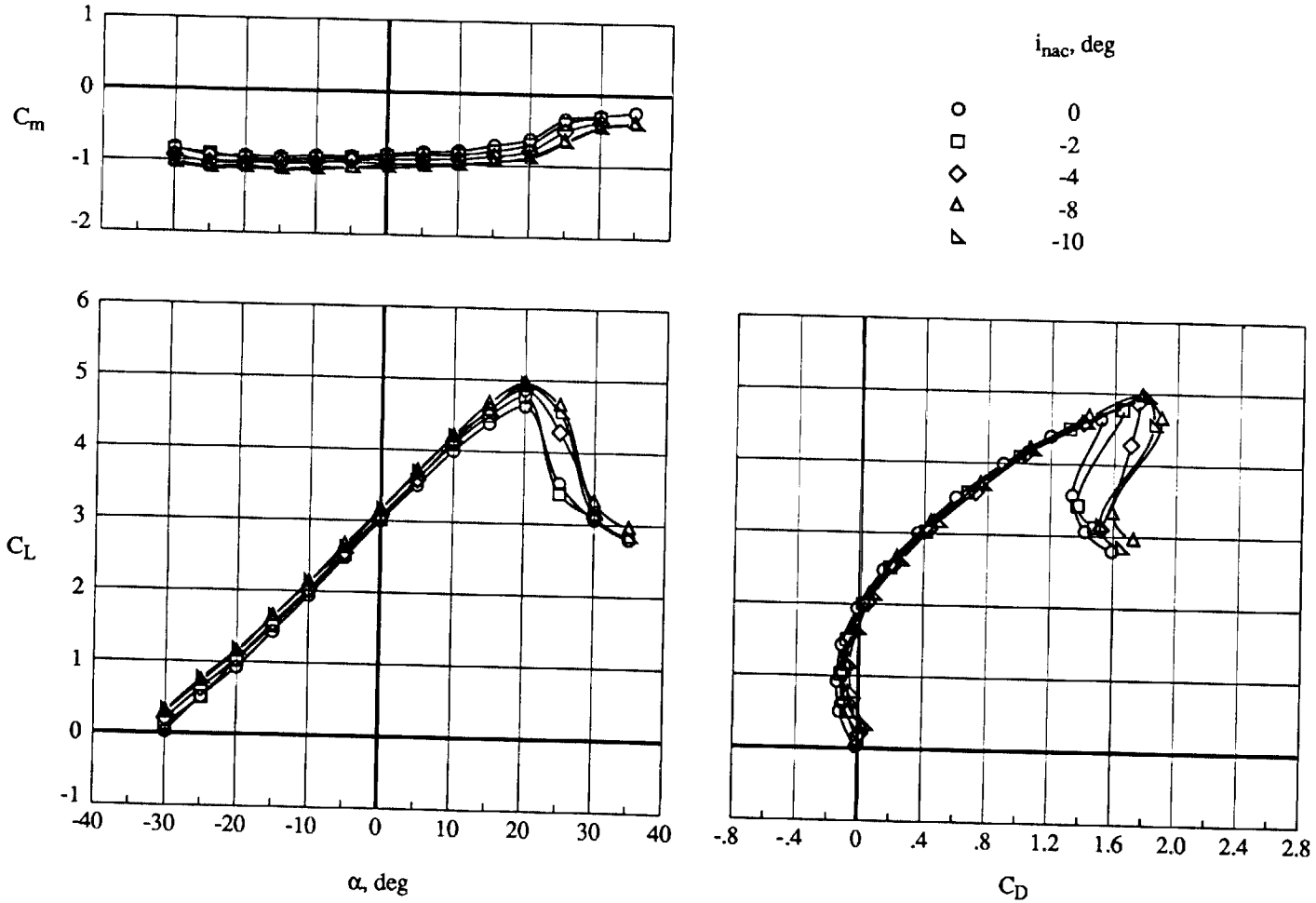

(b) Propeller speed = 11 000 rpm.

Figure 8. Continued.

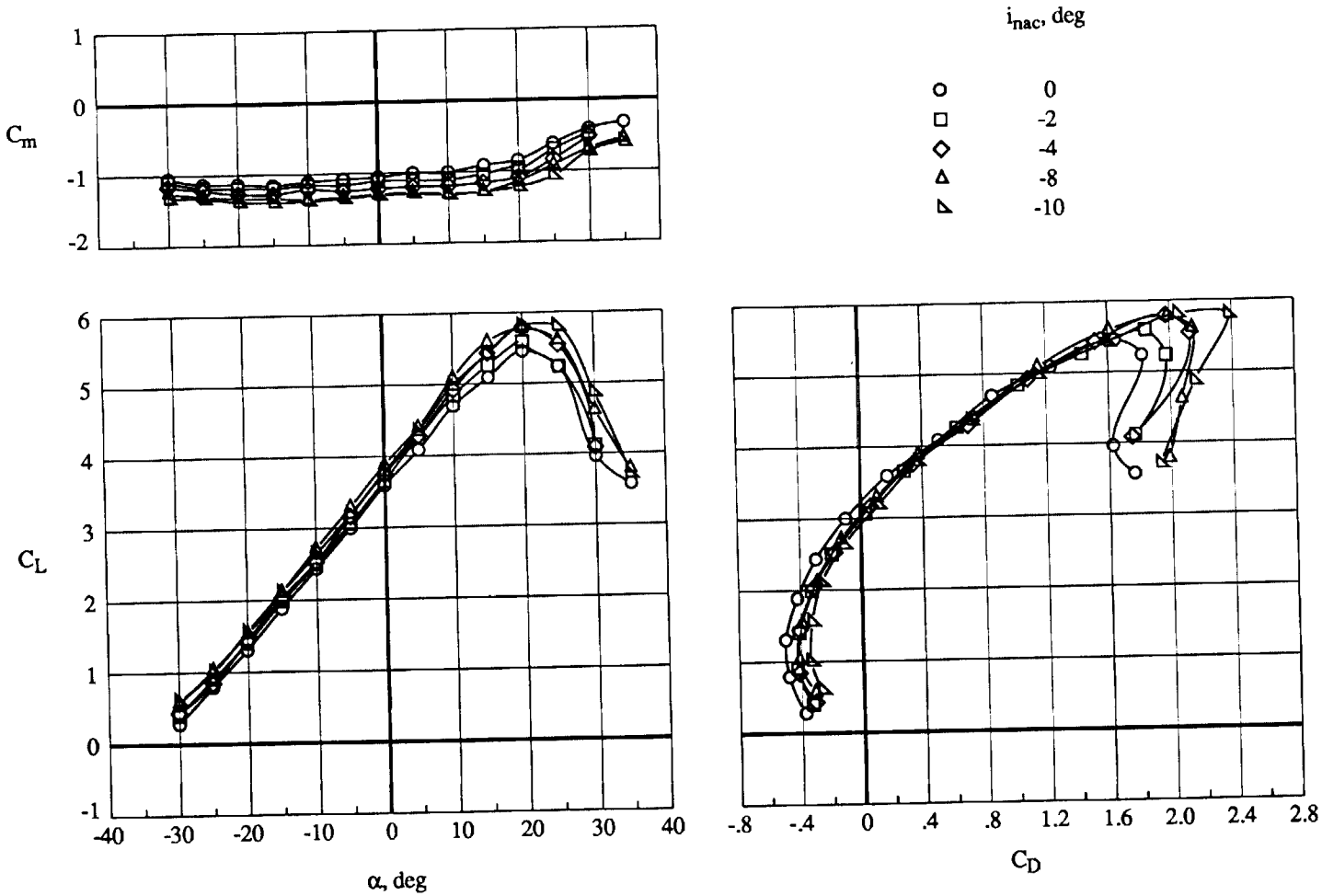

(c) Propeller speed = 14 000 rpm.

Figure 8. Concluded.

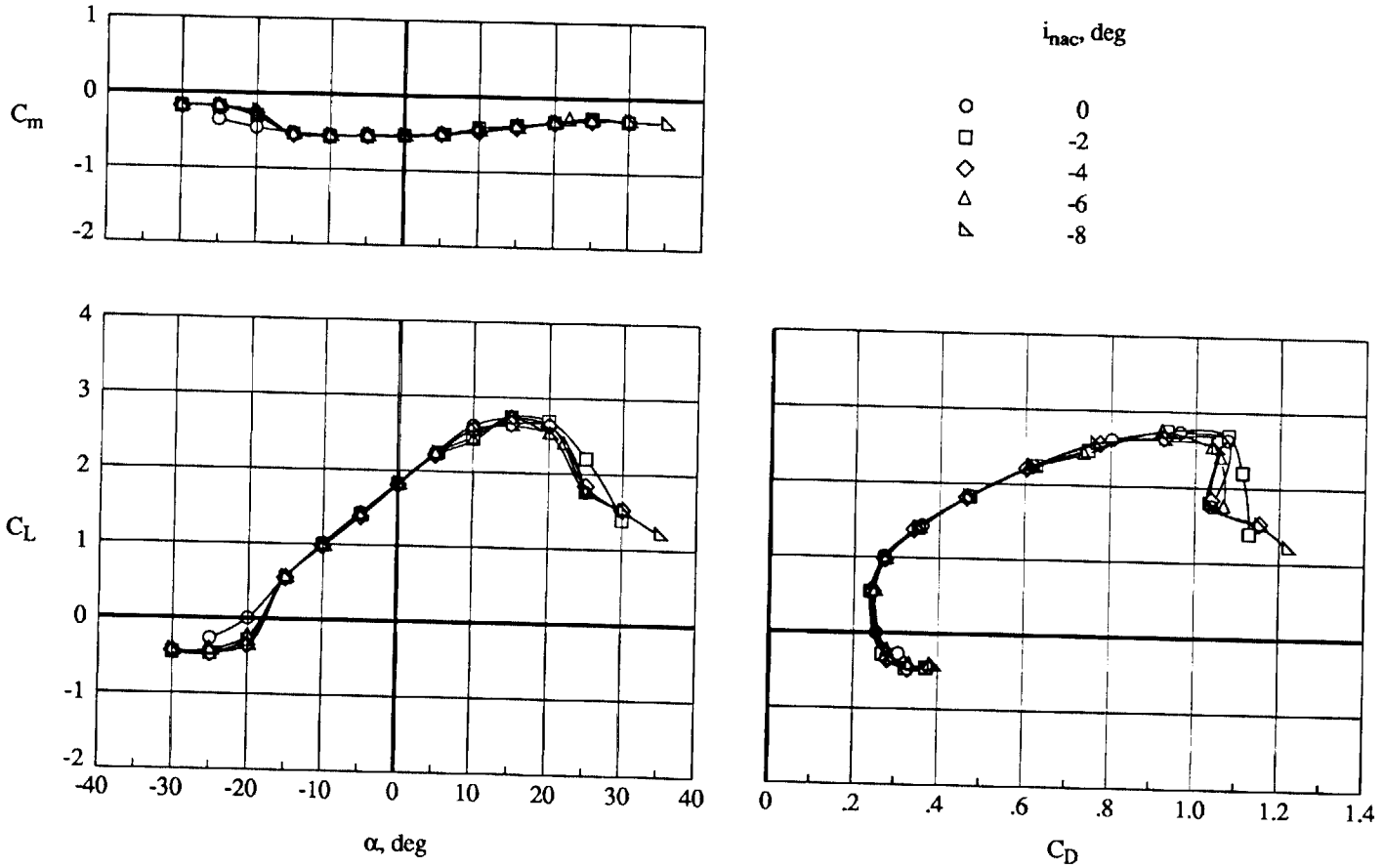

(a) Windmill conditions.

Figure 9. Effect of nacelle inclination on aerodynamic characteristics for $q = 15$ lb/ft^2, $x/c = 0.60$, $z/c = 0.30$, and $\delta_f = 60°$.

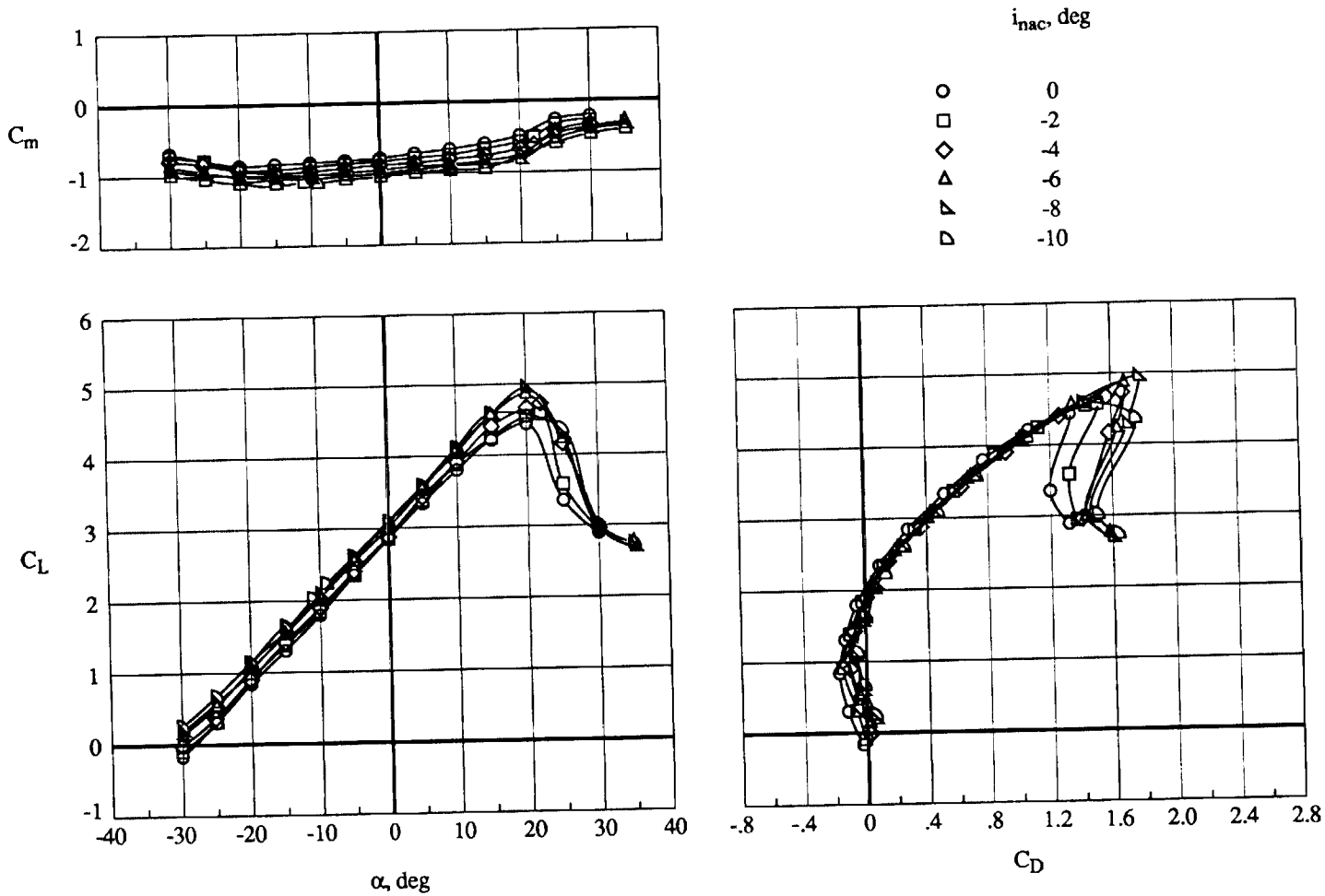

(b) Propeller speed = 11 000 rpm.

Figure 9. Continued.

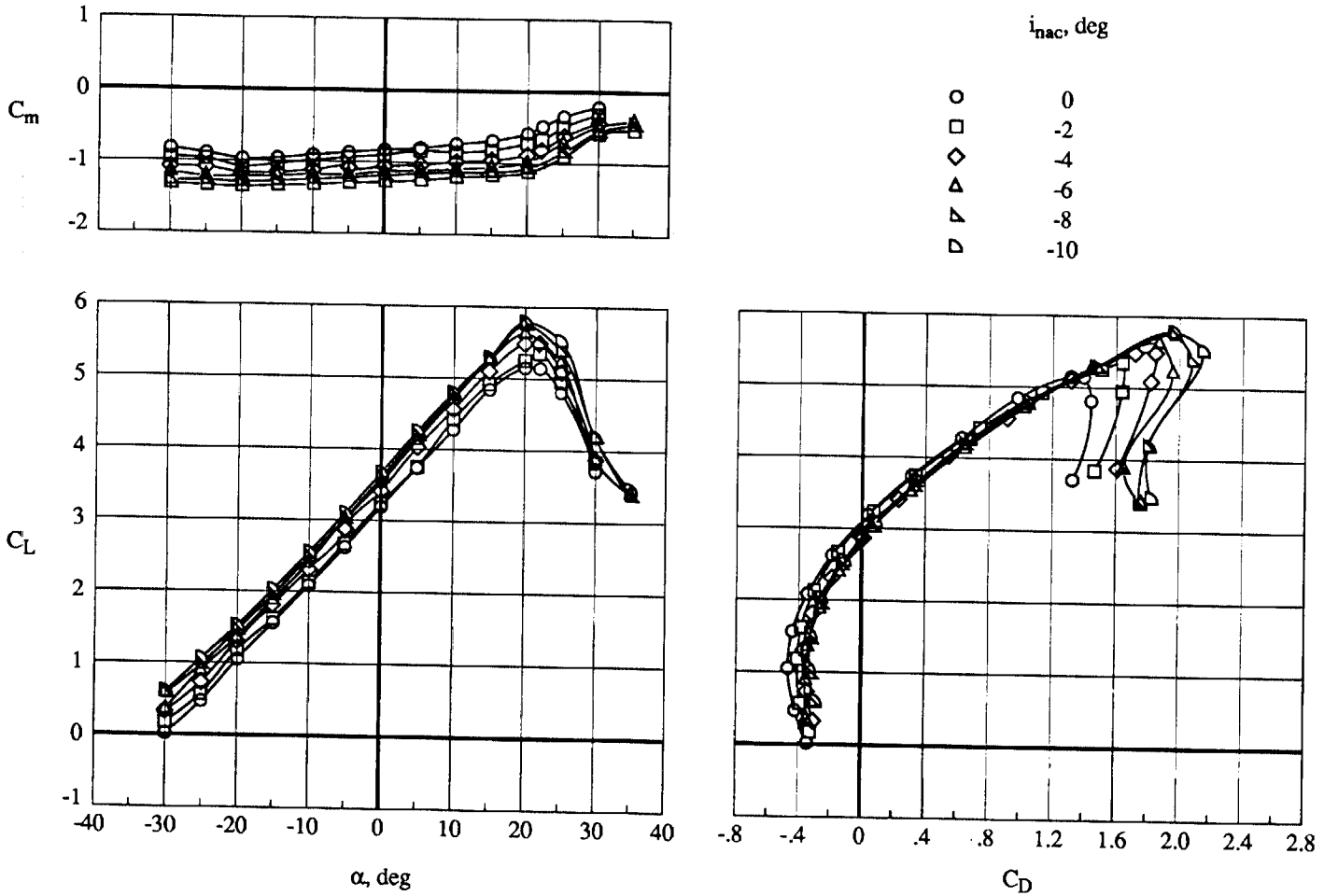

(c) Propeller speed = 14 000 rpm.

Figure 9. Concluded.

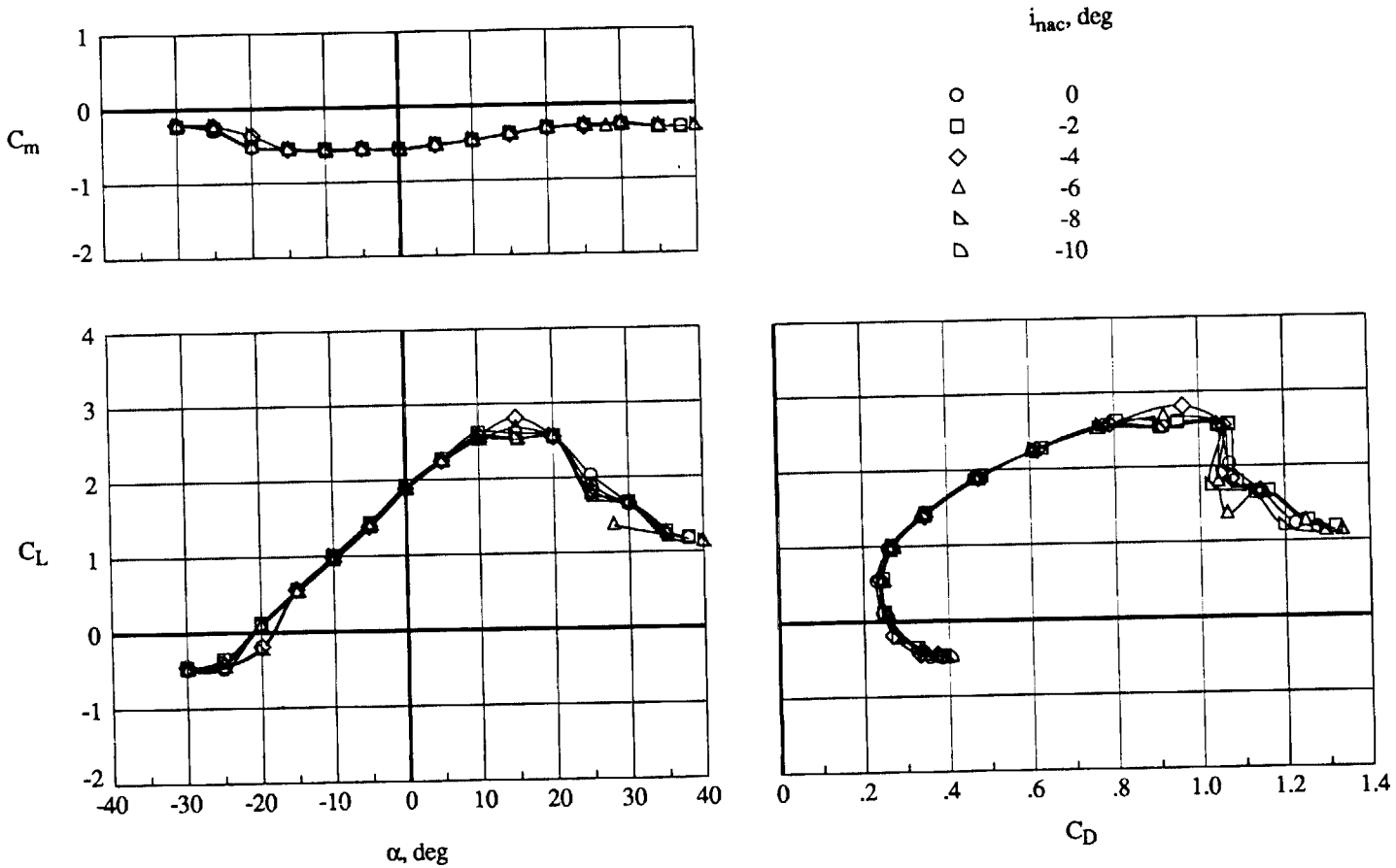

(a) Windmill conditions.

Figure 10. Effect of nacelle inclination on aerodynamic characteristics for $q = 15$ lb/ft^2, $x/c = 0.75$, $z/c = 0.25$, and $\delta_f = 60°$.

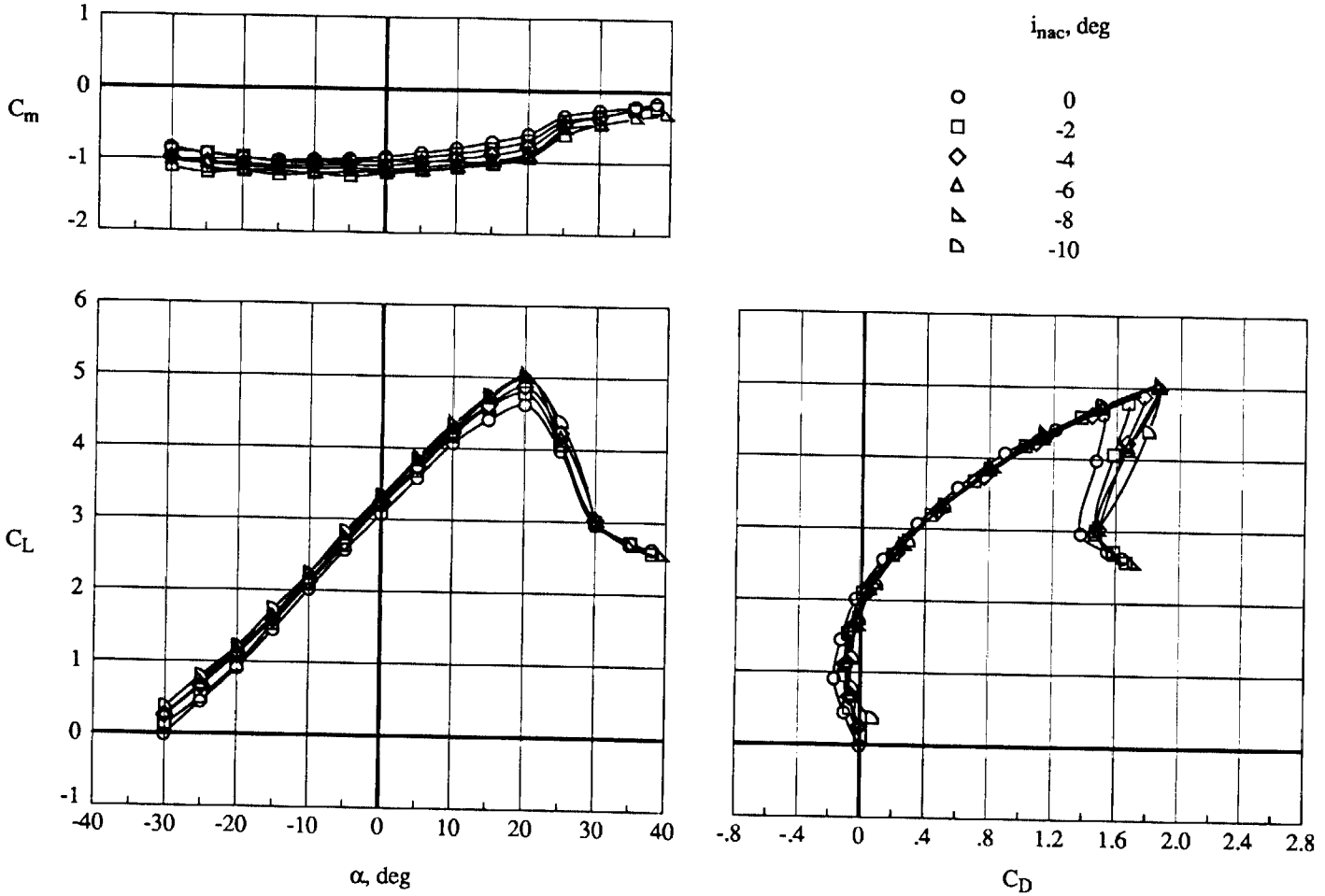

(b) Propeller speed = 11 000 rpm.

Figure 10. Continued.

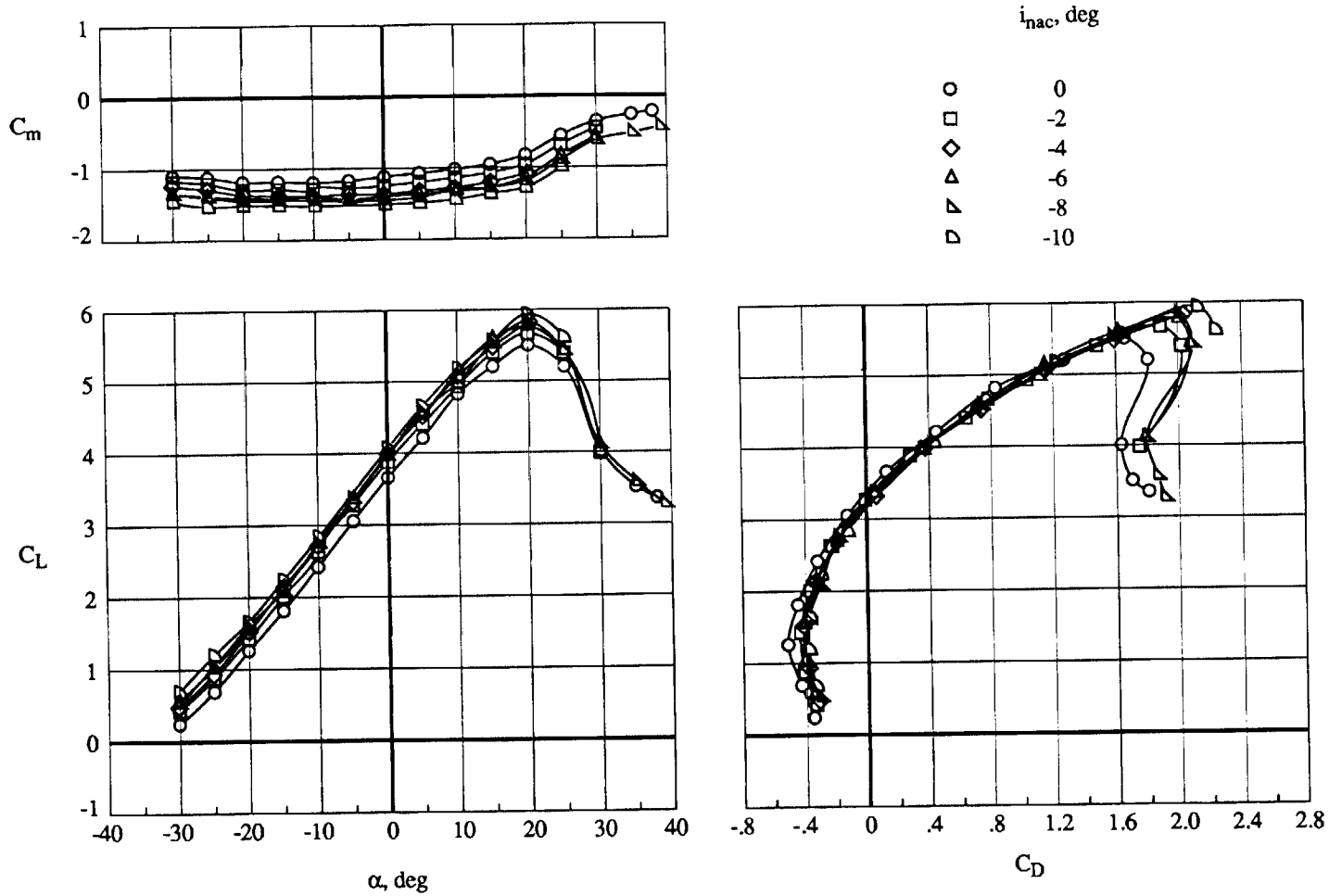

(c) Propeller speed = 14 000 rpm.

Figure 10. Concluded.

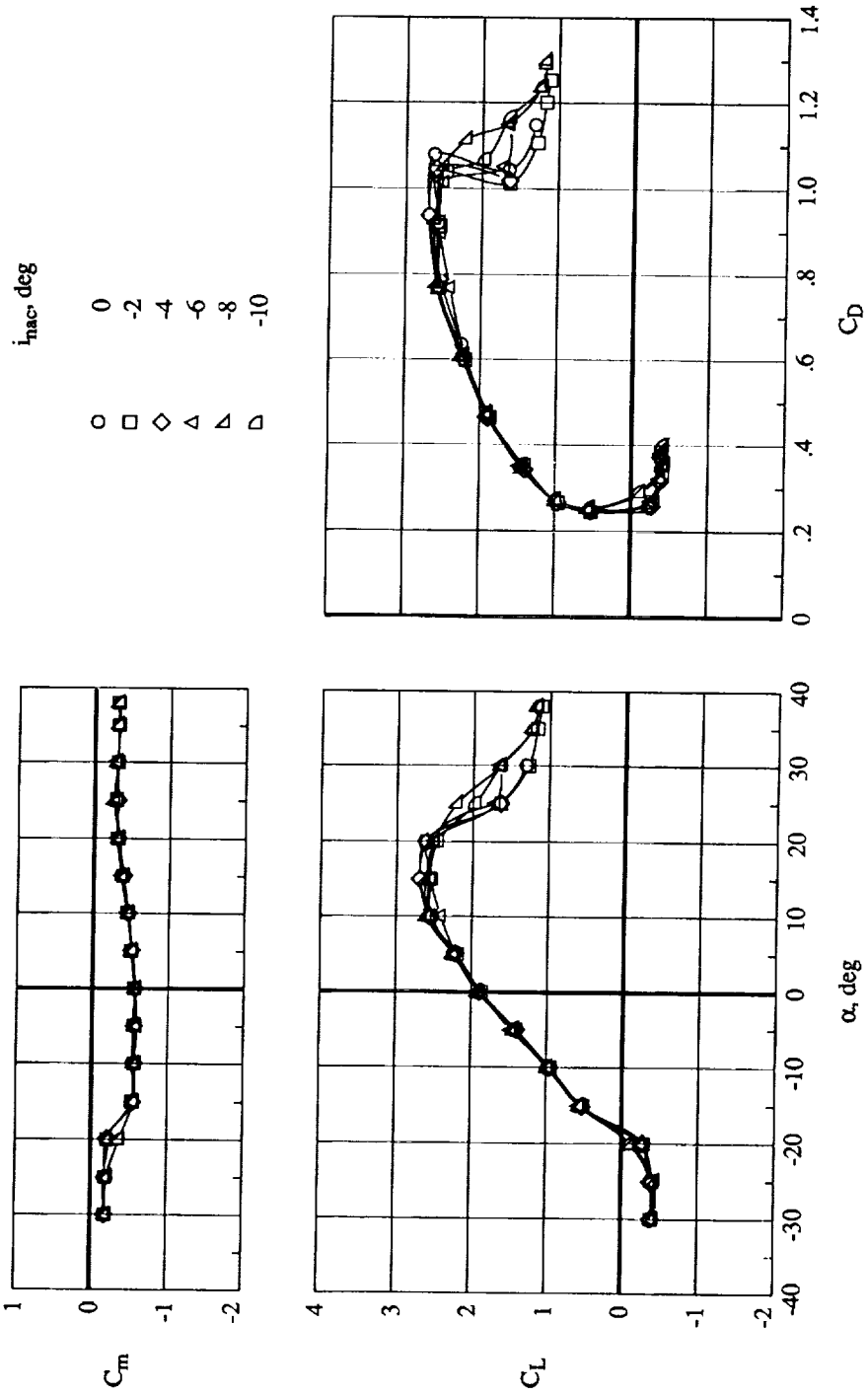

(a) Windmill conditions.

Figure 11. Effect of nacelle inclination on aerodynamic characteristics for $q = 15$ lb/ft^2, $x/c = 0.75$, $z/c = 0.30$, and $\delta_f = 60°$.

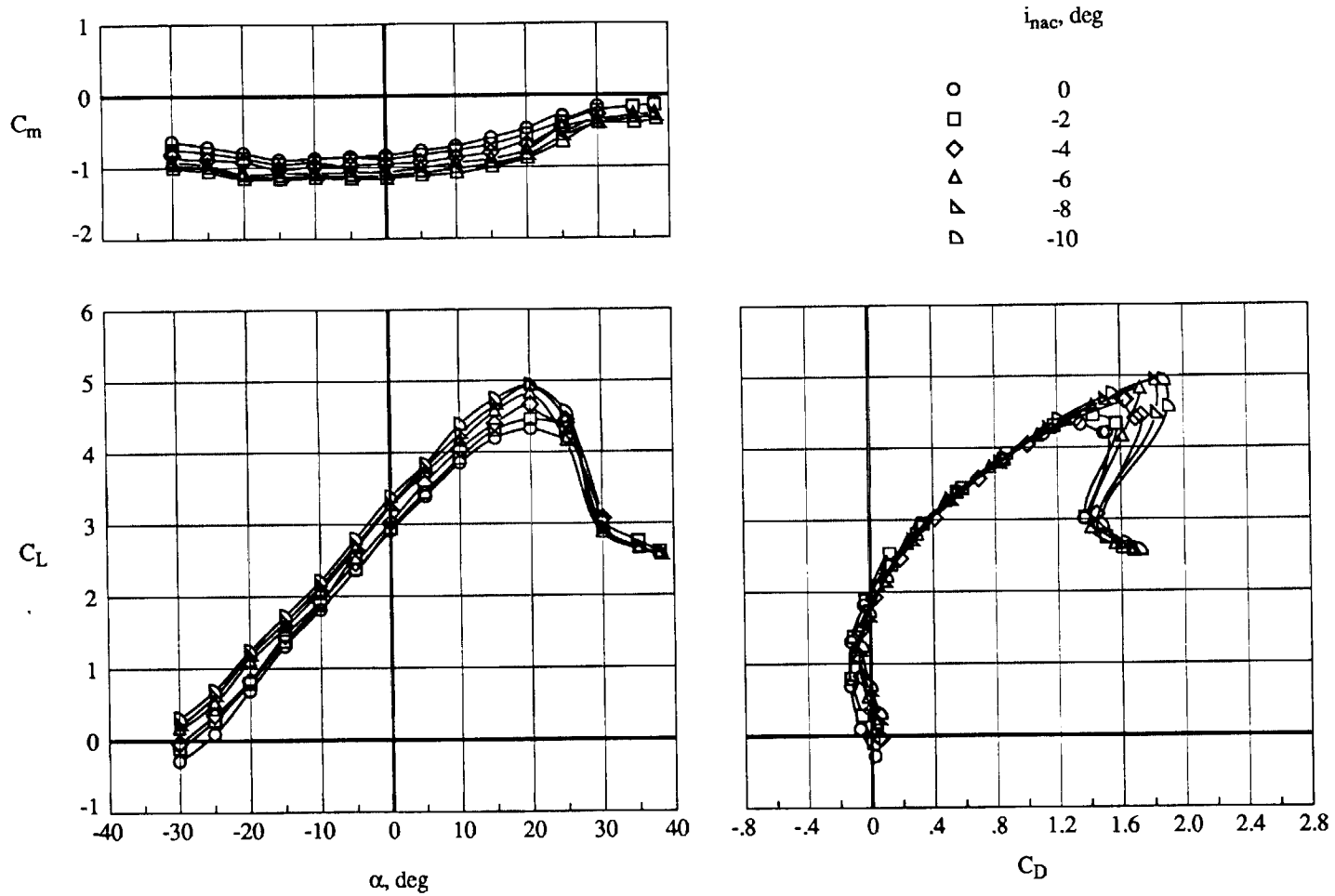

(b) Propeller speed = 11 000 rpm.

Figure 11. Continued.

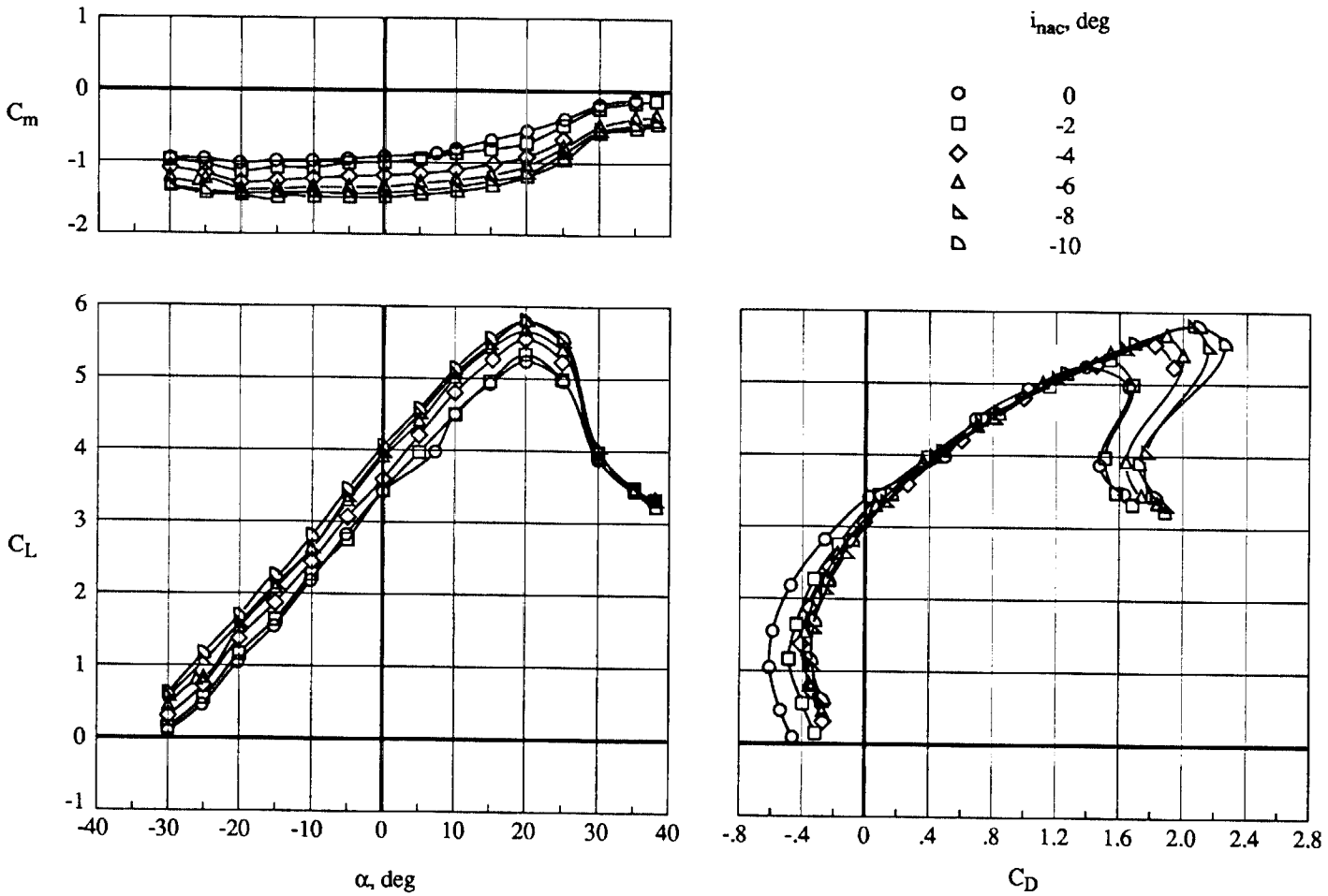

(c) Propeller speed = 14 000 rpm.

Figure 11. Concluded.

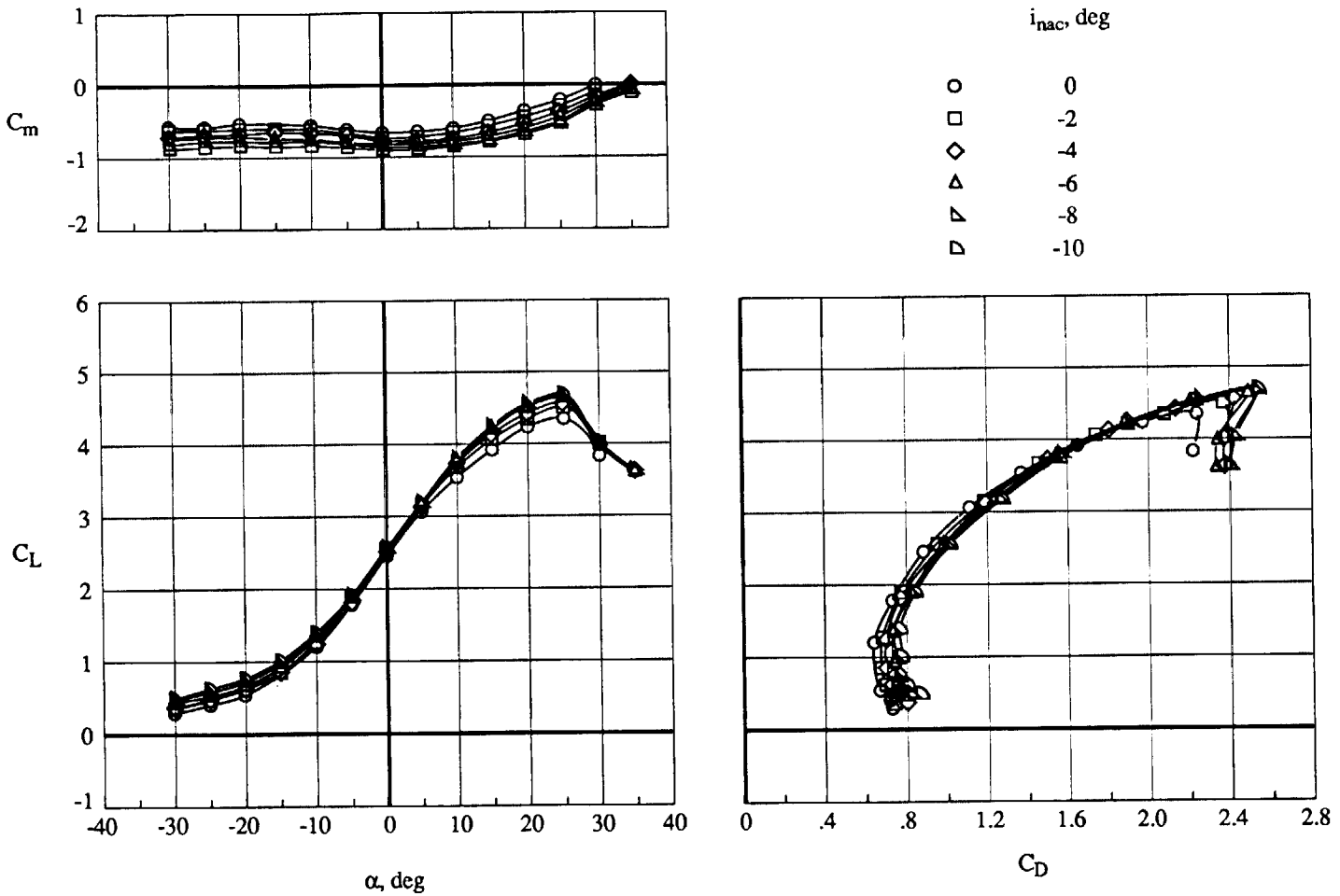

Figure 12. Effect of nacelle inclination on aerodynamic characteristics for $q = 15$ lb/ft^2, $x/c = 0.60$, $z/c = 0.25$, $\delta_f = 60°$, $\delta_K = 60°$, and Propeller speed = 11 000 rpm.

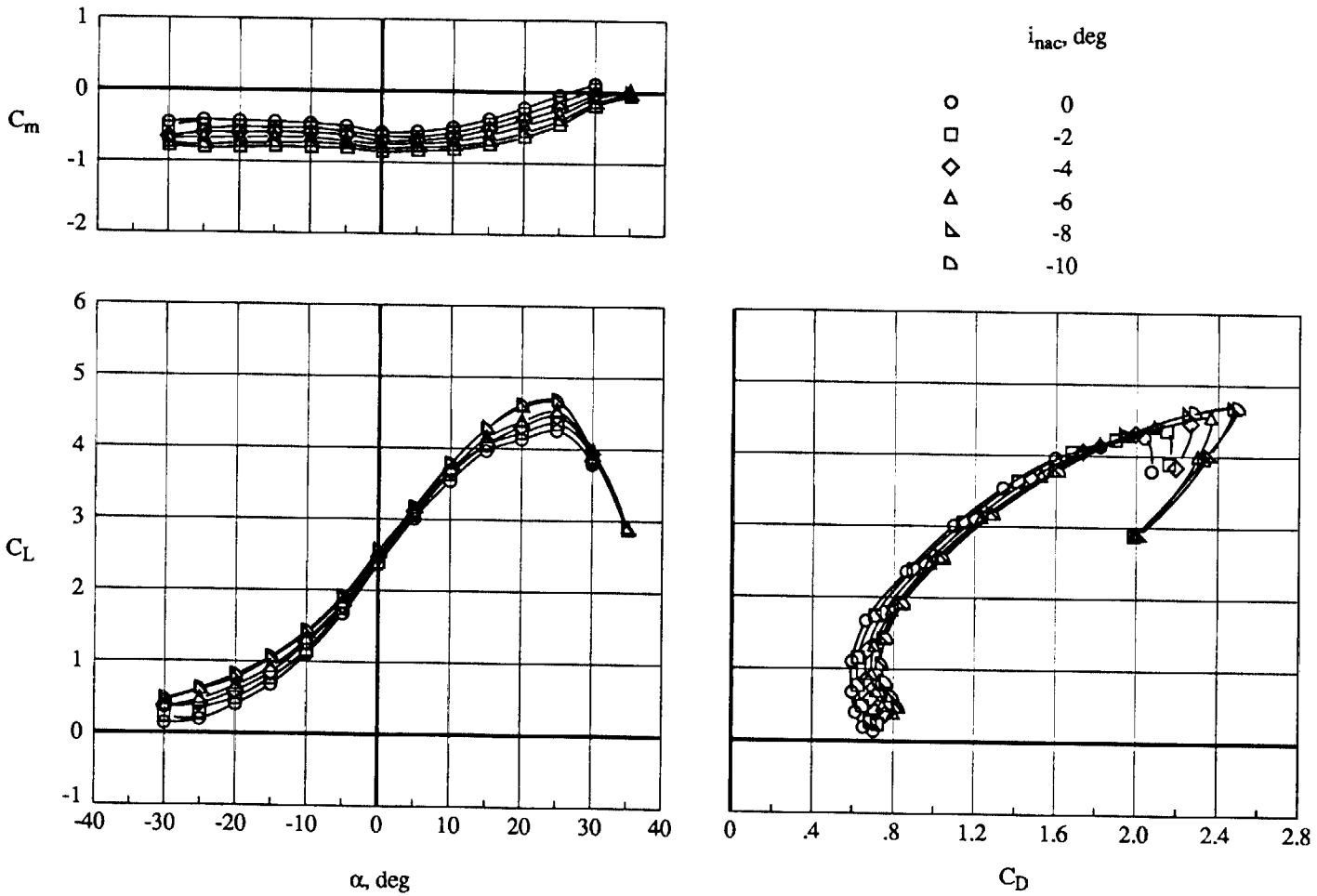

Figure 13. Effect of nacelle inclination on aerodynamic characteristics for $q = 15$ lb/ft^2, $x/c = 0.60$, $z/c = 0.30$, $\delta_f = 60°$, $\delta_K = 60°$, and Propeller speed = 11 000 rpm.

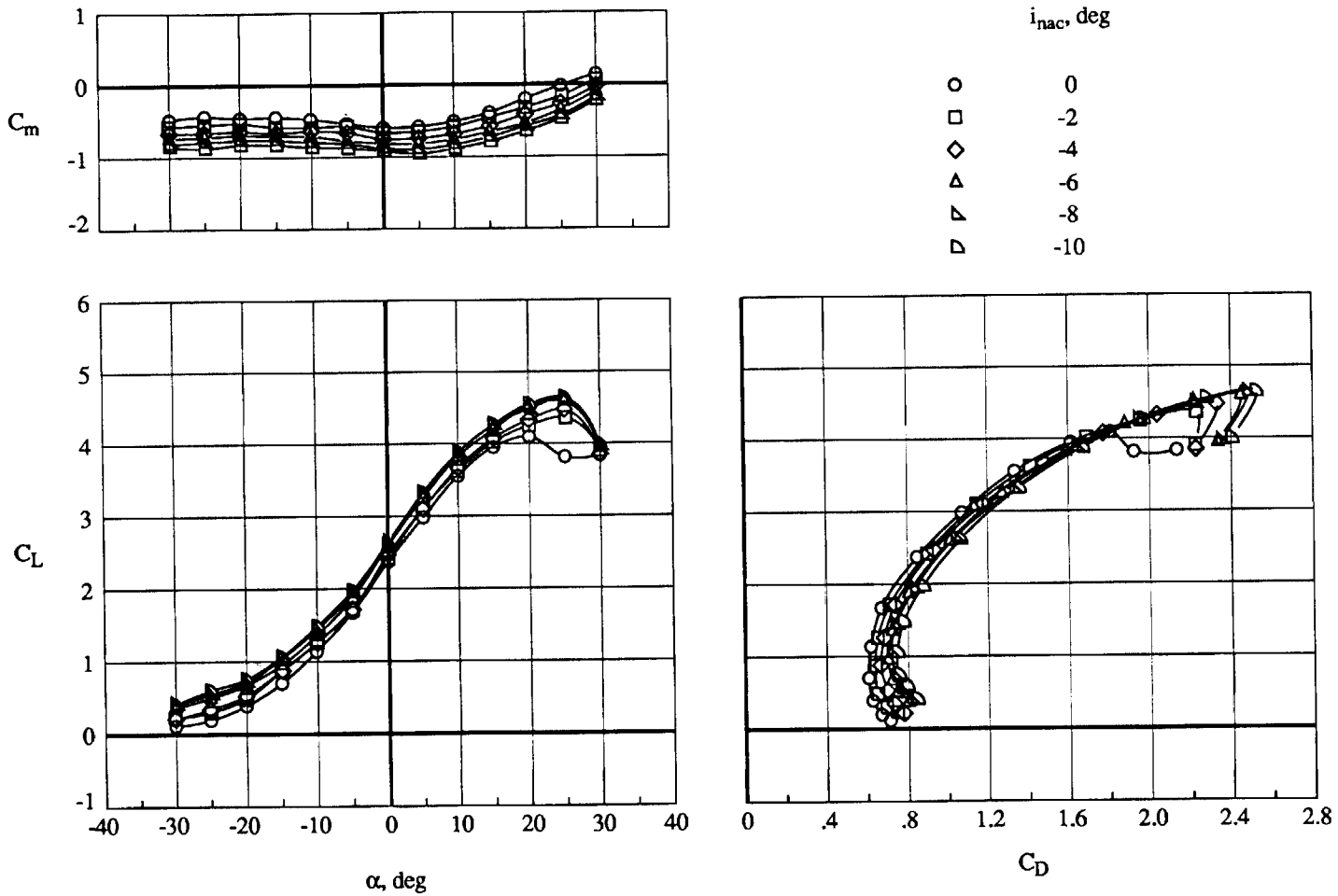

Figure 14. Effect of nacelle inclination on aerodynamic characteristics for $q = 15$ lb/ft^2, $x/c = 0.75$, $z/c = 0.30$, $\delta_f = 60°$, $\delta_K = 60°$, and Propeller speed = 11 000 rpm.

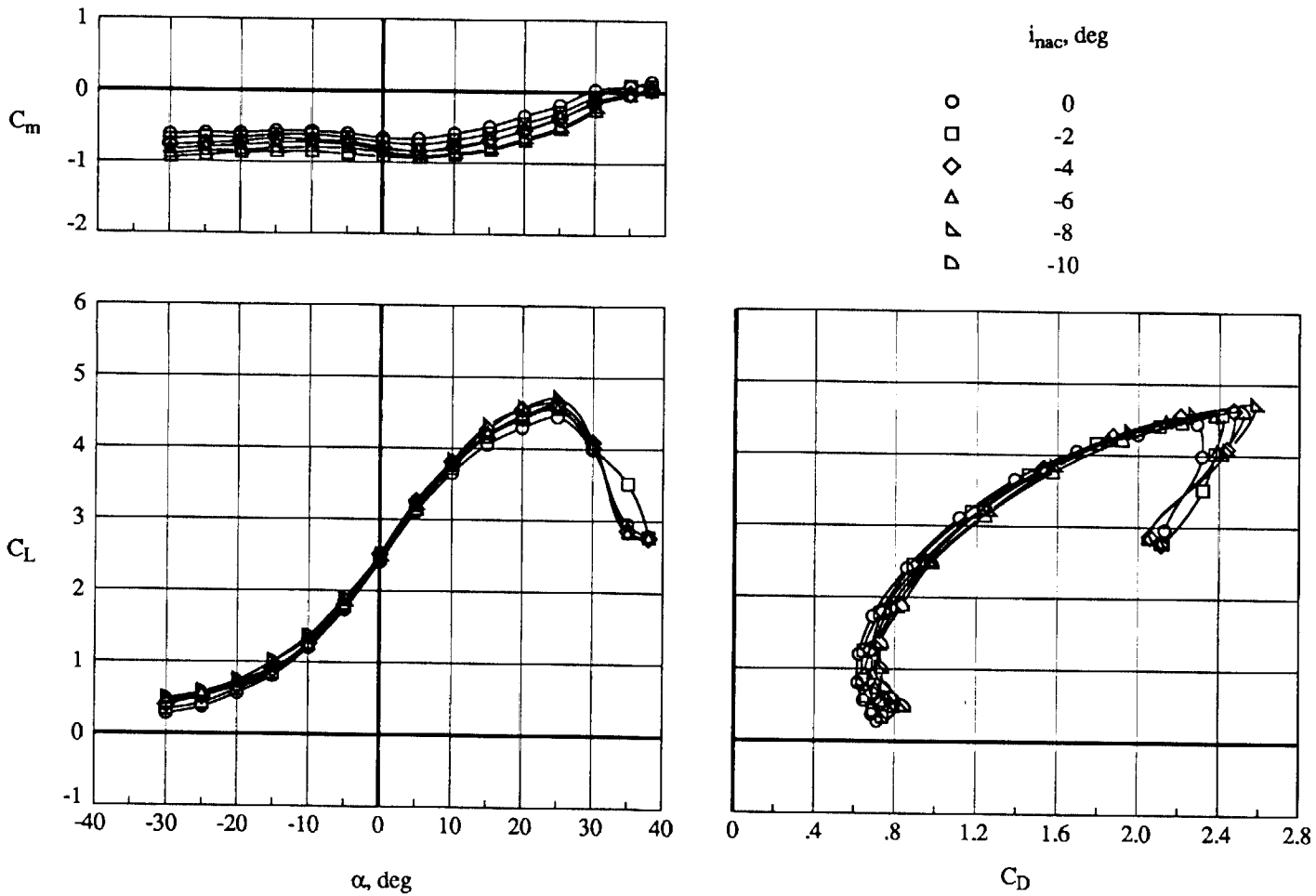

Figure 15. Effect of nacelle inclination on aerodynamic characteristics for $q = 15$ lb/ft^2, $x/c = 0.75$, $z/c = 0.25$, $\delta_f = 60°$, $\delta_K = 60°$, and Propeller speed = 11 000 rpm.

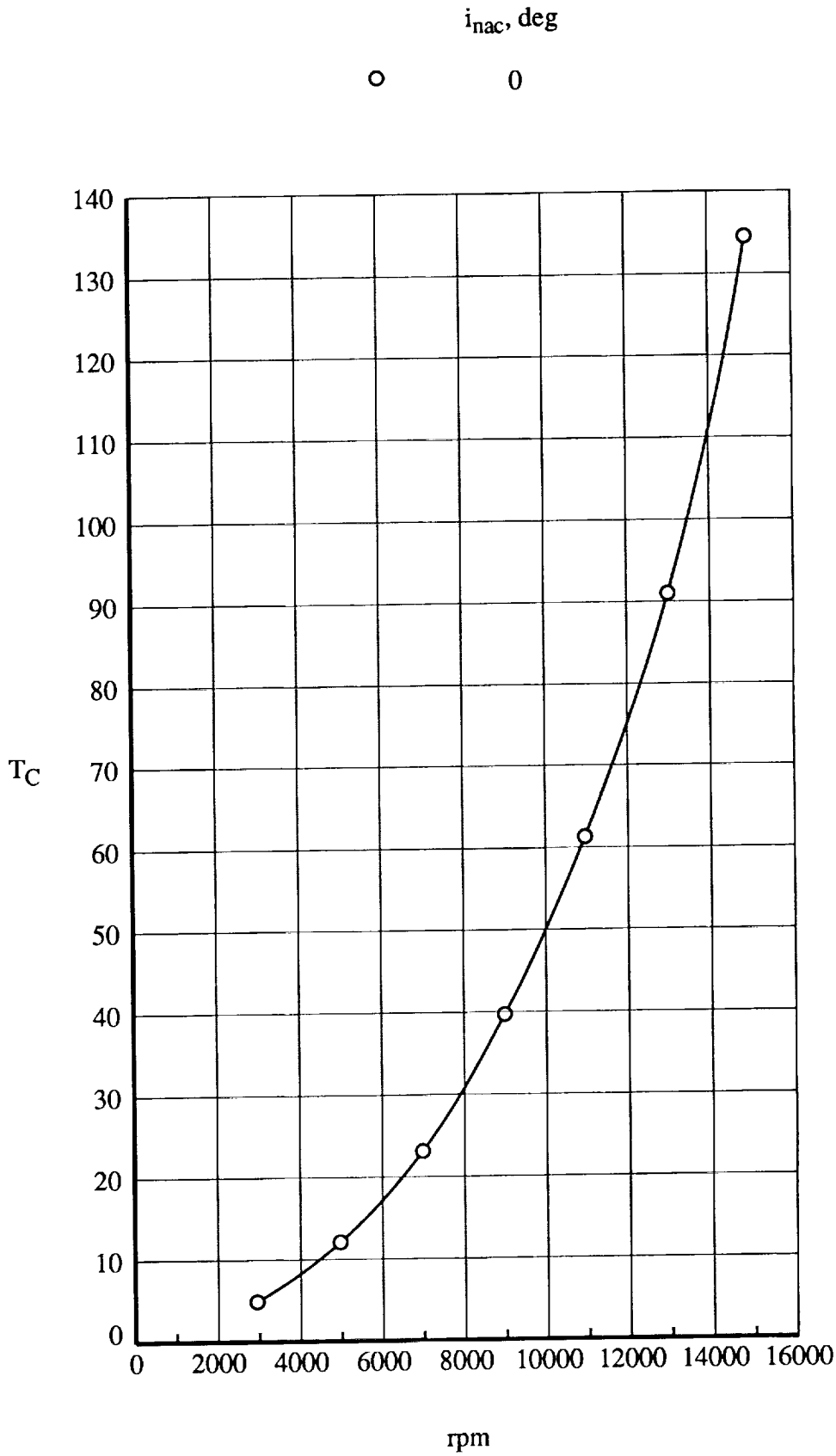

Figure 16. Thrust variation with rpm for cruise configuration at static conditions.

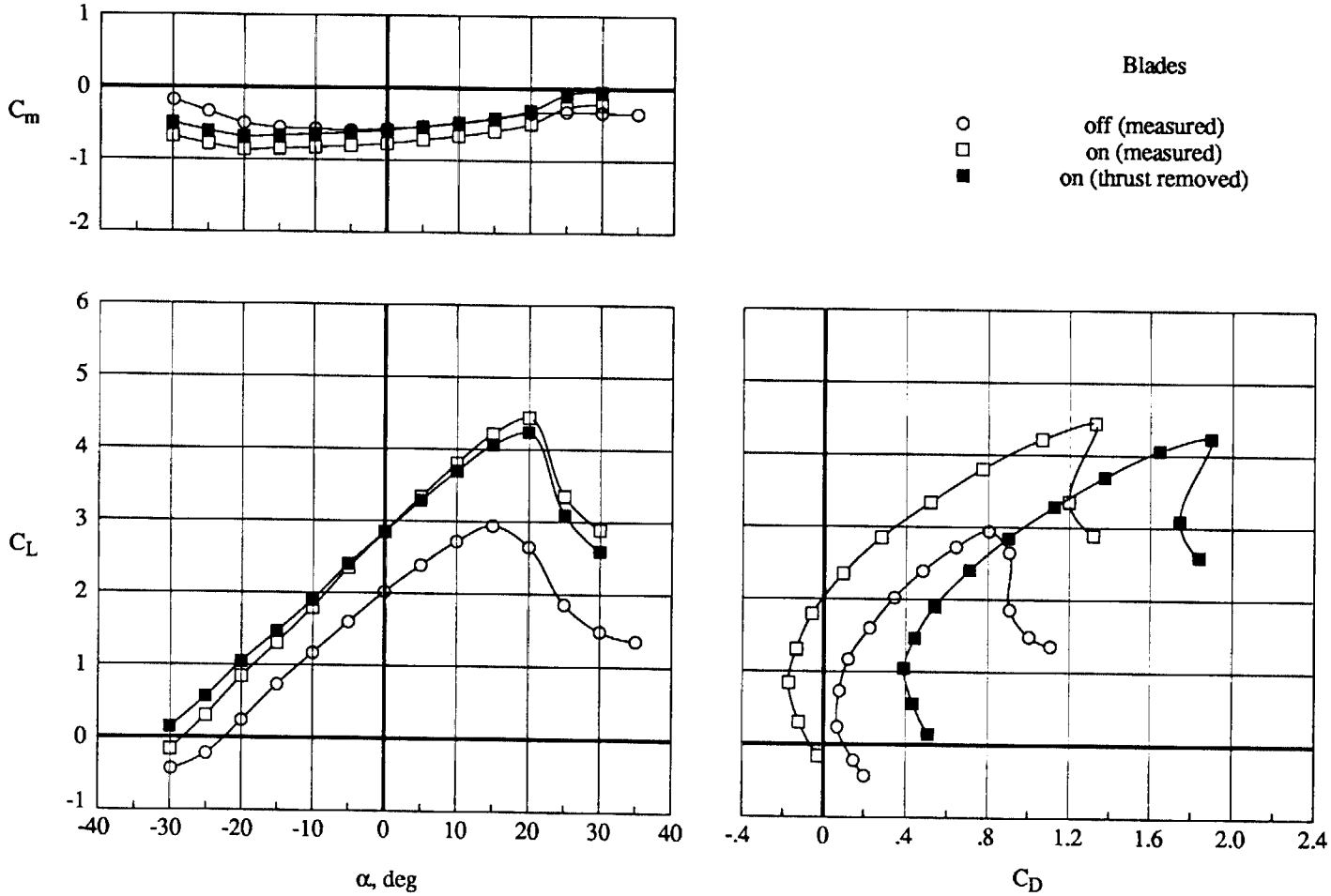

Figure 17. Propeller thrust and slipstream effects on wing aerodynamic characteristics with propeller blades on, and core pressure ratio matched to blades-off configuration for $q = 15$ lb/ft^2, $x/c = 0.60$, $z/c = 0.30$, $\delta_f = 60°$, and Propeller speed = 11 000 rpm.

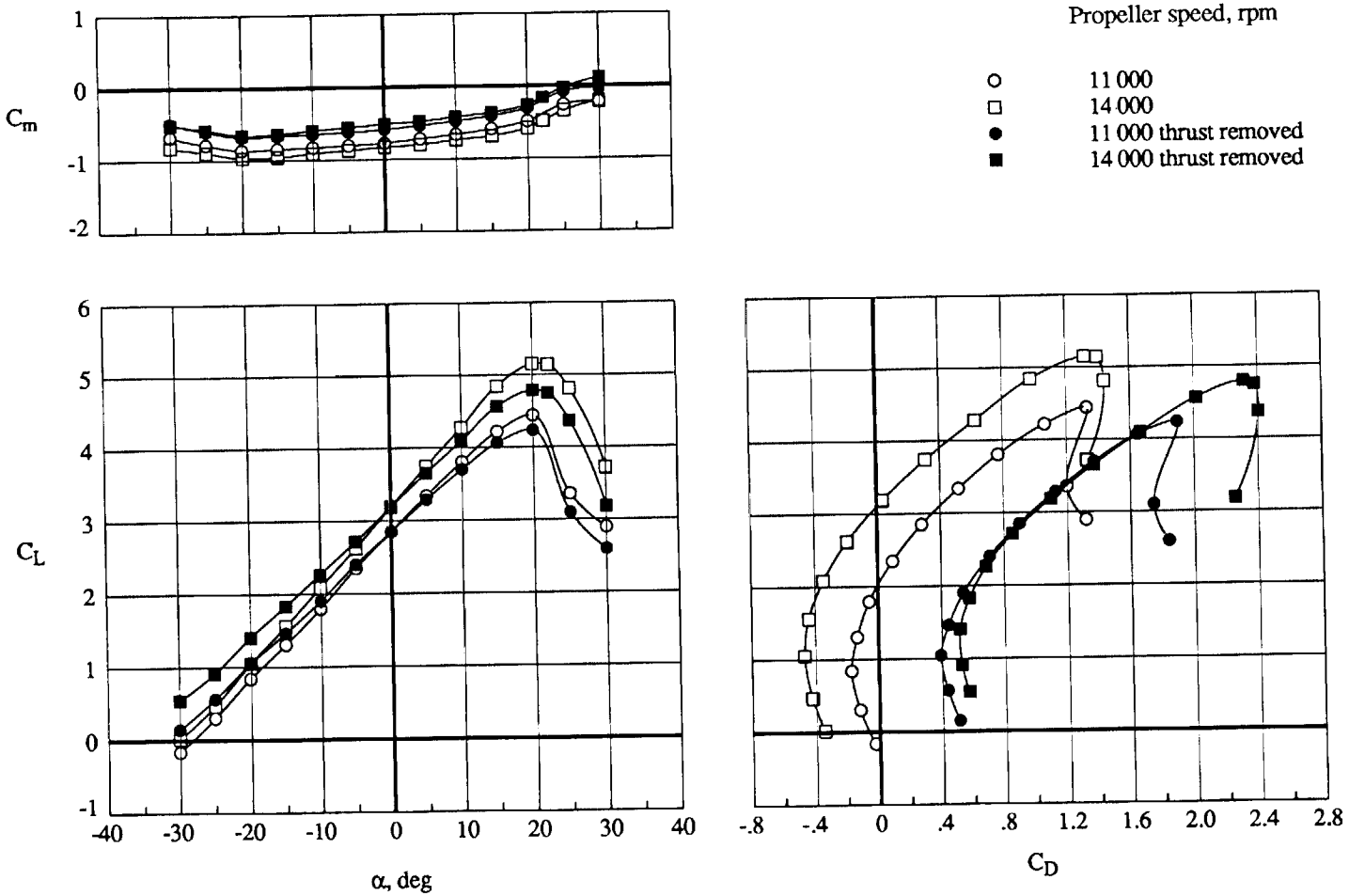

Figure 18. Effect of propeller rotational speed on wing aerodynamic performance for $q = 15$ lb/ft^2, $x/c = 0.60$, $z/c = 0.30$, $\delta_f = 60°$, and $i_{nac} = 0°$.

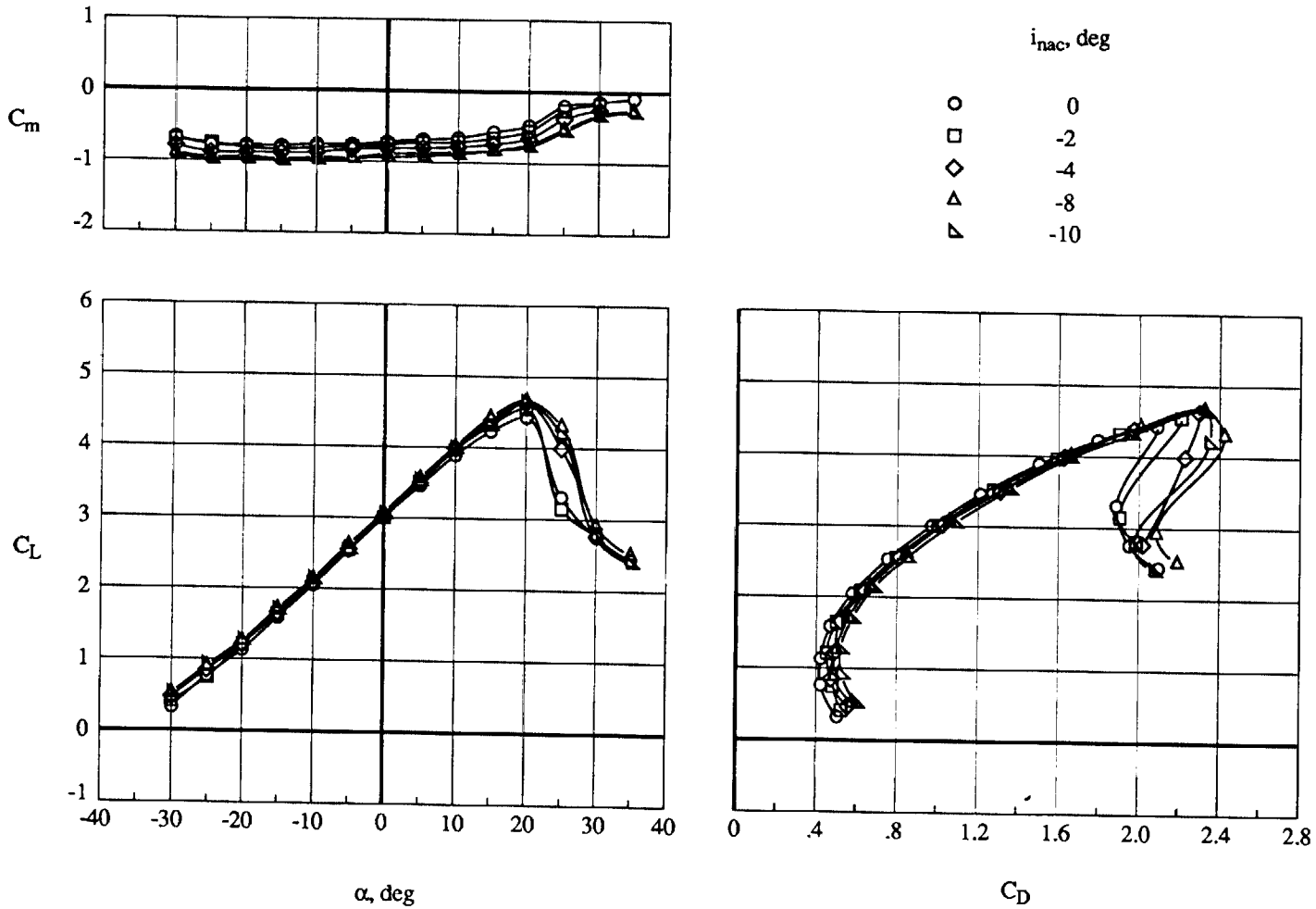

(a) Propeller speed = 11 000 rpm.

Figure 19. Effect of nacelle inclination on thrust-removed aerodynamic characteristics for $q = 15$ lb/ft^2, $\delta_f = 60°$, $x/c = 0.60$, and $z/c = 0.25$.

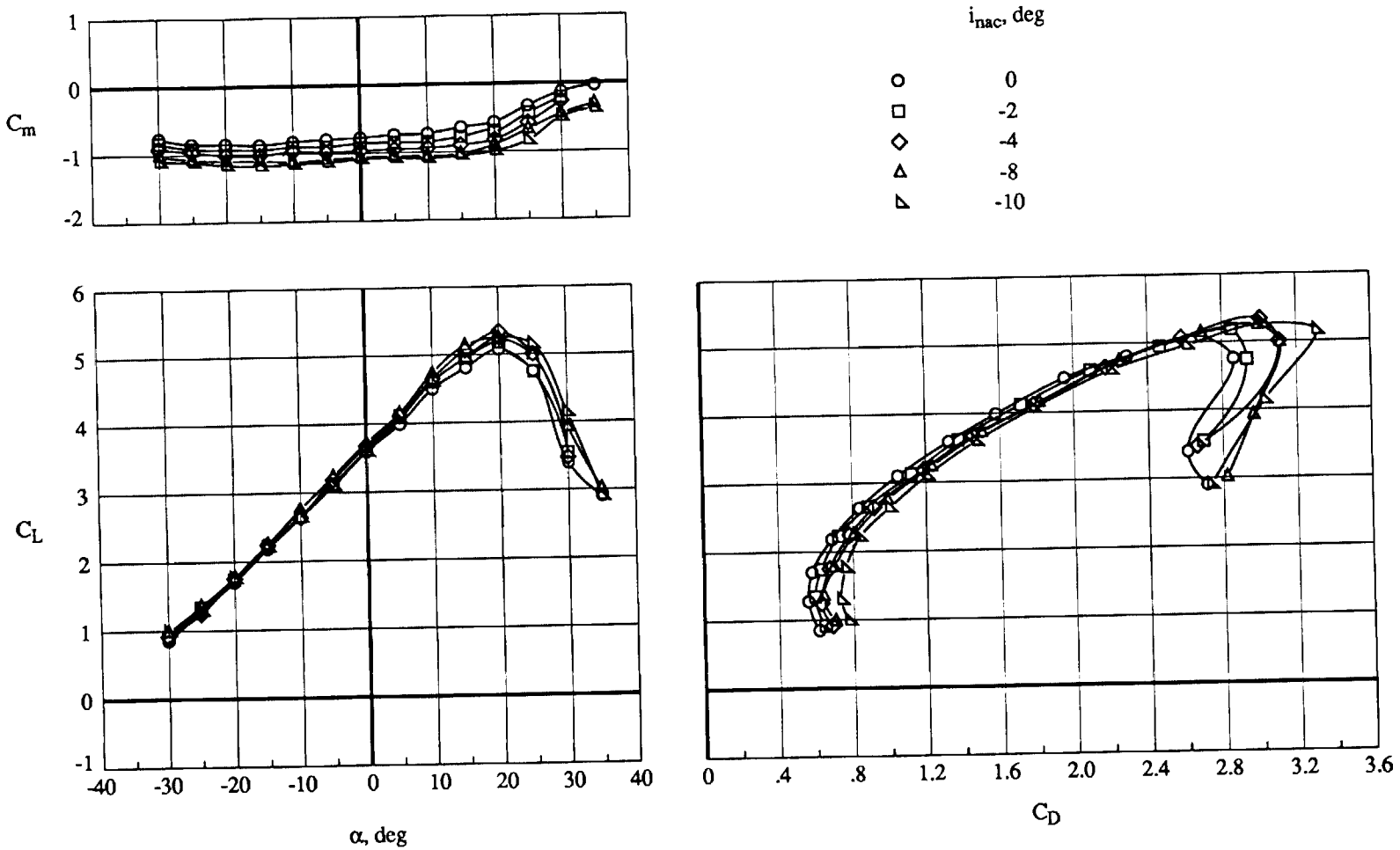

(b) Propeller speed = 14 000 rpm.

Figure 19. Concluded.

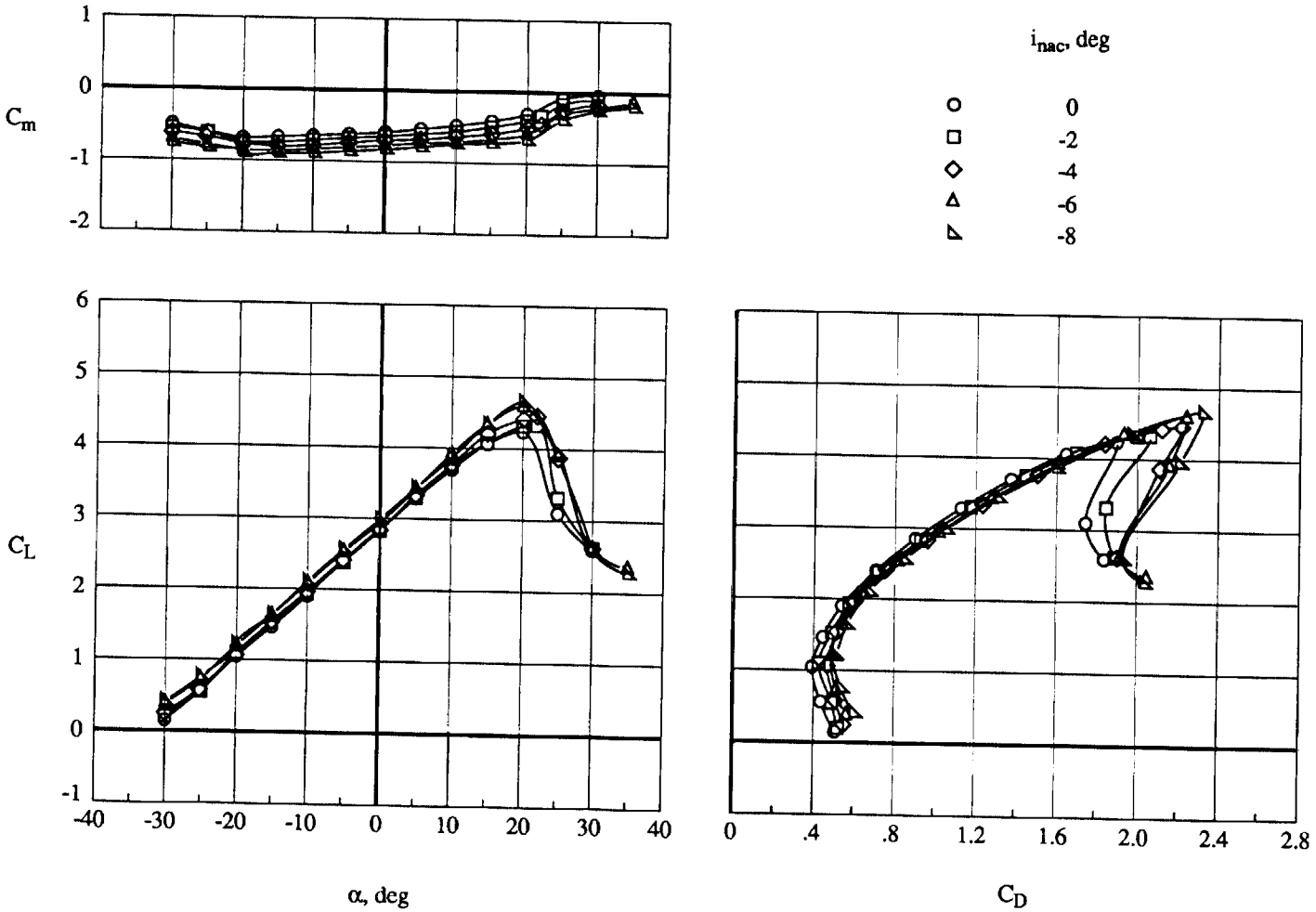

(a) Propeller speed = 11 000 rpm.

Figure 20. Effect of nacelle inclination on thrust-removed aerodynamic characteristics for $q = 15$ lb/ft^2, $\delta_f = 60°$, $x/c = 0.60$, and $z/c = 0.30$.

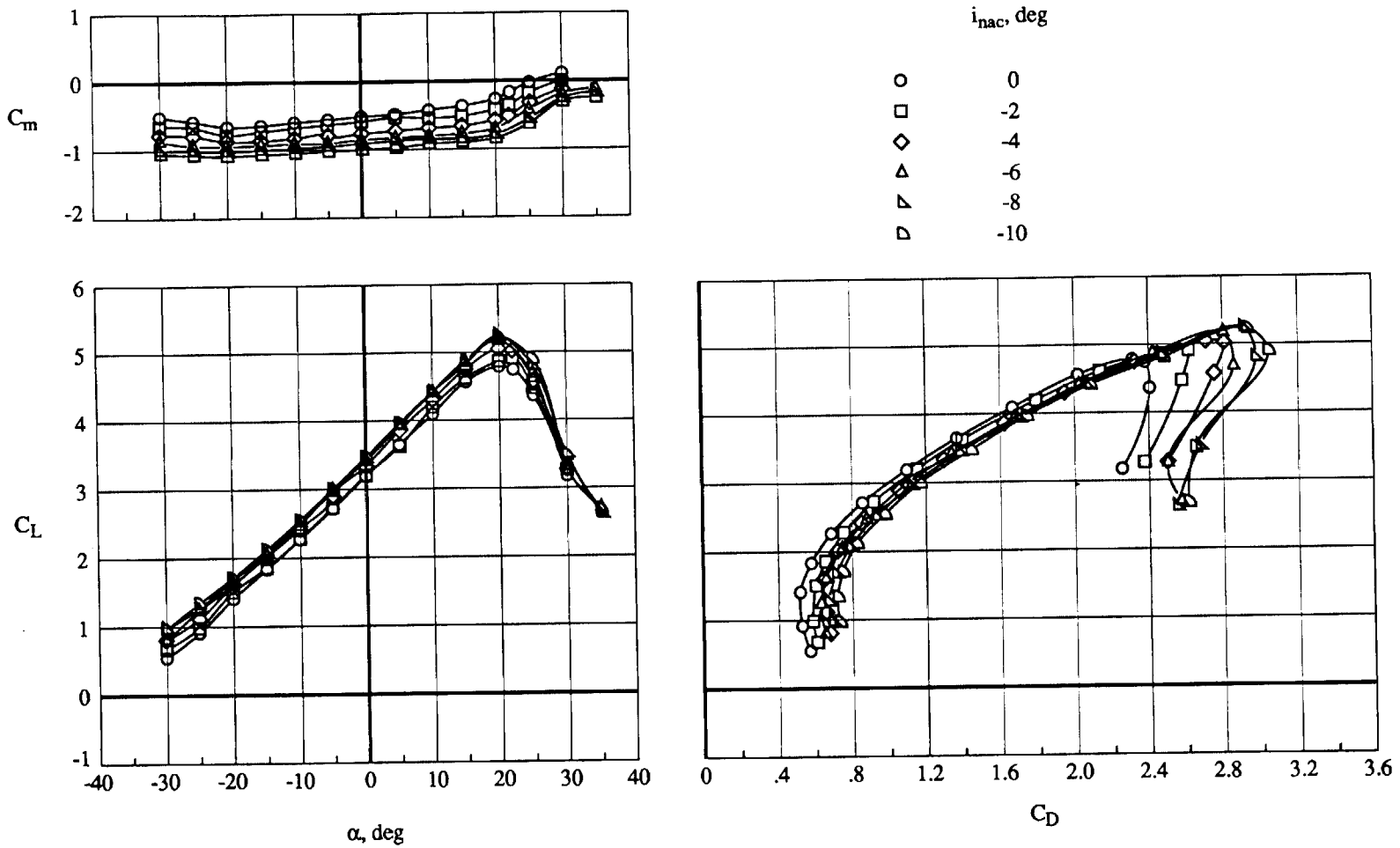

(b) Propeller speed = 14 000 rpm.

Figure 20. Concluded.

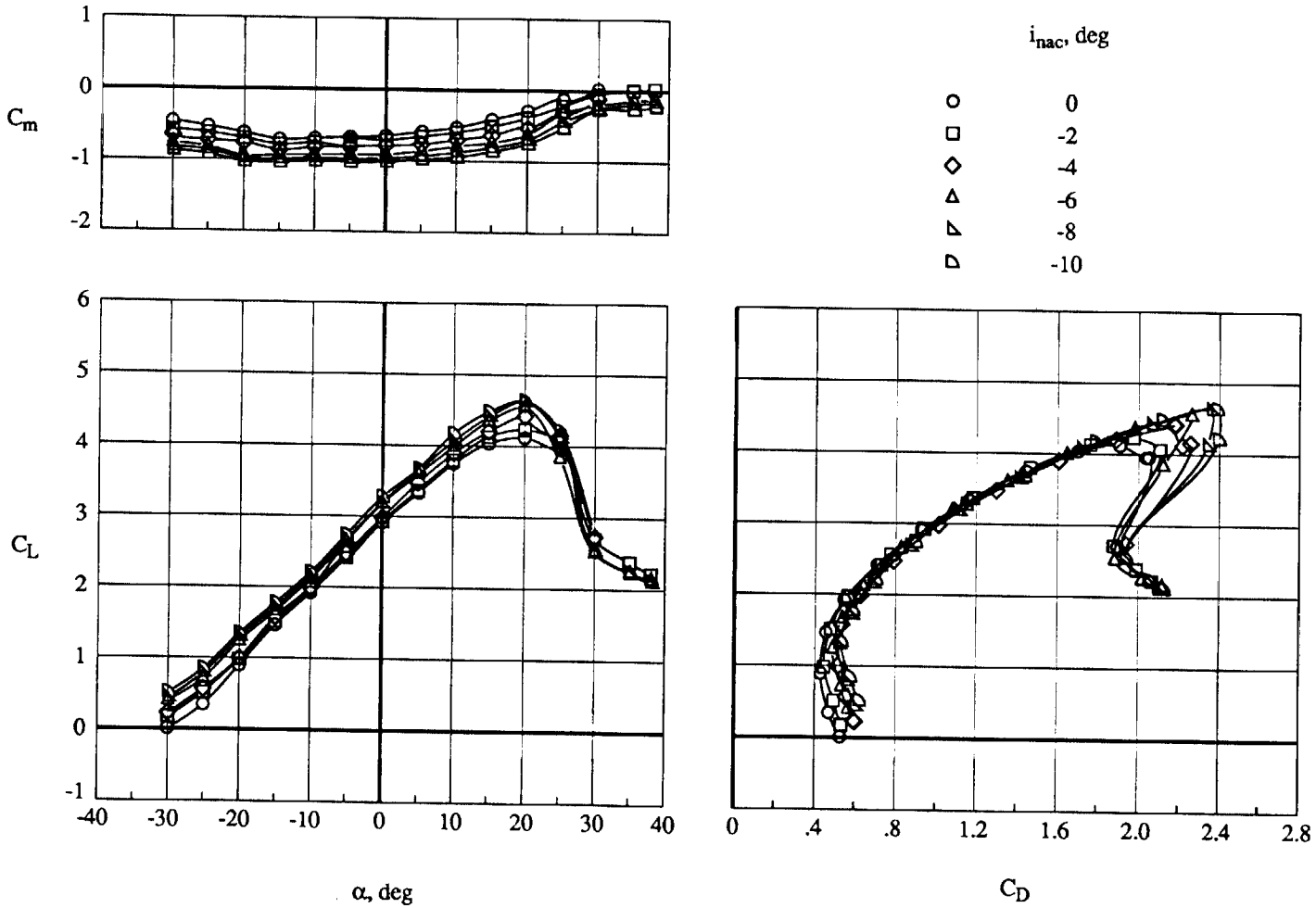

(a) Propeller speed = 11 000 rpm.

Figure 21. Effect of nacelle inclination on thrust removed aerodynamic characteristics for $q = 15$ lb/ft^2, $\delta_f = 60°$, $x/c = 0.75$, and $z/c = 0.30$.

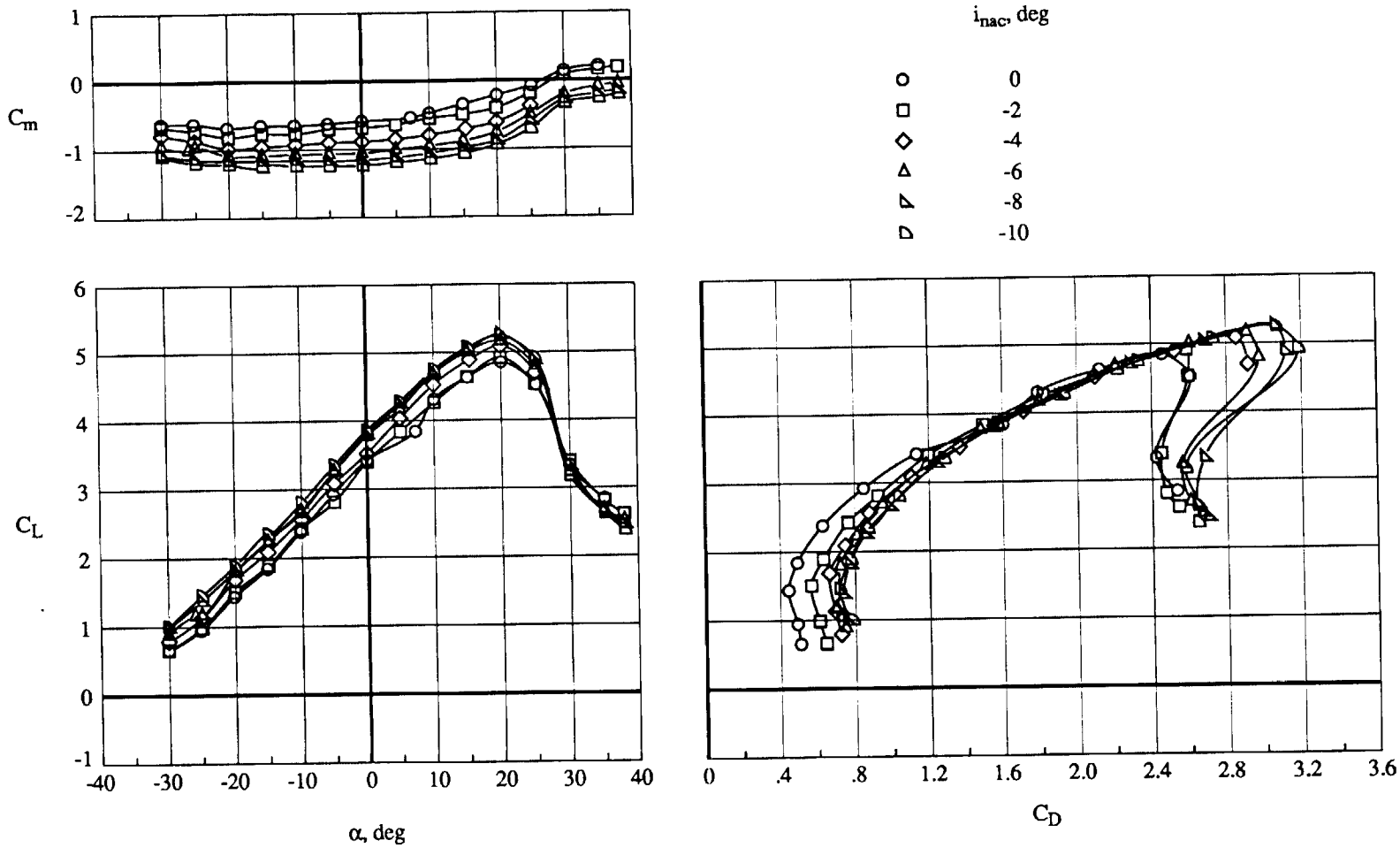

(b) Propeller speed = 14 000 rpm.

Figure 21. Concluded.

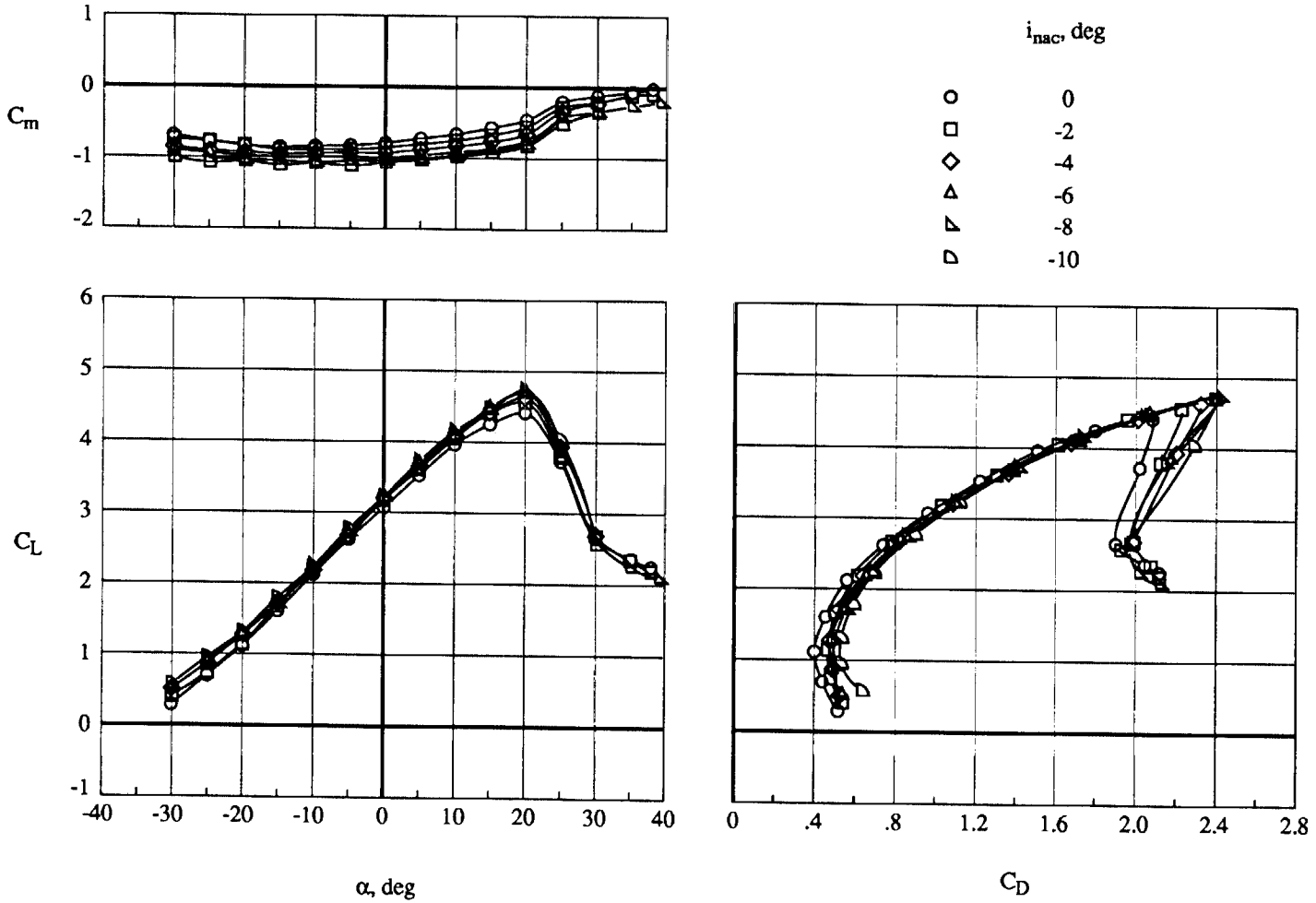

(a) Propeller speed = 11 000 rpm.

Figure 22. Effect of nacelle inclination on thrust removed aerodynamic characteristics for q = 15 lb/ft^2, $\delta_f = 60°$, $x/c = 0.75$, and $z/c = 0.25$.

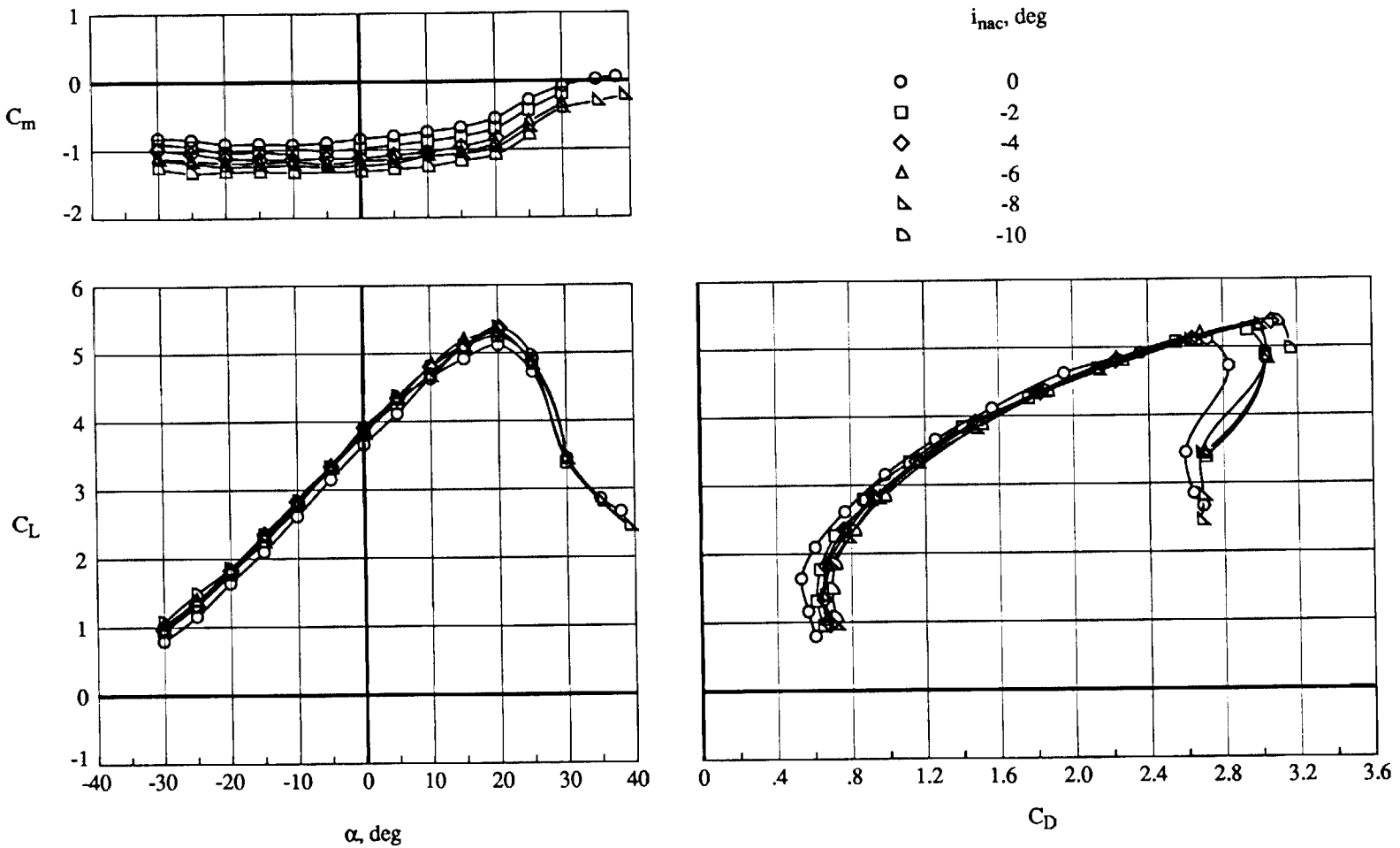

(b) Propeller speed = 14 000 rpm.

Figure 22. Concluded.

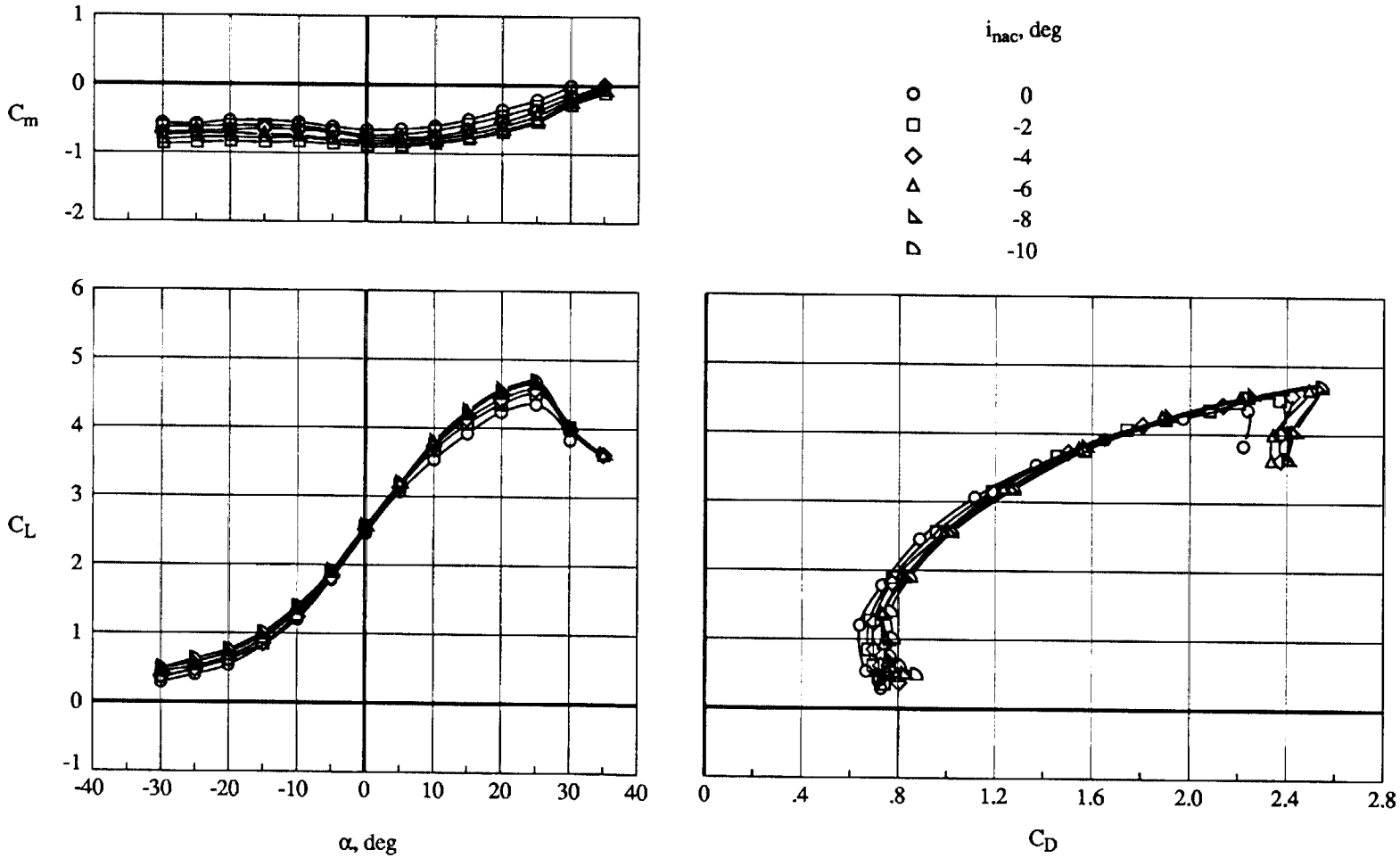

Figure 23. Effect of nacelle inclination on thrust-removed aerodynamic characteristics for $q = 15$ lb/ft^2, $x/c = 0.60$, $z/c = 0.25$, $\delta_f = 60°$, $\delta_K = 60°$, and Propeller speed = 11 000 rpm.

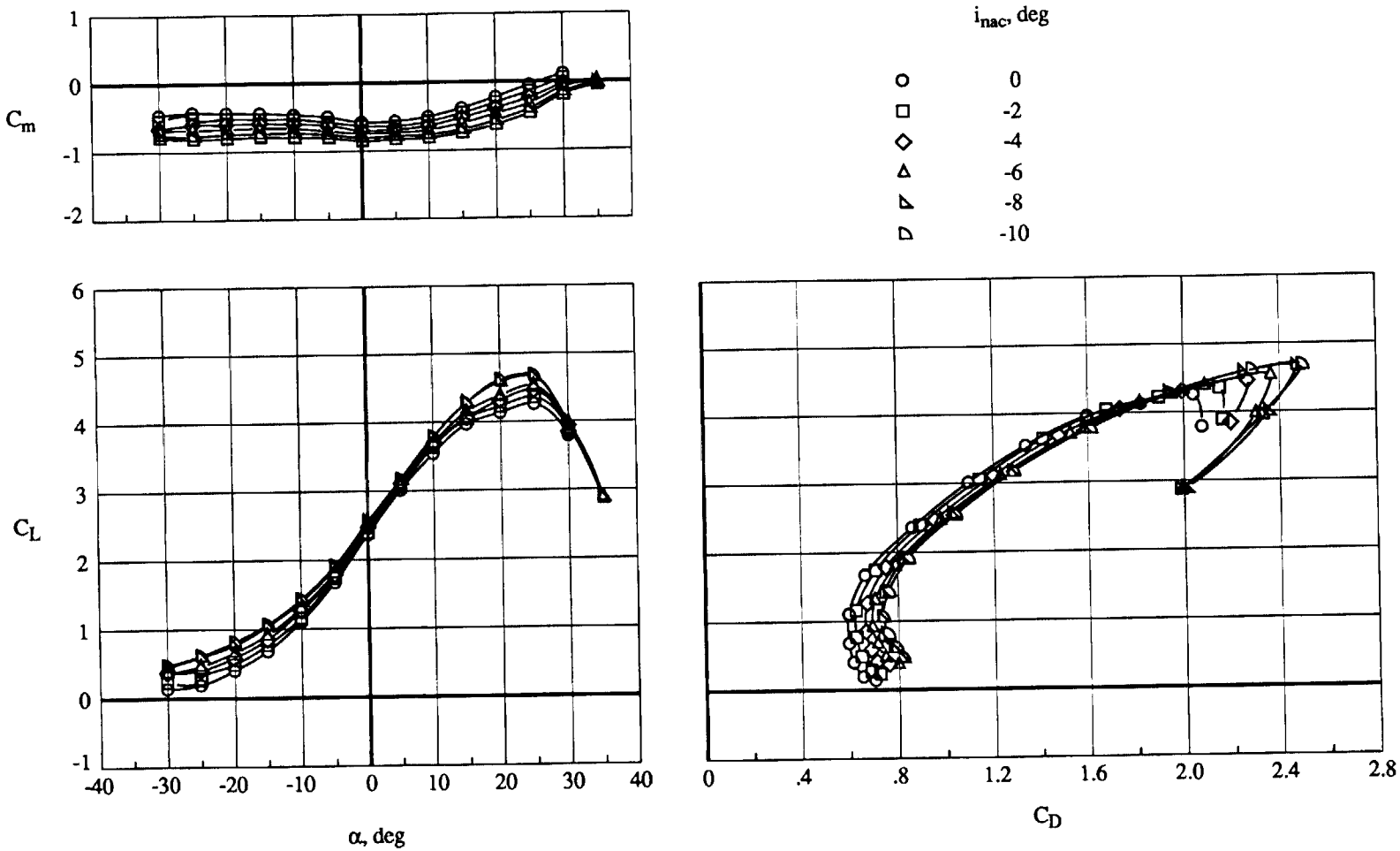

Figure 24. Effect of nacelle inclination on thrust-removed aerodynamic characteristics for $q = 15$ lb/ft^2, $x/c = 0.60$, $z/c = 0.30$, $\delta_f = 60°$, $\delta_K = 60°$, and Propeller speed = 11 000 rpm.

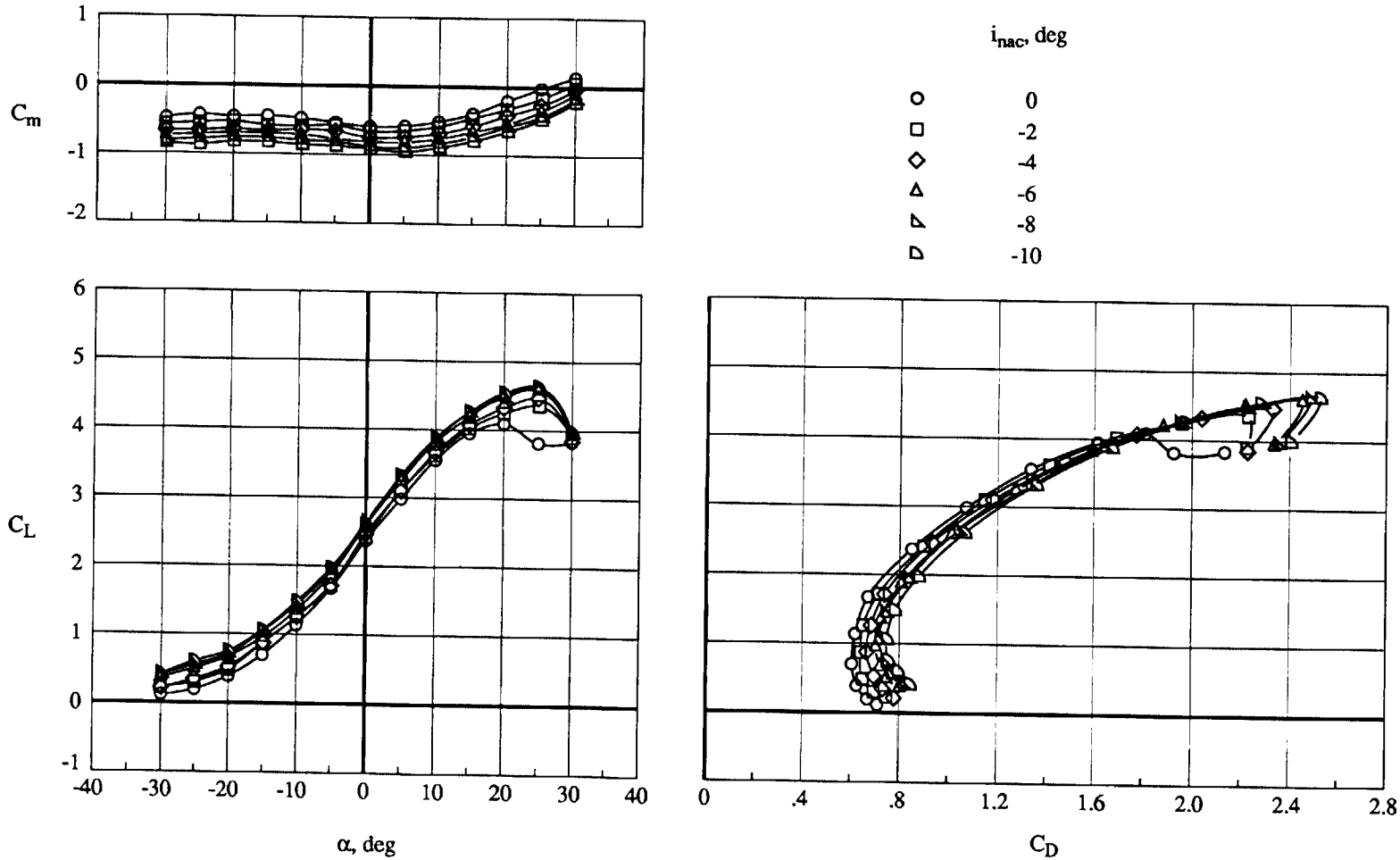

Figure 25. Effect of nacelle inclination on thrust-removed aerodynamic characteristics for $q = 15$ lb/ft^2, $x/c = 0.75$, $z/c = 0.30$, $\delta_f = 60°$, $\delta_K = 60°$, and Propeller speed = 11 000 rpm.

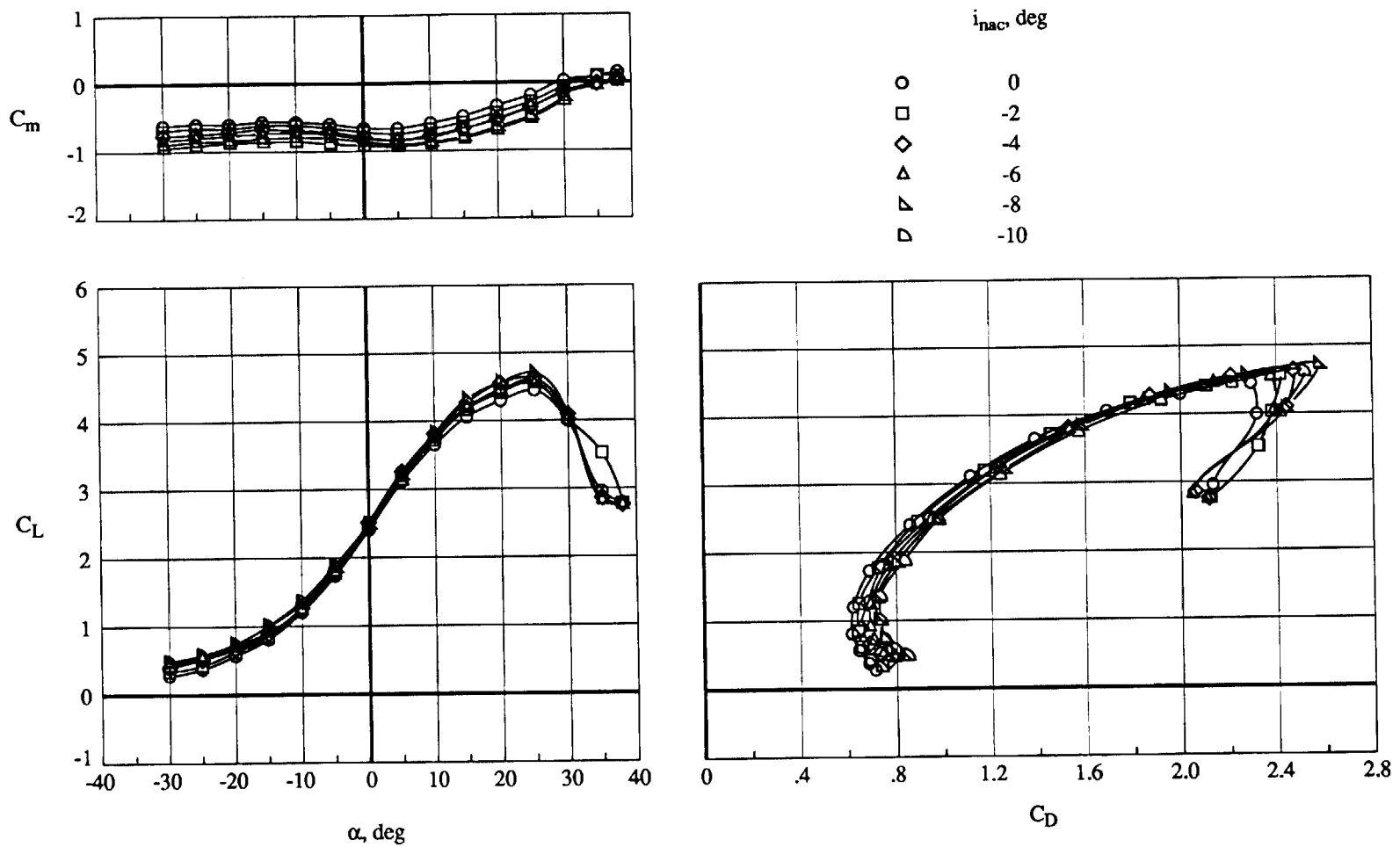

Figure 26. Effect of nacelle inclination on thrust-removed aerodynamic characteristics for $q = 15$ lb/ft^2, $x/c = 0.75$, $z/c = 0.25$, $\delta_f = 60°$, $\delta_K = 60°$, and Propeller speed = 11 000 rpm.

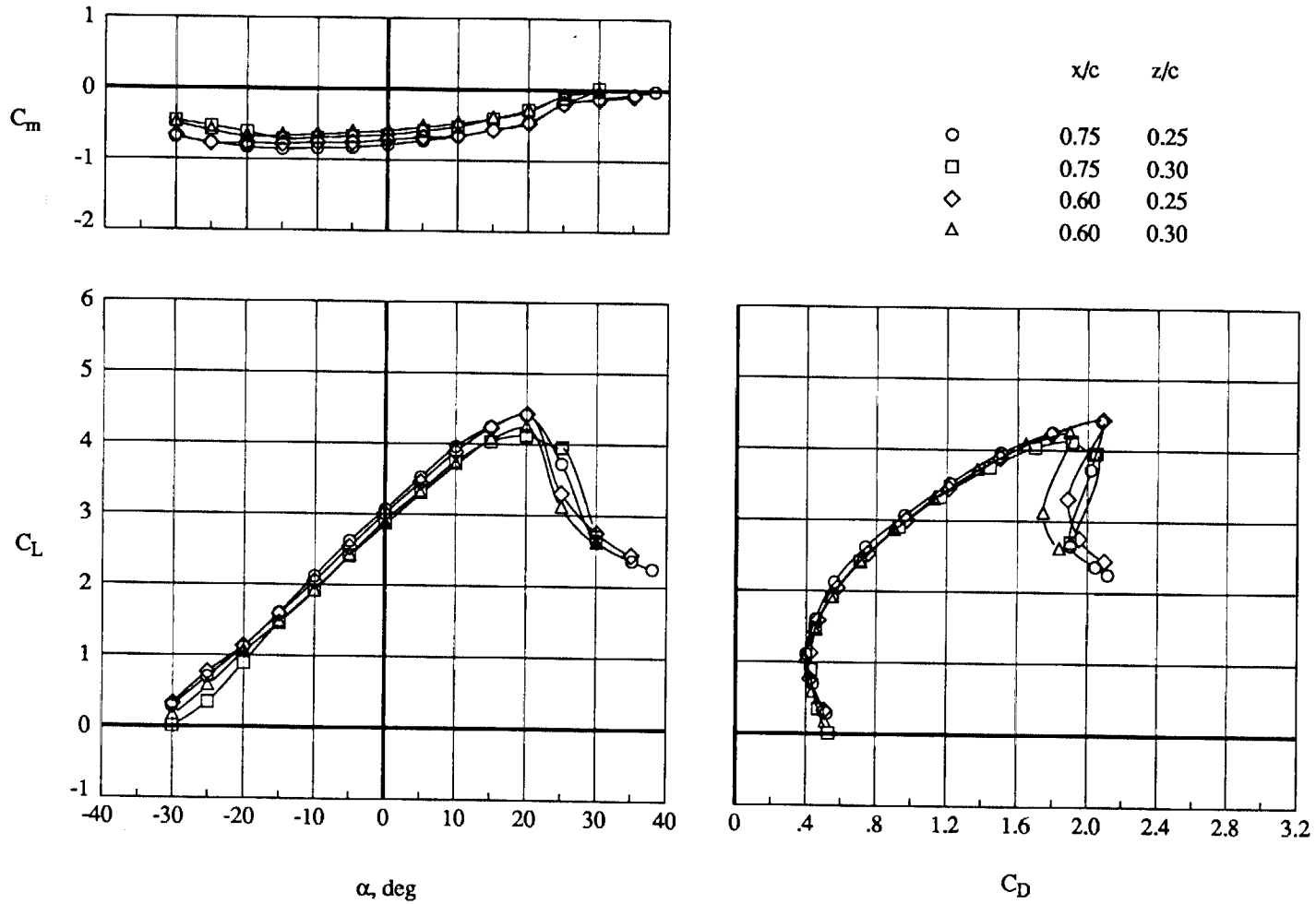

(a) Propeller speed = 11 000 rpm.

Figure 27. Effect of engine position on aerodynamic characteristics for $q = 15$ lb/ft^2, $\delta_f = 60°$, and $i_{nac} = 0°$.

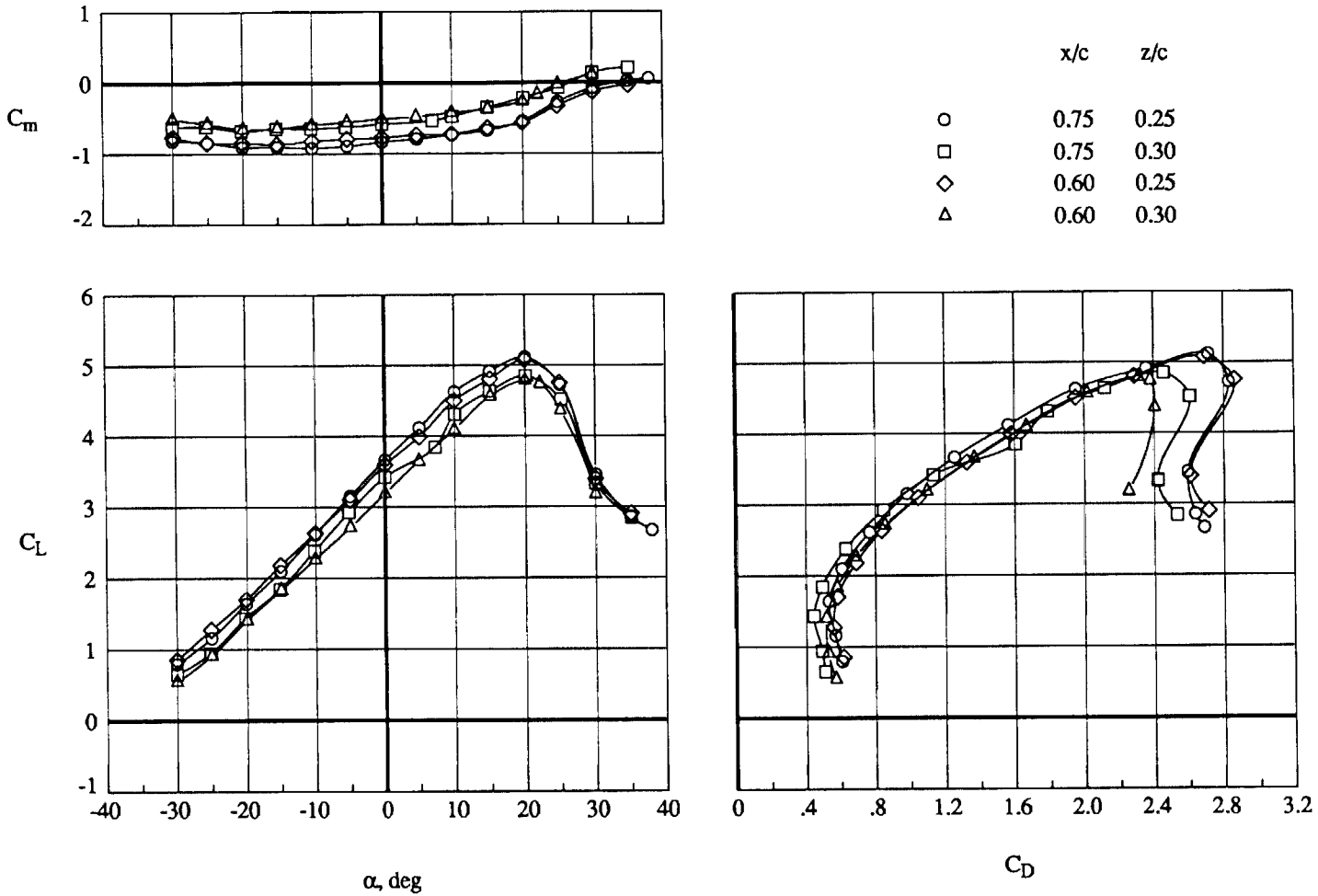

(b) Propeller speed = 14 000 rpm.

Figure 27. Concluded.

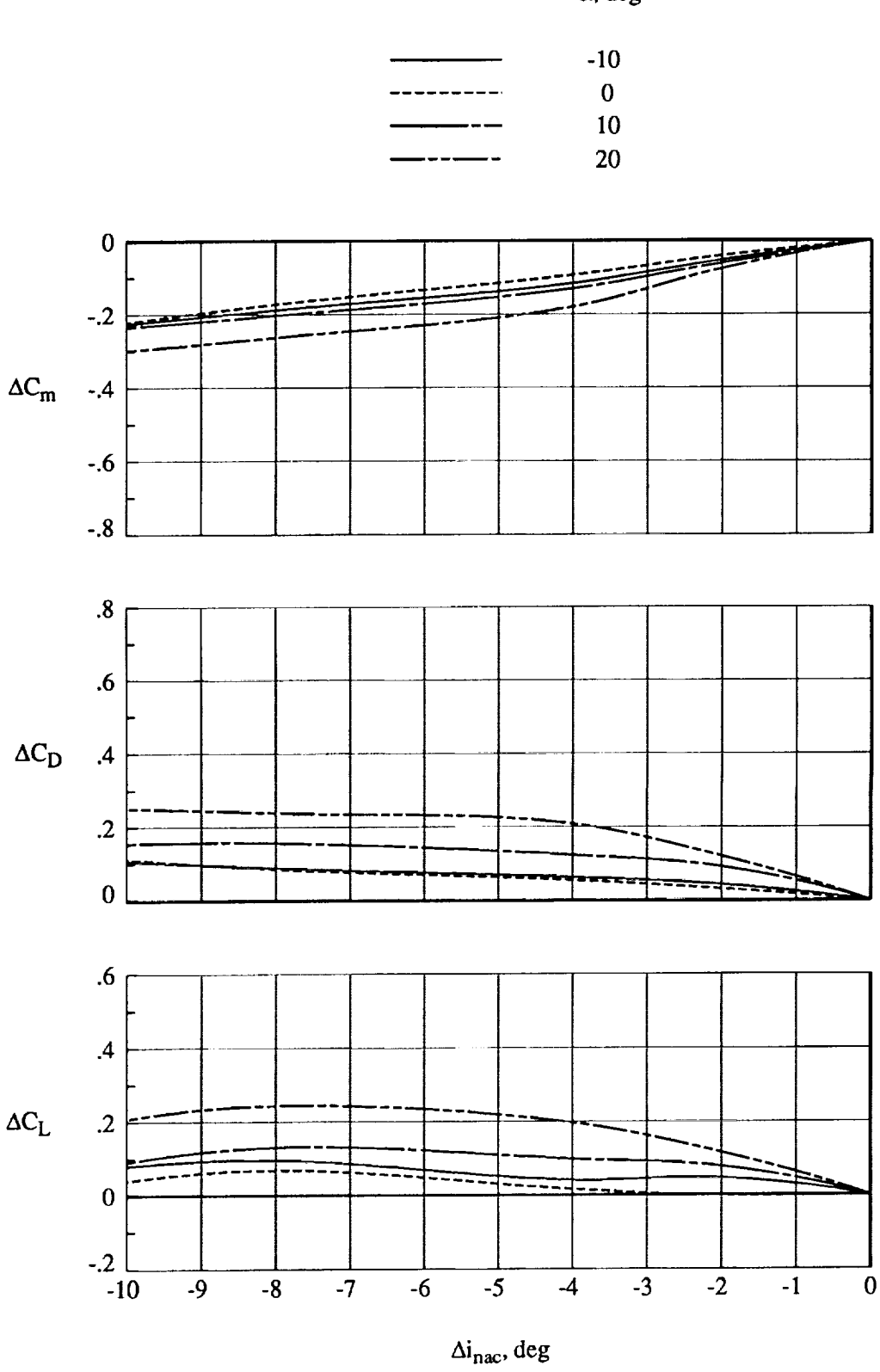

(a) Propeller speed = 11 000 rpm.

Figure 28. Relative effect of nacelle inclination on aerodynamic characteristics for $q = 15$ lb/ft^2, $x/c = 0.60$, $z/c = 0.25$, and $\delta_f = 60°$.

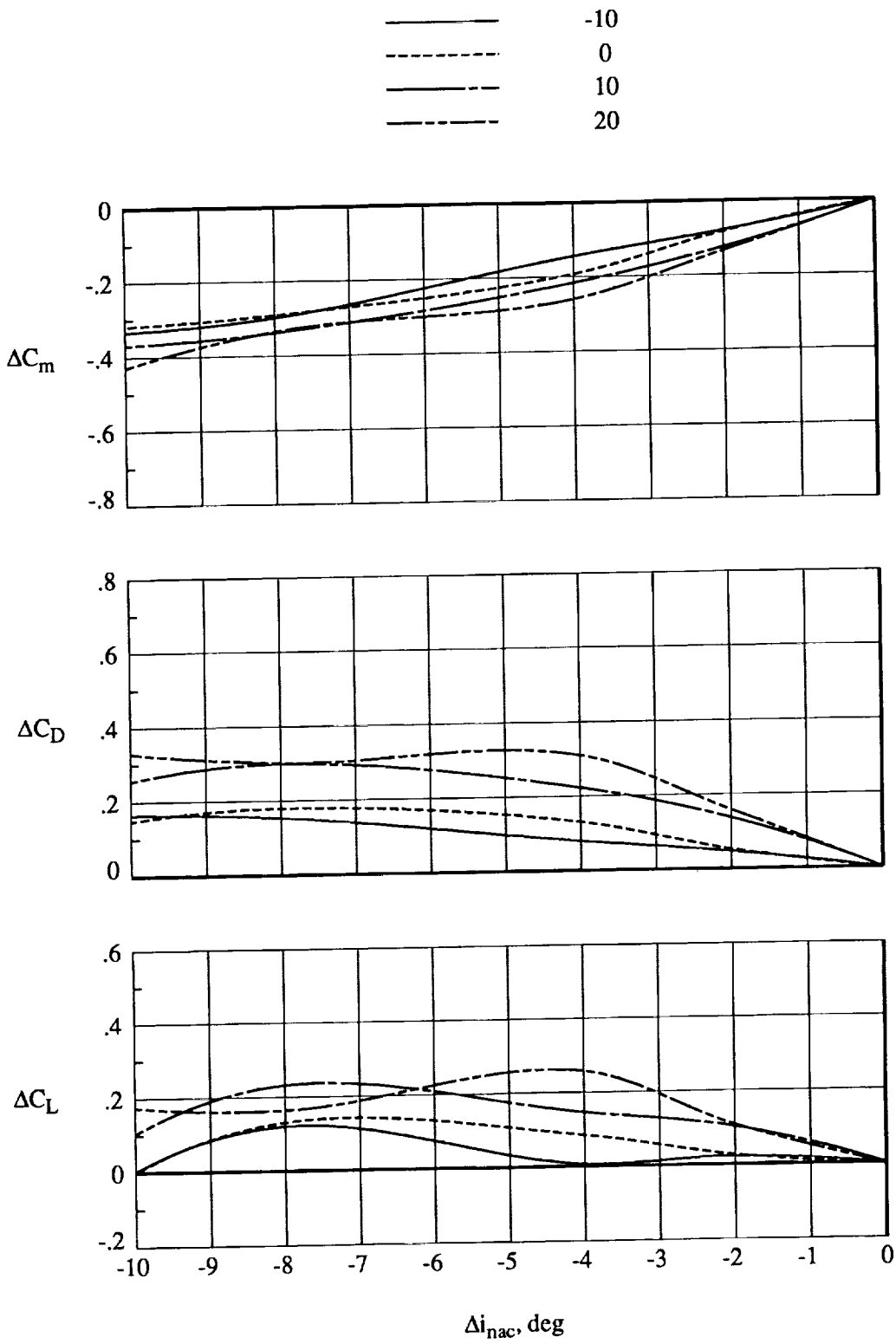

(b) Propeller speed = 14 000 rpm.

Figure 28. Concluded.

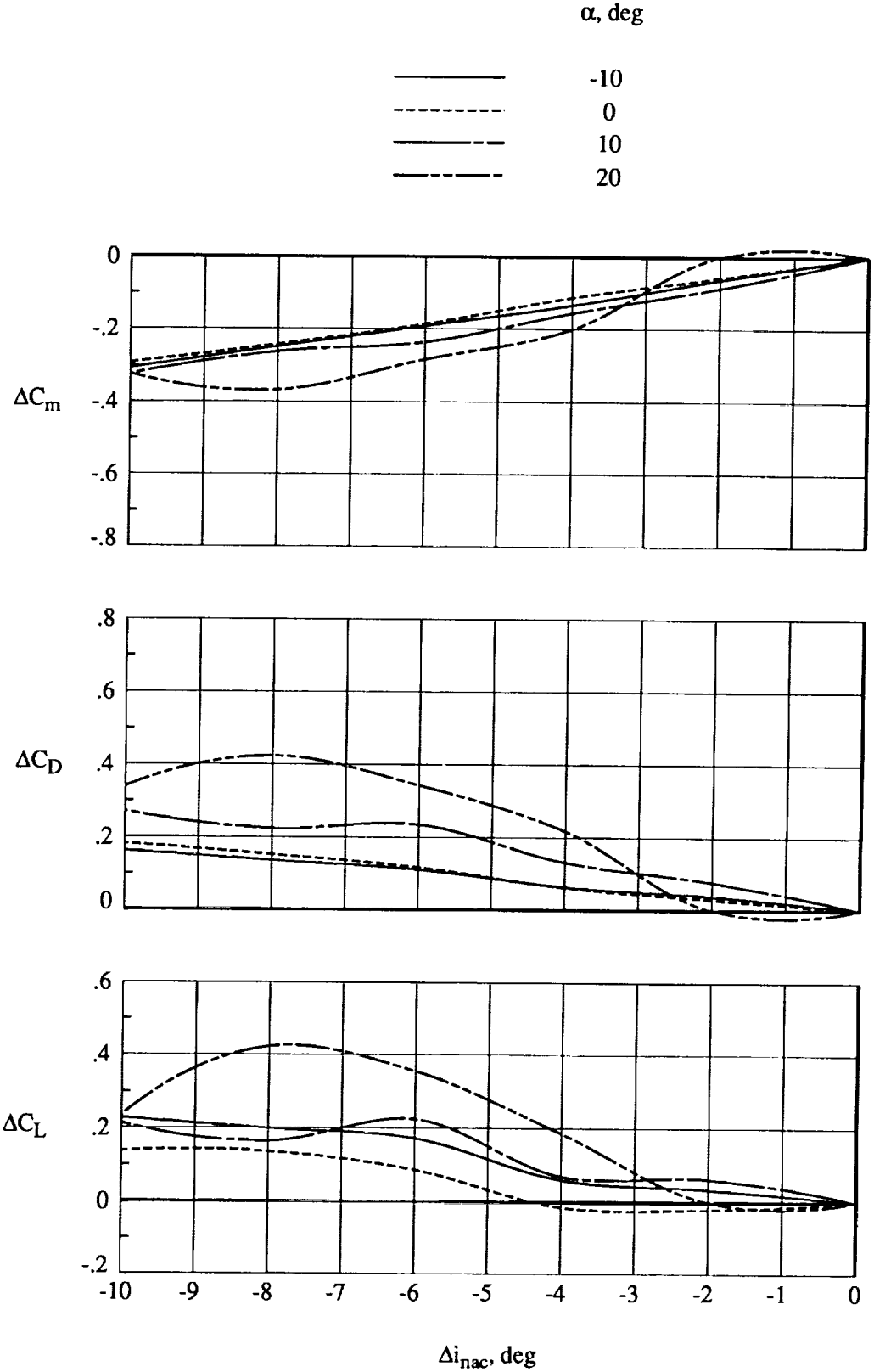

(a) Propeller speed = 11 000 rpm.

Figure 29. Relative effect of nacelle inclination on aerodynamic characteristics for $q = 15$ lb/ft^2, $x/c = 0.60$, $z/c = 0.30$, and $\delta_f = 60°$.

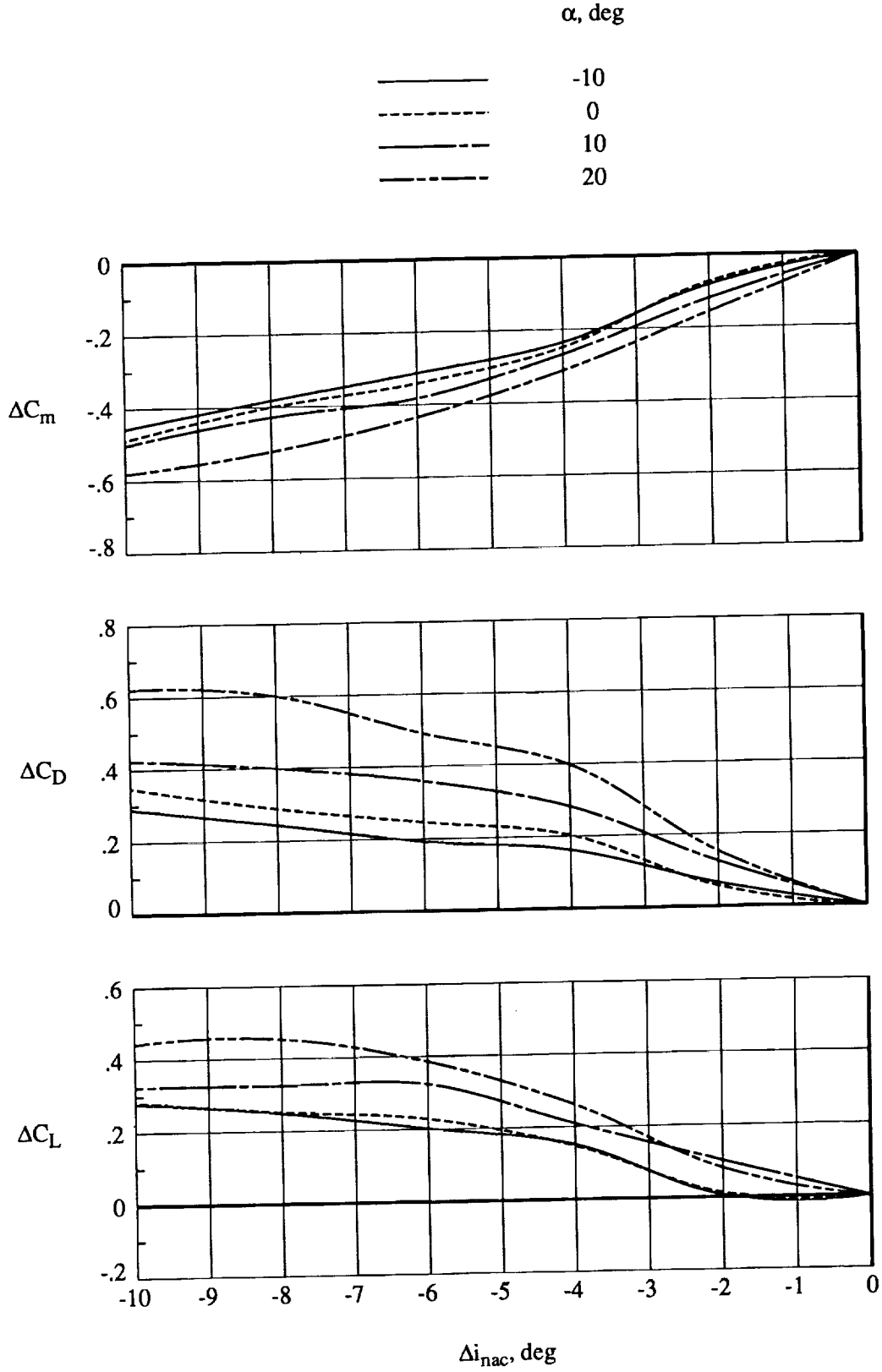

(b) Propeller speed = 14 000 rpm.

Figure 29. Concluded.

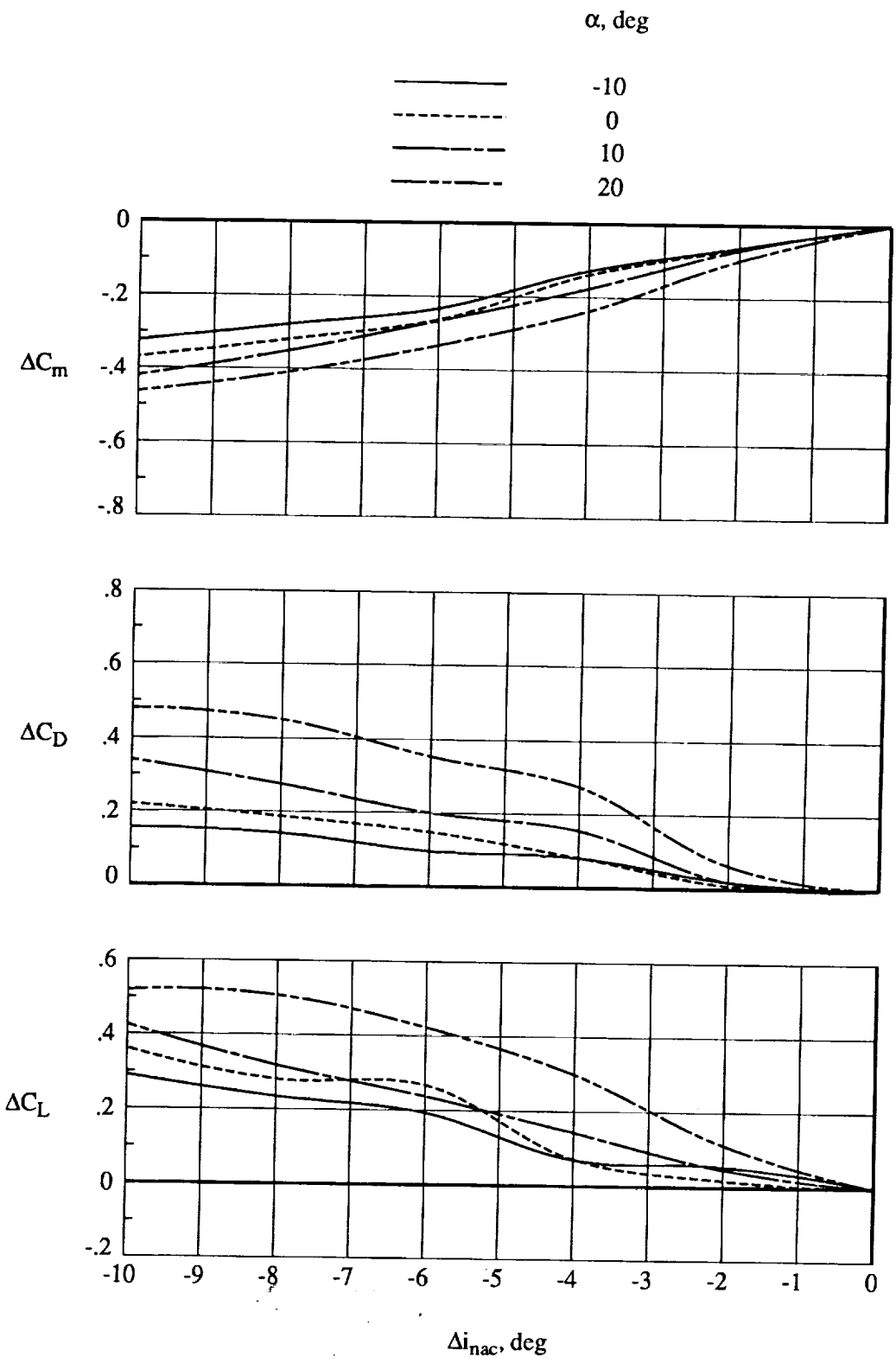

(a) Propeller speed = 11 000 rpm.

Figure 30. Relative effect of nacelle inclination on aerodynamic characteristics for $q = 15$ lb/ft^2, $x/c = 0.75$, $z/c = 0.30$, and $\delta_f = 60°$.

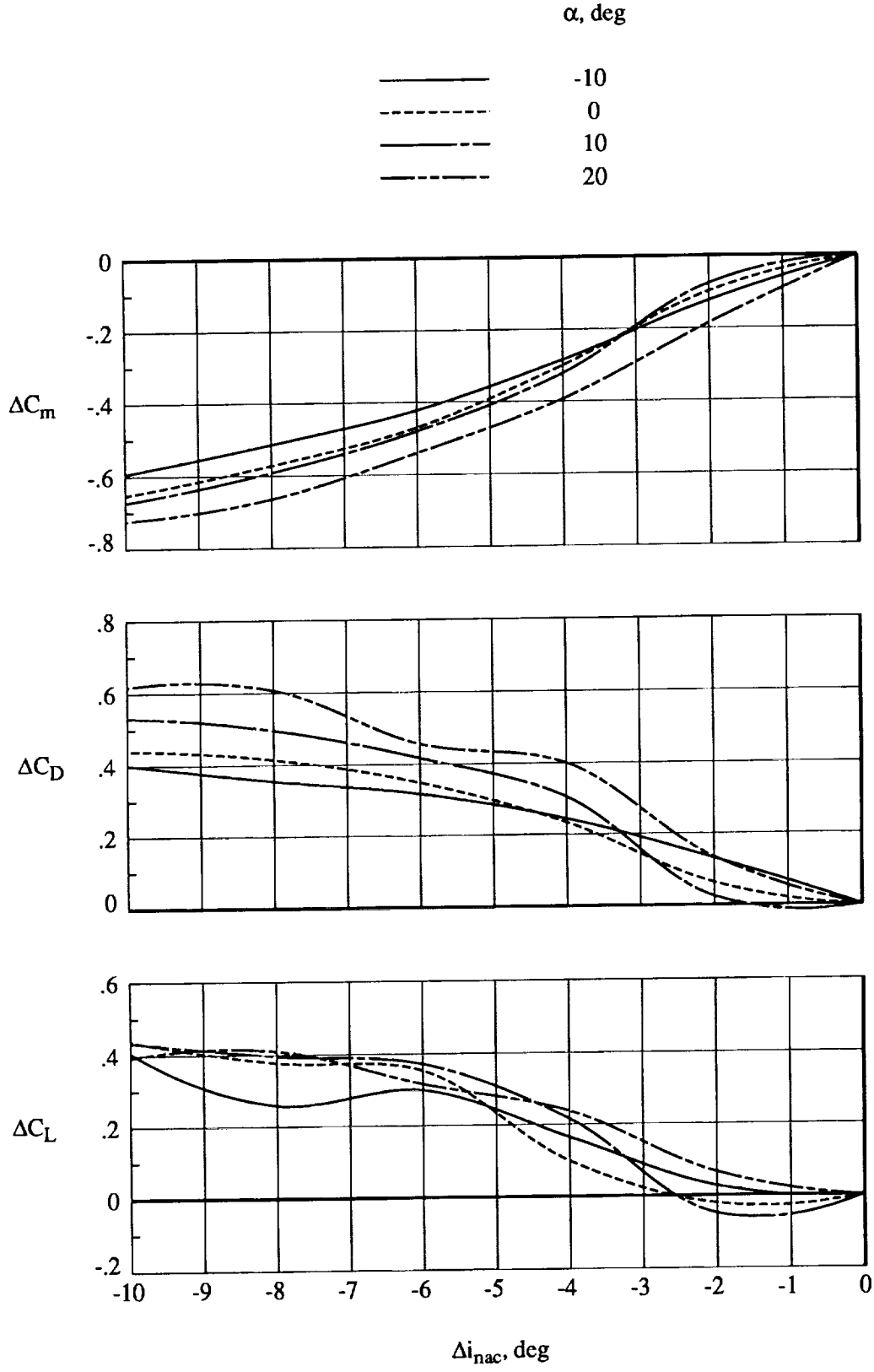

(b) Propeller speed = 14 000 rpm.

Figure 30. Concluded.

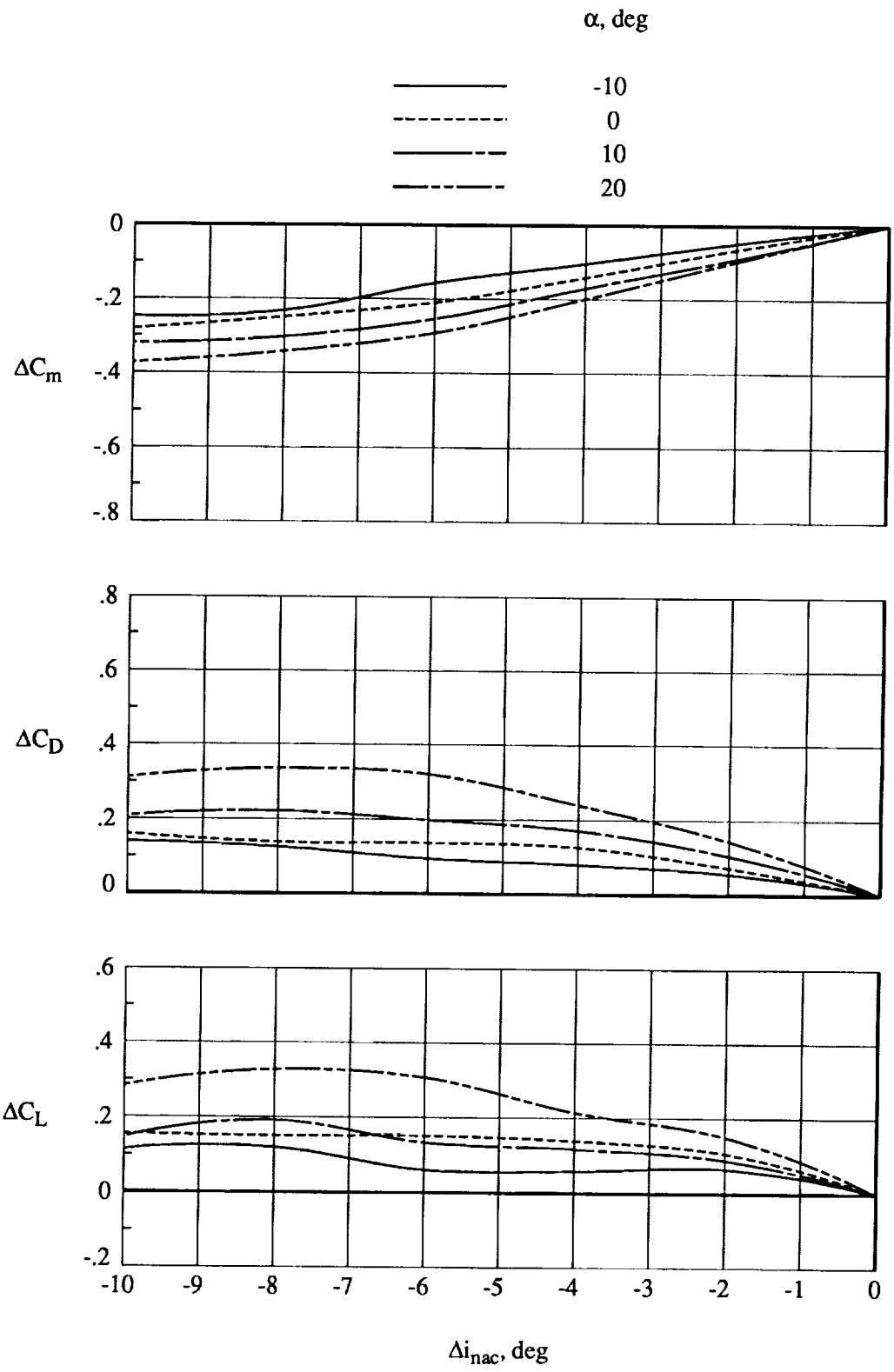

(a) Propeller speed = 11 000 rpm.

Figure 31. Relative effect of nacelle inclination on aerodynamic characteristics for $q = 15$ lb/ft^2, $x/c = 0.75$, $z/c = 0.25$, and $\delta_f = 60°$.

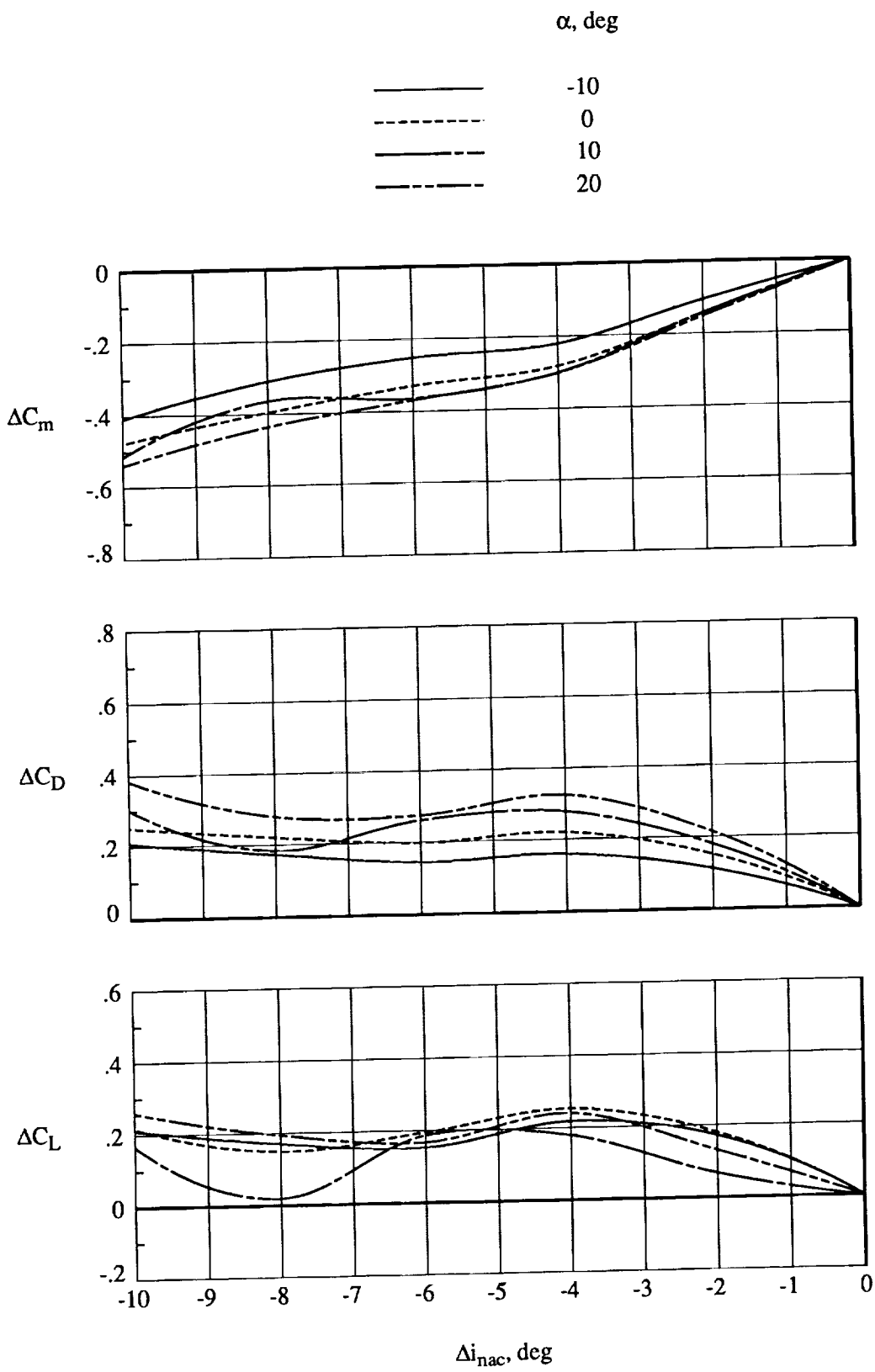

(b) Propeller speed = 14 000 rpm.

Figure 31. Concluded.

REPORT DOCUMENTATION PAGE

Form Approved
OMB No. 0704-0188

1. AGENCY USE ONLY *(Leave blank)*	2. REPORT DATE	3. REPORT TYPE AND DATES COVERED
	April 1994	Technical Memorandum

4. TITLE AND SUBTITLE
Aerodynamic Characteristics of a Propeller-Powered High-Lift Semispan Wing

5. FUNDING NUMBERS
WU 535-03-10-02

6. AUTHOR(S)
Garl L. Gentry, Jr., M. A. Takallu, and Zachary T. Applin

7. PERFORMING ORGANIZATION NAME(S) AND ADDRESS(ES)
NASA Langley Research Center
Hampton, VA 23681-0001

8. PERFORMING ORGANIZATION REPORT NUMBER
L-17259

9. SPONSORING/MONITORING AGENCY NAME(S) AND ADDRESS(ES)
National Aeronautics and Space Administration
Washington, DC 20546-0001

10. SPONSORING/MONITORING AGENCY REPORT NUMBER
NASA TM-4541

11. SUPPLEMENTARY NOTES
Gentry and Applin: Langley Research Center, Hampton, VA; Takallu: Lockheed Engineering & Sciences Company, Hampton, VA.

12a. DISTRIBUTION/AVAILABILITY STATEMENT
Unclassified Unlimited

Subject Category 02

12b. DISTRIBUTION CODE

13. ABSTRACT *(Maximum 200 words)*
A small-scale semispan high-lift wing-flap system equipped under the wing with a turboprop engine assembly was tested in the Langley 14- by 22-Foot Subsonic Tunnel. Experimental data were obtained for various propeller rotational speeds, nacelle locations, and nacelle inclinations. To isolate the effects of the high-lift system, data were obtained with and without the flaps and leading-edge device. The effects of the propeller slipstream on the overall longitudinal aerodynamic characteristics of the wing-propeller assembly were examined. Test results indicated that the lift coefficient of the wing could be increased by the propeller slipstream when the rotational speed was increased and high-lift devices were deployed. Decreasing the nacelle inclination (increased pitch down) enhanced the lift performance of the system much more than varying the vertical or horizontal location of the nacelle. Furthermore, decreasing the nacelle inclination led to higher lift curve slope values, which indicated that the powered wing could sustain higher angles of attack near maximum lift performance. Any lift augmentation was accompanied by a drag penalty due to the increased wing lift.

14. SUBJECT TERMS
Turboprop; Propulsion integration; High lift

15. NUMBER OF PAGES
68

16. PRICE CODE
A04

17. SECURITY CLASSIFICATION OF REPORT	18. SECURITY CLASSIFICATION OF THIS PAGE	19. SECURITY CLASSIFICATION OF ABSTRACT	20. LIMITATION OF ABSTRACT
Unclassified	Unclassified		